CRANFIELD UNIVERSITY

BRIGIDA CORRIERI

HUMAN VS NON-HUMAN BONE.
IDENTIFICATION AND DIFFERENTIATION OF FRAGMENTED SKELETAL
REMAINS USING NON-DESTRUCTIVE METHODS

CRANFIELD FORENSIC INSTITUTE

PhD Thesis
Academic Year: 2017 - 2018

Supervisor: Dr Nicholas Marquez-Grant
Associate Supervisor: Professor Keith Rogers
February 2018

CRANFIELD UNIVERSITY

CRANFIELD FORENSIC INSTITUTE

PhD Thesis

Academic Year 2017 - 2018

BRIGIDA CORRIERI

HUMAN VS NON-HUMAN BONE.
IDENTIFICATION AND DIFFERENTIATION OF FRAGMENTED SKELETAL
REMAINS USING NON-DESTRUCTIVE METHODS

Supervisor: Dr Nicholas Marquez-Grant
Associate Supervisor: Professor Keith Rogers
February 2018

This thesis is submitted in partial fulfilment of the requirements for the degree
of PhD

ABSTRACT

Fragmented human and non-human bones can be found in forensic contexts, such as mass disasters, mass graves, and crime scenes, as well as in archaeological deposits. When fragmented skeletal remains are found, one of the first questions asked is whether or not the fragments are human or non-human. If none of the diagnostic features is visible, the origin of the fragments may be difficult to assess. Most of the methods currently employed to identify the origin of bone fragments, such as microscopic and biomolecular methods, are invasive and time consuming.

The aim of the research presented in this thesis was to explore the potential of non-destructive procedures, such as GIS (Geographic Information System) software, morphological examination and Micro-Computed Tomography, in determining whether or not a bone fragment is human. These techniques were applied on skeletal features not commonly used for the human-nonhuman bone differentiation. Cranial suture patterns, cranial curvature and rib shaft curvature were assessed and measured using a GIS software. In addition, the morphology of the occipital condyles and the linea aspera of the femur were investigated and compared between human and non-human species. Finally, primary nutrient foramina and cross-sectional shape of long bones were analysed using micro-CT. More than 700 human and non-human bones were used; the non-human species selected are the ones whose remains are likely to be found in forensic or archaeological contexts in the United Kingdom.

Most of the bone features considered and the procedures used in this study proved to be reliable for the differentiation between human and non-human fragmented bones. Blind tests performed on fragments whose human or non-human origin was not known further demonstrated the applicability and effectiveness of the methods and features explored in this study. The results of this research provide a valuable contribution to the fields of forensic anthropology, bioarchaeology, and comparative anatomy.

Keywords: forensic anthropology, bone fragments, macroscopic methods, GIS software, Micro-Computed Tomography

ACKNOWLEDGEMENTS

TABLE OF CONTENTS

LIST OF FIGURES

LIST OF TABLES

Chapter 1: INTRODUCTION

Bone fragments, ranging from 5 millimetres to 10/12 centimetres, can be found in both forensic and archaeological contexts, such as crimes scenes, burial sites, mass graves or mass disasters. Natural, accidental or manmade mass disasters after which human and non-human commingled remains might be found are earthquakes, floods, transportation accidents, bombings, and hurricanes (Stout, 2009). Furthermore, a skeleton or a single bone might undergo many processes before its discovery and recovery, such as animal gnawing and scavenging, cannibalism (although rare), peri-mortem trauma, post-mortem dismemberment, specific funerary rites, and burial disturbance, during excavation or in antiquity by human, non-human or natural activity (Lyman, 1994; Knüsel and Outram, 2004).

The analysis of the bone remains is carried out by a forensic anthropologist, or bioarchaeologist in case of archaeological contexts, though a forensic anthropologist can be involved in an archaeological case and sometimes a bioarchaeologist can be involved in a forensic case (Ubelaker, 2016). When severe or extreme fragmentation occurs, the forensic anthropologist or the bioarchaeologist determines whether the fragment is bone or other material; if the fragment is securely identified as bone, the next step is to determine its human or non-human origin. In case of human remains, the biological profile of the individual(s), which includes sex, age at death, ancestry, height, pathologies and trauma, is reconstructed, in order to determine his or her identity, cause of death, or mobility (Obenson, 2014; Christensen *et al.*, 2015). In case of non-human remains, the investigation is not further carried out, or a zooarchaeologist is called, particularly in archaeological contexts (Reitz and Wing, 2008).

As mentioned above, when fragmented bones are found in forensic contexts or in archaeological sites, one of the first questions to address is whether or not the remains are human, or in case of commingling following disasters or mass-graves, which bones are human and which ones are non-human (Anstett and Dreyfus, 2015).

Understanding the origin of bone fragments is vital for the ongoing investigation, as in the majority of cases the investigation would be interrupted if the remains turned out to be non-human, saving time and money. Furthermore, in case of commingling, knowing the human or non-human origin of the fragments is important to calculate the minimum number of human (and in some cases non-human) individuals (Klein and Cruz-Uribe, 1984). In several cases, remains are recovered and sent to police departments, but they are identified as non-human or even not bone. According to the FBI,

10-15% of the remains initially identified as human sent to them turned out to be non-human or other materials (Ubelaker and Scammell, 2006).

The differentiation between human and non-human skeletal remains is straightforward when the remains are complete, but it becomes increasingly difficult in case of fragmentation, especially when the diagnostic features, such as long bone epiphyses or facial bones, are no longer visible. This might become more difficult with burnt bones, as the burning process leads to colour, dimensional and morphological changes, dehydration, and mass loss (Adams, 2007; Fairgrieve, 2008; Thompson, 2005). The non-human remains that are commonly misidentified as human are those of animals used for meat consumption or animal exploitation in general, such as chickens, pigs or calves. The fragmented bones of these animals may appear human (for example, chicken bones look similar to human juvenile bones), as they share a number of characteristics with the human bones (see Chapter 2, 5, 6 and 7 of this thesis). Furthermore, their remains are often found in both archaeological and forensic scenes, but in most cases they turn out to be just leftovers from meals (Adams, Crabtree and Santucci, 2008).

When fragments are too small or miss the commonly accepted diagnostic features, the procedures considered as most appropriate for the human/non-human origin distinction are the microscopic methods, such as histology or genetic analysis, which require destructive sampling. However, some of these methods might produce incorrect results (see Chapter 3; Dirkmaat, 2014). The observation of bone morphology is currently not considered a strong method for the human/non-human differentiation of bone fragments, as it is less standardized and more related to the experience of the observer, therefore more prone to bias (France, 2009).

The main aim of the research presented in this thesis is to assess methods of distinction between human and non-human remains that do not require invasive sampling and that can rely on macroscopic procedures only, focusing on bone features that have not been previously considered or have not been fully explored from this point of view. A GIS software was used to identify the pattern of the sagittal suture and measure the curvature of parietals and rib shafts; occipital condyles and linea aspera were morphologically examined; Micro-Computed Tomography was employed to analyse the primary nutrient foramina and the cross-sectional shape of long bones. These bone features can appear very similar between human and non-human species, and therefore lead to a misidentification of fragments; an investigation was needed, in order to highlight the differences among species and use them as a tool to distinguish human from non-human bone fragments.

The results obtained in this study represent a valuable contribution to the field of biological anthropology, and are applicable to forensic anthropology, bioarchaeology, comparative and evolutionary anatomy. Non-destructive methods of origin identification allow the anthropologists to distinguish bone fragmented remains without using destructive, costly and time-consuming procedures.

1.1 Thesis outline

This thesis presents the research carried out on human and non-human bones, where macroscopic methods were applied on certain bone features in order to assess their utility for the human/non-human differentiation of bone fragments. Chapters 2 and 3 introduce the human/non-human bone differentiation topic through the explanation of the main differences between human and non-human skeletons and the techniques currently used to distinguish them in fragmentation scenarios, respectively. In chapter 4, the aims and objectives of this research are specified, and chapter 5 describes in detail the materials and methods used. Chapter 6 contains the results of this study, which are discussed in chapter 7; chapter 8 draws conclusions about the results obtained and discussed in the two previous chapters. Appendices A and B display tables with the values obtained from the cranial and rib curvature calculation.

1.2 Examples of cases where human-nonhuman bone differentiation was required

This section shows some examples of forensic and archaeological scenarios where differentiating between human and non-human skeletal remains was essential. Separating human remains from the non-human ones is vital when mass and natural disasters occur, or when mass graves are found, in order to proceed with the identification of the human remains (subsections 1.2.1, 1.2.2, 1.2.3). There are cases where fragmented skeletal remains are found, and determining their human or non-human origin is important to decide whether further investigations are needed or not (subsection 1.2.4). Finally, in many forensic cases the distinction between human and non-human remains is a necessary step in identifying the victims of crimes (subsection 1.2.5).

1.2.1   Mass disasters: 9/11/2001

The outcome of the terrorist attacks at the World Trade Center in New York that took place on September 11 2001 is an example of commingled human and non-human fragmented remains found on the same site. The other two locations of the attacks, the Pentagon and the crash site of the United 93 flight in Shanksville, Pennsylvania, had teams of anthropologists who had to distinguish between human and non-human remains, separate the commingled ones and identify every small fragment, as the airplanes impact resulted in high fragmentation of both vehicle and occupants (Kontanis and Sledzik, 2008). However, these two scenarios were less challenging than the one present at the WTC in New York, as they represented closed populations (with known number and identity of the victims), and the victims were indeed all identified in three months, particularly through ante-mortem data such as DNA, fingerprints and dental prints (Sledzik *et al*., 2009; Stout, 2009).

The aftermath at the Twin Towers was the most challenging for the anthropologists, as extreme commingling and fragmentation occurred, and non-human remains coming from the restaurants in the buildings mixed with the many human ones and had to be separated (Adams, 2007). Furthermore, in this case there was an open population, not for the passengers of the two flights, the American Flight 11 and the United Flight 175, but for the people who were in the towers (Sledzik *et al*., 2009). Many things made the recovery and subsequent identification of the remains extremely difficult: the impact of the planes with the towers and their subsequent collapse, the fire and then the water to

extinguish the fire, the heavy machines that were used to remove the debris, and the long time the recovery process took made remains fragment and DNA degrade. Burnt bone undergoes physical changes associated with shrinkage, warping, ablation of surface tissues and bone cortex, spalling, increased porosity and fracturing (Beisaw, 2013). The bone transformation can be divided in four phases: dehydration, at a temperature between 100°C and 600°C; decomposition, with colour changes and further weight loss, at 300-800°C; inversion, with increase in crystal size, at 500-1100°C; fusion, with reduction in dimensions and changes in porosity, at a temperature over 700°C (Thompson, 2005). The colour changes are related to the microstructural alterations to the hard matrix of bone, caused by the increasing temperatures. Bones appear black when they have lost the periosteum, and their inorganic components are combusted; grey when crystals alter their shape and size; white when the loss of organic portion and recrystallization are complete (Klepinger, 2006). The last stage is the one where peak dimensional alterations occur and histological examination becomes fruitless; the amount of useful biological data for identification is reduced, and the accuracy of identification techniques is affected, including DNA analysis (Fairgrieve, 2008). In heavily burnt bone fragments, DNA can be highly degraded and contaminated. The identification via DNA analysis is still possible with semi-burnt bones, but becomes increasingly difficult and less reliable with bones burnt at higher temperatures (Schwark, Heinrich, Preusse-Prange, von Wurmb-Schwark, 2011). When the extraction and profiling of DNA is possible, a reliable identification of a specific individual remains unlikely (Von Wurmb-Schwark, Simeoni, Ringleb, Oehmichem, 2004). Even in the case of the WTC, the identification of the victims was not based on DNA testing alone, but on morphological and genetic analyses combined; in many cases, the identification was not possible, but only the minimum number of individuals was determined, given the high degree of alteration of the remains (Budimlija *et al.*, 2003).

The remains, around 20,000, were taken to the Fresh Kills landfill in Staten Island, and here the anthropologists spent months separating human remains from non-human ones, before sending the human remains to the OCME (Office of the Chief Medical Examiner) mortuary. Years later, in 2005 and 2006, the anthropologists had to deal with the same issues, following the discovery of human remains in the area of the World Trade Center. New researches began in hundreds of subterranean structures and on the roofs of the buildings nearby, including the Deutsche Bank Building, where 783 bone fragments were found, the Haul Road and the Liberty Street Parcel, where 600 bone fragments were recovered, and the site of the St Nicholas Greek Orthodox Church, destroyed when the Towers collapsed, where around 270 bones were found (NYT, 2006; Sledzik *et al.,* 2009).

1.2.2 War crimes and mass graves: Bosnia and Herzegovina

Fragmented human remains can be found in mass graves, as a consequence to a conflict or a human rights violation, where hundreds of individuals need to be identified. Some examples of scenarios where anthropologists had to deal with thousands of fragmented and commingled human remains are Bosnia and Herzegovina, Rwanda, East Timor, Cyprus, Chile, Guatemala, and Argentina (Christensen, Passalacqua and Bartelink, 2014).

In Bosnia and Herzegovina, the mass graves were hidden in the natural caves that its mountainous terrain has, where the human remains were mixed with non-human ones in order to conceal the evidence of the crimes (Komar and Buikstra, 2008).

In the early 90s, the Serbs nationalists were seeing Muslims and Croats as an obstacle for the creation of the Greater Serbia, which was supposed to include Montenegro and most of Bosnia and Herzegovina, and thought their populations had to be killed (Malcolm, 2002). The starting point for the killings of Bosnian Muslims and Croats by the Serbs was the declaration of independence of Bosnia and Herzegovina by the European Union and the United States on the 6th of April 1992 (Maass, 1997). Hundreds of thousands of Muslims and Croats were imprisoned and killed, and after three and a half years 250,000 of them died and 30,000 were missing (Glenny, 1997). In July 1995, in only one week 8,000 Muslim men were killed after the fall of Srebrenica (Rohde, 2012). The only way Serbians found to deal with thousands of bodies was to bury them in clandestine mass graves, caves, wells and even rivers, and at times the bodies were left unburied in forests and fields. In many cases, rocks and animal bones from nearby slaughterhouses were thrown into the caves to cover the bodies (Silber and Little, 1997). The exhumations started in October 1995. The majority of the bodies recovered from the caves were skeletonized or badly decomposed, due to the long time that had passed from their death to their recovery, and because water was continuously dripping in the caves where the bodies lied (Klonowski, 2007).

1.2.3 Natural disasters: the 2011 tsunami in Japan

Disasters or mass fatality accidents can range from a house fire to a plane crash, or can be related to a natural cause, as happens in earthquakes, tsunami or hurricanes (Christensen, Passalacqua and Bartelink, 2014).

Two examples of natural disasters that caused extreme fragmentation of the victims remains are the Hurricane Katrina, a deadly tropical cyclone that was responsible for 1,833 fatalities (source: FEMA-Federal Emergency Management Agency), and the earthquake with subsequent tsunami that struck Japan in 2011.

The earthquake of magnitude 9.0 that hit the Northeast of Japan (Tohoku region) on 11th March 2011 caused a powerful tsunami, with waves whose height reached over 39 meters. Over 15,800 casualties were reported (Mimura *et al.,* 2011). The violent collision of the bodies against surfaces caused by the strong waves, and in some cases the wide-scale fires caused by the explosion of propane gas canisters, led to severe fragmentation of human and non-human remains (Takezawa, 2016).

Years later, in 2016, the Japanese police was still searching for the remains of the over 2,500 missing people, and working on the found remains in order to identify them (TheJapanTimes, 2016).

1.2.4 Bone fragments of doubtful origin: the cases in York, Canada, in Colorado, USA, and in Bucharest, Romania

There are cases where bone fragments are found in construction sites, caves, or in suspicious bags in airports. In all these cases, it is important to determine the human or non-human origin of the remains, as the presence of human remains would require further investigations.

An example is the case of Thornhill, a neighbourhood in the Regional Municipality of York in Ontario, Canada, where suspected human remains were found in a construction site. During an archaeological assessment of the area, very close to Thornhill's first official cemetery, established between 1804 and 1830, a number of bone fragments were found; more precisely, rib and teeth fragments, along with a small iron clasp, were found in what appeared to be a small grave (Queen, 2016). At first the remains were considered human, and the main hypothesis was that the remains of

an individual buried in the nearby cemetery could have been disturbed, so the construction works were interrupted. However, as soon as an expert archaeologist looked at the bones, it turned out that those fragments came from a small cow or a horse, given the number of ribs and the size of the teeth. The presence of bovine remains was justified by the fact that the site had been used as a tannery for a short period of time (Javed, 2016).

In another case, skeletal remains found in a cave in Colorado were firstly identified as those of a human infant; money and time were spent because this was being treated as a forensic case. However, when Diane France, a professional anthropologist who dedicated her life to comparative anatomy, saw the fragments, they turned out to be porcupine bones (Evidence Technology Magazine, 2016).

Bear paws have a skeletal structure that appears extremely similar to that of human hands and feet, especially when the distal phalanges are removed (Pickering and Bachman, 2009). Since bear hunting is a common practice in some countries, and bear paws are eaten or used in traditional Chinese medicine (Leung, 2016), is not uncommon to find bear paws in the field or during baggage checks in airports. An example is the case of the Henri Coanda International Airport, Bucharest, Romania, where what seemed a human foot was found in a passenger's luggage. The foot, immediately seized by the police, was subjected to osteological and radiological examination, and identified as a bear paw. The characteristics that allowed to identify the foot as a bear paw were the following: the presence of 11 sesamoids, 1 between the navicular and the medial cuneiform and 10 semilunar ones on the head of each metatarsal; a ridge at the centre of the metatarsal heads that separates the sesamoids; a deep V-shaped groove on the head of the proximal phalanges, and a deep groove at the base of the intermediate phalanges; calcaneal tuberosity, sustentaculum tali and 5th metatarsal styloid process more developed than in humans (Dogăroiu, Dermengiu and Viorel, 2012).

1.2.5 Crime scenes and forensic cases: Jeffrey Dahmer, the disappeared woman, and the missing children

In many forensic cases fragmented remains of unknown origin are found. There are cases where the identification of the remains is the key for the investigation, and others where the perpetrator has already been found and committed, but other findings need to be properly identified.

This is the case of Jeffrey Dahmer, arrested in 1991 in his home in Milwaukee, Wisconsin, after he carried out 17 murders. He used to pick up men to whom he offered money for photographic sessions, but as soon as they were in his house he drugged and strangled them, and mutilated their dead bodies; he also claimed to practice cannibalism. He was charged 957 years of prison, but in 1994 he died for a head injury following an attack by a prison inmate (Pearson, 2015).

His first murder was discovered only when he was arrested in 1991, after the police searched his parent's home in Bath, Ohio. Dahmer had killed Steven Hicks, an 18 year old man, with a strike on the head with a barbell, and then strangled him. Dahmer dismembered the body with a bowie knife, and placed the body parts closed in plastic bags behind the house. He confessed that later he decided to dig up the plastic bags and to crush them with a sledgehammer, after which he scattered the fragments in the same place. When the police interrogated him, Dahmer told them about his first victim and the police started searching for the remains of Hicks in his parent's house. They found hundreds of fragmented human bones mixed with non-human ones, which turned out to be domestic animals such as chickens and cows. The anthropologists called from the Smithsonian Institution in Washington, D.C., had to separate the human bones from the non-human ones. The human fragments were 250, and all of them turned out to be from Hicks (Ferllini, 2003).

The identification of the human or non-human origin of the remains was the key in the case of a woman disappeared with her car in 1986 in Missouri, and whose remains were found and identified only years later. Two years later her disappearance, her car was discovered in a storage facility at 49 km where she was seen for the last time, and 31 small bone fragments were found inside it (Stout, 2009). After a microscopic analysis made to establish if the fragments were bone material, the next step was to understand if the remains were of human or non-human origin. Among others, the cortical thickness, the lack of plexiform bone (commonly present in large fast-growing animals such as cows and pigs), and the typically human osteonal cross-sectional area, allowed to identify the bone fragments as human, and specifically those of an individual between 50 and 65 years of age (calculated on the basis of the osteon population density; Dix, Stout and Mosley, 1991). The

microscopic analysis of the samples showed that the fragments were from the skull, and that the individual consumed antibiotics within three months before dying. The bone sections were examined using fluorescent microscopy, and tetracycline-like banding was observed. The bands of tetracycline (an antibiotic) were all located on bone surfaces, which means that the antibiotic had been administered recently. The human bone remodelling units require approximately three months to be completed, therefore the antibiotic was administered within three months prior to death. The medical records of the woman confirmed this hypothesis. The DNA test confirmed that the remains found in that car were those of the missing woman (Stout and Ross, 1991).

Two similar cases, the April Jones case in the United Kingdom and the José Bretón case in Spain, show the importance of identifying the human or non-human origin of fragmented (and burnt) skeletal remains. In both cases, severely fragmented bone remains were found in a fireplace and among bonfire remains, respectively, and the determination of their human or non-human origin took months (BBC News, 2013; Albert, 2012). In both cases, the determination of the human origin of the fragments was essential for the investigation and for the conviction of the murderers (The Telegraph, 2017; Albert, 2013).

Chapter 2: MAIN DIFFERENCES BETWEEN HUMAN AND NON-HUMAN BONES

This chapter explains the main macroscopic differences between human and non-human bones, and mentions those present on a microscopic level. The section dedicated to macroscopic differences is divided in subsections focused on the single bones that form a vertebrate skeleton.

This chapter, as the research presented in this thesis, focuses on the superclass *Tetrapoda*, namely the four-limbed vertebrates, and more specifically on the clade *Amniota*, which includes birds and mammals. The similarities between human and non-human primate bones were not considered in this research, because they would need to be investigated in a separate research. Humans and apes are part of the same superfamily, *Hominoidea*, therefore their bones are very similar; being apes our closest relatives, the relations between humans and apes are investigated in evolutionary anthropology and primatology (France, 2009). Furthermore, non-human primates are not indigenous to the United Kingdom; they are present only in zoos or rarely as pets (illegally in most cases; Garrod, 2016).

2.1 Macroscopic differences

The mammal skeleton is made up of over 200 bones; the specific number of bones varies among species, but the overall structure of the skeleton, divided in axial and appendicular portions, is the same in all species, including humans (Lyman, 1994). Avian skeletons share with mammals the general number and structure of bones, with some significant differences, due to the adaptation to flight; light bones with a thin cortex, fused in multiple areas such as the vertebral column and the limbs, make avian skeletons different from the mammal ones, as discussed in this chapter (Evans, 2016).

When bones or skeletons are complete, they are clearly identifiable as human or non-human, and in case of non-human species, at least the animal class (bird, mammal, reptile, amphibian, or fish) can be identified straightforwardly. The differences observable in the skeletons of different animal species, including humans, are due to different types of locomotion, biomechanics, growth, development, environment, and nutrition (Jurmain, Kilgore, Trevathan and Ciochon, 2014).

Locomotion and function are the main factors that influence the shape of animal bones. For example, the adaptation to flight makes the bones of flying birds very light and with a thin and smooth cortex, while mammals have much more robust bones with a thick, wood-grain like cortex, as they are involved in activities that include running, digging, or jumping (Dumont, 2010; Fig. 2.1-2.2).

Fig. 2.1-2.2. Pheasant (2.1) and human (2.2) humerus

Non-human mammal bones tend to be denser and thicker relative to size than human ones. In humeri and femora the cortical thickness is about ¼ of the total bone diameter in humans, and ½ in non-humans; however, this is a very generic rule, as in many cases the cortical thickness may be greater in humans than in non-human mammals. For example, the cortical bone at the femoral mid-shaft in

humans was proved to be thicker than in other mammals, such as sheep and kangaroo: the cortical thickness index, or proportion of shaft diameter occupied by the cortex, is 51.5% in humans, 34.6% in kangaroos, and 25% in sheep. This may be due to the higher load on the human femur, as in humans a larger body mass is carried on two legs, instead of four (Croker, Clement and Donlon, 2009).

The trabecular (internal) bone of bird long bones is characterized by large air pockets, and is denser at the articular ends; as for mammals, the trabeculae cover the medullary surface in human long bones, while in non-human mammals the medullary surface tends to be relatively smooth, as the trabeculae are largely absent (Fig. 2.3-2.5). For this reason, the boundary between cortical and trabecular bone is well defined in non-human bones and less visible in human bones (Beisaw, 2013).

Fig. 2.3-2.4-2.5. Internal structure of avian bone, with large air pockets (left, blogs.bu.edu), human bone, with clearly visible trabeculae (Visuals Unlimited, Inc.), and mammal bone, with a smooth internal surface.

The articular surfaces are generally smoother in humans, as the range of movements that characterizes the human skeleton is larger than that seen in most non-human mammals, whose joints tend to be more massive and interlocked, therefore less efficient in motion but much more stable (Komar and Buikstra, 2008).

2.1.1 Skull

Human crania appear generally as more rounded than the non-human ones, although the differences in curvature might become less obvious when fragmentation occurs. The bones of the cranial vault, when fragmented, can be difficult to identify as human or non-human, as human crania share some characteristics, such as curvature, suture patterns, and occipital condyles appearance, with some non-human mammals (as shown in Chapter 5 of this thesis). Human cranial vault bones tend to show a clear sandwich-like structure, with spongy bone enclosed between two inner and outer cortex tables; this structure is not always visible in non-human mammal crania (Watson and Mc Clelland, *n.d.*). Birds' crania are very thin, and in many cases translucent, and cannot be misidentified as human bone even in a fragmentary state (see Chapters 5 and 6 of this thesis).

The facial bones, including the more robust ones such as zygomatic, maxilla, and mandible, show more differences between human and non-human species, therefore they would be less challenging to identify in a fragmentation scenario. Human skulls have an orthognathic (non-projecting) face, with a bulbous vault, while non-human skulls tend to have a prognathic (projecting) large and elongated face, with a smaller vault (Beisaw, 2013). Human orbits are located at the front of the skull and above the nasal aperture; conversely, non-humans have their orbits located laterally and posterior to the nasal aperture. Birds have very large eye orbits showing an ossicular ring, and a brain case that is small relative to the size of the skull (Kaiser, 2007)

Both in human and non-human skulls, the mandible has a much denser bone than the rest of the skull. Generally, the mandible is U-shaped in humans and V-shaped in non-humans (including birds, whose mandible is called dentary). Non-human mandibles are often not fused at the mandibular symphysis, depending on the type of occlusion (the human mandible fuses by 6-12 months of age), and never show a chin, which is only seen in human mandibles (Becker, 1986; Lieberman and Crompton, 2000).

2.1.2 Teeth

Humans have vertically implanted anterior teeth, small canines, and bunodont (with rounded cusps) molars, as a consequence of an omnivorous diet; among the very few non-human species that have bunodont teeth there are pig and bear, raccoon, hedgehog, and the members of the family *Hominidae*,

which includes, besides humans, orangutans, gorillas, and chimpanzees (Fig. 2.6-2.7). An adult human has generally 32 teeth, 8 in each quadrant of the mouth: 2 incisors, 1 canine, 2 premolars and 3 molars; the dental formula, or number of teeth per quadrant, of non-human mammals is highly variable (Christensen, Passalacqua and Bartelink, 2014). Variation in number, size and shape of teeth also occurs within species. In most mammals, sexual dimorphism can be seen in tooth size (usually based on crown diameter), as males tend to have larger teeth than females (Hillson, 2003).

Non-metrical dental variations are an important tool for identification of human individuals. The most common non-metrical traits considered for human teeth are the presence, number, morphology and position of molar cusps, the pattern of fissures in molar occlusal surfaces, and the presence or absence of teeth, in particular the third molar (Hillson, 1996). In humans, there are also ancestry-related differences, more marked in the permanent dentition. For example, shovel-shaped incisors (with a concave lingual surface bound by mesial and distal ridges) are typically found in Asian individuals, particularly those from North-East Asia and the Americas; other characteristics seen in Asian dentition are large incisors, small premolars, large molars, and a parabolic arch (Moreno, 2013). In Black individuals, a midline diastema and an increased tendency for the existence of supernumerary teeth are commonly observed; in Caucasians, the cusp of Carabelli, an additional cusp usually found on the first molar, is a common trait, rarely present in Asian and Black dentitions (Brook *et al.*, 2009).

Fig. 2.6-2.7. Pig (left) and black bear (right) teeth (utep.edu; uwsp.edu)

Generally, carnivore species have small incisors and large and conical canines, and sharp premolars and molars, adapted for raw meat grabbing, ripping and eating. Herbivores have small or missing canines, and broad and tall cheek teeth with deep pits, or *infundibula*, to grind up plants (Hillson, 2003).

Rodents (*Rodentia*) have large incisors and robust mandibles, adapted for gnawing, and do not have canines; premolars (sometimes absent) and molars are flat and have shallow valleys between the peaks (Beisaw, 2013).

Since teeth are among the most valuable source of information (e.g. diet, health, disease, ancestry) in a skeleton, they are commonly investigated in separate researches; for this reason, they were not considered in this thesis. Dental anthropology and forensic odontology are the disciplines that focus on studying teeth (Hillson, 1996).

2.1.3 Hyoid

The hyoid bone, located in the anterior portion of the neck in humans, is present in many non-human species, including mammals, birds and fish (Liebich and König, 2007). Non-human mammals have a hyoid apparatus that appears as more complex than in humans, with more developed horns and a lingual process (Fig. 2.8-2.9). The avian hyoid bone is extremely different from the human one, as it is very thin and is part of the cranium (Fig. 2.10; Kaiser, 2007).

Fig. 2.8. Human hyoid (width: 4.5 cm), antero-lateral view (Taxform.me); a: greater horns, b: lesser horns, c: body. *Fig. 2.9.* Horse hyoid, antero-lateral view (asu.edu); a-b: proximal and distal ends of cornu, c: corniculum, d: body. *Fig. 2.10.* Avian hyoid, superior view (etc.usf.edu). The hyoid bone wraps around the skull; the lingual process (arrow) supports the tongue.

2.1.4 Shoulder girdle

Human scapulae are triangular in shape and elongated supero-inferiorly, with a projecting acromion and coracoid process; in non-human mammals, scapulae tend to be elongated medio-laterally (for quadrupedal locomotion), or quadrangular, as seen in bears, and have much less projecting acromion and coracoid process, because of a limited range of motion (Christensen, Passalacqua and Bartelink, 2014). Most non-human mammals do not have clavicles, because the scapulae need more freedom of motion, particularly in fast-running animals (Kardong, 1995). The clavicle is present in the non-human mammals that have grasping hands, such as primates and squirrels (Beisaw, 2013).

The shoulder girdle of birds has a peculiar structure, which is formed by scapulae, coracoids and furcula. Birds scapulae do not share their appearance with the mammals ones, but appear as thin ribs; the coracoids have a unique shape, as they have a fanlike blade and a hook-shaped proximal articulation (Fig. 2.11). The furcula is formed by the two fused clavicles, and appears as a convex V-shaped bone that projects anteriorly (Kaiser, 2007).
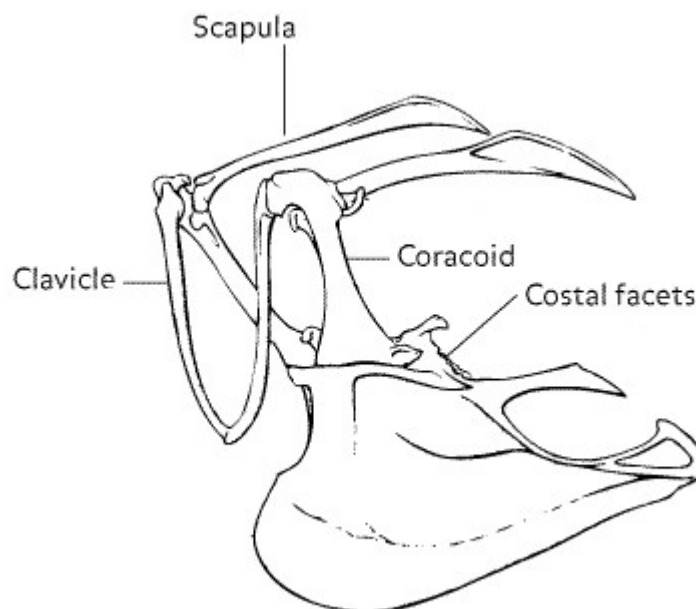
Fig. 2.11. Avian shoulder girdle and sternum (eku.edu)

2.1.5 Sternum and ribs

Human and non-human mammal sterna have the same structure, as they are both formed by the manubrium, the mesosternum made of sternebrae, and the xyphoid process. Non-human mammal sterna tend to be less curved and have more pronounced attachments for ribs (Arbabi, 2009).

As seen in Fig. 2.11, birds' sternum is a very large three-sided bone, with thin walls but robust borders, characterized by a prominent keel, for attachment of pectoral muscles used to fly; in flightless birds, the sternum has the same shape, but does not show the prominent keel (Kaiser, 2007).

Human ribs tend to be more curved than the non-human mammal ones, and show a well-defined costal groove, which is absent in non-humans (Christensen, Passalacqua and Bartelink, 2014). Bird ribs are flat in cross-section, and are divided in dorsal ribs, which articulate with the vertebrae, and ventral ribs, which articulate with the sternum; the dorsal ribs have an uncinated process that attaches caudally to the rib below (Kaiser, 2007).

When the ribs are complete, the shape of the vertebral articular facets can help with the differentiation between human and non-human ribs, as they differ among species; however, when only fragmented shafts are discovered, their origin identification can become much more difficult, as none of the diagnostic features would be visible (Hillson, 2003). The identification can become particularly challenging with those non-human species whose bones share multiple similarities with the human ones, and that are frequently found in archaeological and forensic contexts; fragmented pig ribs, for example, can be misidentified as human bone (see Chapter 5 of this thesis).

2.1.6 Vertebrae

The human vertebral column has an S-like shape when seen from a lateral point of view; this peculiar shape is one of the adaptations of the human skeleton to bipedalism (Williams and Russo, 2015). In a non-human mammal quadruped, the spine is only slightly curved, and does not have multiple curves as occurs in the human spine; this important difference in the curvature of the spine is responsible for the different appearance of human and non-human vertebrae (France, 2011). Human vertebrae are wedge-shaped, and are gradually larger because of the increasing weight they have to sustain; the vertebral bodies are relatively flat and broad, and the spinous processes are short (Mallett, Blythe and

Berry, 2014). Conversely, in non-human mammals the spinous processes tend to be much larger and longer (particularly in the thoracic vertebrae), and the vertebral bodies are more cylindrical, with concave or convex articular surfaces, in some cases with a ventral ridge that runs cranio-caudally (Hillson, 2003). In quadrupeds, vertebrae do not sustain an increasing weight as in humans, therefore the vertebral bodies are similar in height and length, with the exception of the small caudal vertebrae (Aspinal and Cappello, 2015). The differences in the shape of the first cervical vertebra or atlas and the atlanto-occipital joint are discussed in Chapter 7, in relation to the occipital condyles shape.

Birds' vertebral bodies are saddle shaped and strongly locked to each other, as rigidity is needed for flight; for the same reason, in many cases the thoracic vertebrae are fused, forming the *notarium,* which in adult age fuses with the synsacrum (sacrum fused with lumbar and some caudal vertebrae). On the sides of most cervical vertebrae there are the *hypaphophyses*, namely thin rear-facing projections (Adams, Crabtree and Santucci, 2008). The last caudal vertebrae fuse to form the pygostyle, where tail muscles and feathers attach (Kaiser, 2007).

2.1.7 Pelvic girdle

Bipedal locomotion and childbirth made the human pelvic girdle different from the non-human mammals. In humans, the pelvis is wide and broad, to hold the internal organs, while in non-human mammals is long, acting as a lever arm for the antero-posterior movement of the legs (France, 2011). The human pubic bones connect through the pubic symphysis, a fibrocartilaginous joint; in some non-human mammals, the pelvis is fused along the pubic symphysis (Christensen, Passalacqua and Bartelink, 2014; Fig. 2.12-2.13).
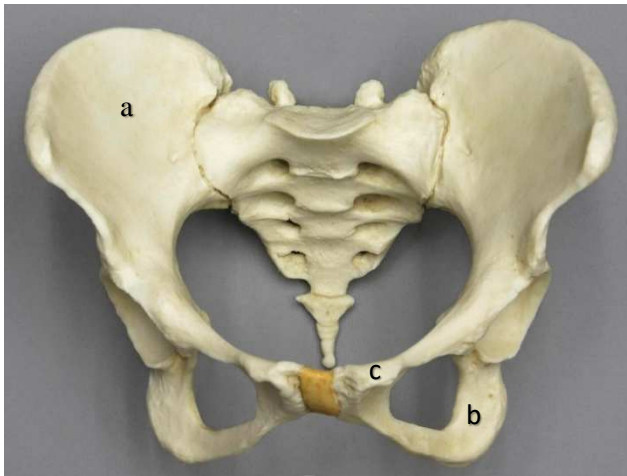
Fig. 2.12-2.13. Human female pelvis (width: 17.8 cm), with sacrum and coccix (left, BoneClones, Inc), and goat pelvis. A: ilium; b: ischium, c: pubis.

In birds, the pelvic girdle is formed by ilium, ischium and pubis fused with the synsacrum. As the rest of the avian skeleton, the pelvis comprises many bones fused together for stability, but is very light, for flight (Fig. 2.14); in lateral view can be seen up to three foramina (depending on the bird species), namely the sciatic foramen, the obturator foramen, and the acetabulum (Beisaw, 2013; Fig. 2.15).

Fig. 2.14-2.15. Pheasant pelvis, frontal view (left) and lateral view (right); a: synsacrum, b: ilium; c: ischium, d: pubis.

Some non-human mammal species, in particular primates, rodents, and carnivores, have an additional bone named baculum, or penis bone, which has a rod-like structure with an inferior groove for the passage of the urethra (Ewer, 1998). The peculiar shape and the absence of the baculum in the human skeleton make this bone impossible to misidentify as human bone, even if fragmented; furthermore, it can considerably change among species, and for this reason it can be used to identify specific non-human species (Ramm, 2007).

2.1.8 Long bones

Human long bones are generally more gracile than the non-human ones, with less marked muscle markings (with some exceptions) and smoother articular surfaces, adapted for bipedal locomotion and joints flexibility (Komar and Buikstra, 2008).

The humeri of many non-human mammals, in particular ungulates (with hooves) such as horse, cattle, pig and deer, have a large greater tubercle (Fig. 2.16); in digging animals like badgers or beavers, the deltoid tuberosity is very pronounced (France, 2011). The proximal epiphysis of avian humerus is different from the mammalian one, as it has a fan-like shape (Fig. 2.1).

Fig. 2.16. Pig humerus, antero-medial view

Radii and ulnae of species with prehensile hands, including humans, have a styloid process at the distal articulation; furthermore, radius and ulna are equal in size and have a rounded and simple proximal articulation, in order to allow flexible pronation and supination of the forearm (Beisaw, 2013). Conversely, most non-human mammals show complex articulations, as radius and ulna need to be rigidly locked to increase stability (France, 2011). In birds, radius and ulna are long and thin; avian ulna is generally characterized by the presence of *quill knobs*, namely bony bumps running along the shaft that are the attachment for the wing feathers (Kaiser, 2007).

Human femora have femoral heads that are more rounded than non-humans, and are larger relative to the size of the femur (Christensen, Passalacqua and Bartelink, 2014). Generally, human and non-human femora, including birds, are similar, especially in the diaphysis or shaft (see Chapters 5 and 6 of this thesis).

The patella is present in humans (where patellar ossification begins at three years of age) and in most bird and non-human mammal species, with the exception of marsupials. In humans, the patellae are circular-triangular sesamoid bones that protect the knee joints and the quadriceps tendon, and allow for a more effective knee flexion (Fox, Wanivenhaus and Rodeo, 2012). In non-human mammals, the patellae are more robust than in humans, and provide an enhanced lever system for the knee joint, which helps the hindlimbs in resisting gravity; their shape varies among species, as it can be triangular, rounded, or oval (Samuels, Regnault and Hutchinson, 2017). In birds, the patellae are the extension of the cnemial crest, a bony protrusion on the frontal, proximal end of the tibiotarsus (König, Korbel, Liebich and Klupiec, 2016).

Bipedal locomotion is responsible for the large and thick proximal surface of human tibia, as this bone, along with the femur, has a weight bearing function (Cartmill and Smith, 2009). In humans, tibia and fibula allow the rotation of the foot, while in non-human mammals (except for pig, dog and cat) these bones are fused together, and only part of the shaft or the remains of the fibular extremities are visible. The avian tibia, called tibiotarsus, is generally characterized by a proximal-lateral small crest lying on the attachment with fibula, and by a shallow canal that runs along the posterior and distal portion of the shaft (France, 2011).

The main long bones - humerus, radius, ulna, femur, tibia - can be straightforwardly identified as human or non-human when the epiphyses are present, as these show clear differences among the species and are therefore diagnostic for the identification. When fragmentation occurs and the epiphyses are not visible, the differentiation between human and non-human long bones can become more challenging. The long bone shafts are commonly found both in archaeological and forensic contexts, as the relatively thick cortex allows them to be better preserved than other bones (Adams and Byrd, 2008). Human and non-human shafts, relatively complete or fragmented, without the epiphyses can be very similar. There are some non-human species in particular, such as pig, sheep, and deer, whose long bones may appear human; the long bones of some birds, such as chicken or duck, may be misidentified as human juvenile bones. In these cases, the species identification is still possible when other features, for example cross-sectional shape, nutrient foramina, muscle markings, or cortex appearance, are considered (see Chapters 5, 6, 7 of this thesis).

Humans have five metacarpals in the hand and five metatarsals in the foot. Both are tubular bones, with squarish proximal bases and rounded distal articular surfaces (White and Folkens, 2005). In non-human mammals, metacarpals and metatarsals are robust; metacarpals are smaller in size, and are generally D-shaped in cross-sections, while metatarsals have a squared cross-section (Beisaw, 2013). The number of metapodials varies in non-human species. For example, pigs have 4 metapodials per limb, cats and dogs have 5 metacarpals and 4 metatarsals, cows have two metapodials per limb (the third and the fourth), and horses have only one metapodial per limb, which is the third digit, called *cannon bone*, flanked by the *splint bones*, namely the remnants of the second and fourth metapodials (Hillson, 2003). In birds, the carpometacarpus is the result of the fusion between the distal row of carpals and metacarpal, and the tarsometatarsus is formed by the distal row of tarsals and 4 metatarsals fused together (Adams, Crabtree and Santucci, 2008).

In humans, hand and foot phalanges are flattened on palmar view and rounded in dorsal view; foot phalanges are smaller and shorter (Christensen, Passalacqua and Bartelink, 2014). Non-human phalanges tend to have one or multiple ridges running posteriorly in proximal-distal direction, and strong articular surfaces that give stability to the paws (Adams, Crabtree and Santucci, 2008). Human and non-human distal phalanges are extremely different (with the exception of primates), as in non-human species they are claws or hooves (Klepinger, 2006).

2.1.9 Carpals and tarsals

Non-human mammal carpals and tarsals have the same basic shape of human carpals and tarsals, and in many cases when found complete they can only be identified as generically mammal or avian, with the exception of calcaneus and talus/astragalus (Beisaw, 2013). In birds, most carpals and tarsals are fused together (Kaiser, 2007).

2.2 Microscopic differences

On a microscopic level, the mammal bone can be woven or immature, and mature or lamellar. Woven bone develops in prenatal life, being generally replaced by mature bone when growth occurs, and is also present in the new bone produced after trauma and in some bone tumours; it appears in form of bundles of collagen fibres arranged in a random pattern (White and Folkens, 2005). Conversely, the lamellar bone is dense and strong bone characterized by an organized structure, with parallel aligned lamellae, and is found both in cortical and trabecular bone (Kardong, 1995).

The trabecular bone receives its nutrients from blood vessels, while the cortical bone is nourished through the Haversian system, made by parallel canals contained within osteons through which blood, lymph and nerve fibres pass; Volkmann's canals run obliquely and link to the Haversian canals. In each lamella there are canaliculi, channels that transport nutrients to the lacunae, small cavities that contain osteocytes or bone cells (Young, Lowe, Stevens and Heath, 2006).

Generally, human bone has circular osteons, and non-human bone exhibits plexiform bone, which has a "brick-wall" appearance, and fibrolamellar bone (Vigorita, 2008). Plexiform bone forms more rapidly than Haversian bone, and is not usually found in humans, although it might be present in the bones of immature individuals; furthermore, non-human bones might have Haversian canals, particularly near muscle attachments in large animals (Mulhern and Ubelaker, 2009; Mulhern and Ubelaker, 2012). Fibrolamellar bone is also found in human foetal and pathological bone (Hillier and Bell, 2007).

Osteon banding, namely the organisation of osteons into distinct layers, is generally not seen in human bone (Mulhern and Ubelaker, 2001). The osteons present in non-human bone are likely to be more rounded than those present in human bone (Crescimanno and Stout, 2012).

2.3 Concluding remarks

In this chapter, the main differences between human and non-human bones were shown, with particular attention to the species considered in this thesis. The differences are mostly related to locomotion, nutrition, and size, and are clearly visible when bones are complete. However, most of the differences between human and non-human bone are much more difficult to detect in case of fragmentation, particularly with cranial bones, ribs and long bones. There are several techniques, both macroscopic and microscopic, that are used to distinguish between human and non-human bone when fragmentation occurs. The most common techniques used for this purpose are discussed in Chapter 3.

Chapter 3: METHODS USED TO DISTINGUISH HUMAN FROM NON-HUMAN FRAGMENTED BONE

In this chapter, the main techniques to differentiate human from non-human fragmented bone are introduced. The macroscopic, microscopic and biomolecular procedures presented are the most common ones and those accepted as valid for the human/non-human differentiation.

3.1 Introduction

When complete or nearly complete bones are found, their human or non-human origin can be identified straightforwardly if the human and the basic non-human bone anatomy are known, or with the use of atlases or reference collections (White and Folkens, 2005). However, when fragmentation occurs, a different approach must be used in order to determine whether the material is human or non-human. The choice of the approach to be used depends on the condition of the bone fragment and the circumstances under which it is found.

Before the identification of the human or non-human origin of a fragment, in many cases the first step is to establish if the fragment is actual bone, as there are some materials with a similar appearance, such as rocks, wood, drywall or plastic, especially if exposed to heat or taphonomic alteration (Gilchrist, Vooght and Soames, 2011). In many cases, a high-quality dissecting microscope is sufficient to detect the structure of the fragment, and to determine whether it is bone or not, but if the alteration is very high many diagnostic features may be lacking and the type of material may not be detected; furthermore, the preparation procedure is destructive and may preclude molecular analysis (Adams and Byrd, 2008). Scanning Electron Microscopy with Energy Dispersive Spectroscopy (SEM/EDS), a technique that combines microscopy with chemical microanalysis, is very useful for the differentiation between bone and other types of material, as it produces highly magnified images and compositional spectra that help identifying the fragment (Ubelaker, Ward, Braz and Stewart, 2002).

To identify the human or non-human origin of a bone fragment, knowing the environment and the economy of the region of interest, namely which non-human species are present and which ones are

used for meat consumption, clothes production, or as pets, might be an advantage (France, 2011). Information about the context where the fragments are found should not influence the human/non-human differentiation itself, as the latter should be unbiased. However, since there are some non-human species whose fragmented bones can be very difficult to distinguish from the human ones, it might be helpful to know if those specific species can be present in the area (see Chapters 6 and 7 of this thesis). Although there are cases where nonlocal species are found in an archaeological or forensic site, because of long-distance trade networks, it is always recommended to check the local non-human species before considering the exotic ones (Beisaw, 2013). The presence of butchery marks on a bone may help assessing a non-human origin, but this is not always the case, as there are cases of human body dismemberment, carried out to hinder the identity of the victim or to facilitate the transportation of the remains (Adams, Crabtree and Santucci, 2008).

3.2 Macroscopic methods

Morphological observation is the first procedure to be used for the identification of a human or non-human fragment; the overall morphology of skeletal features, their presence or absence, and their degree of expression are among the criteria used (France, 2009).

Morphological differences dictated by evolution, size, nutrition and locomotion can still be visible in bone fragments, depending on the degree of fragmentation. As seen in Chapter 2, teeth, facial bones, scapulae, vertebrae, and pelvis are among the most diagnostic bones for the human/non-human differentiation, while some cranial bones, ribs, and long bones (excluding metacarpals, metatarsals and phalanges) are the ones where human and non-human species show many similarities.

The use of bone reference collections can be very helpful in the morphological observation of fragments; if a reference collection cannot be accessed, photographic atlases with human and non-human bones can be used (Adams, Crabtree and Santucci, 2008; Elbroch, 2006; France, 2009 & 2011; Hillson, 2003).

A macroscopic approach has advantages and limitations. It is considered less standardized and more prone to bias than microscopic and biomolecular methods, and more subjective, since it relies on the experience and training of who examines the bones. Furthermore, the presence of specific pathological conditions (such as tuberculosis, scoliosis, ankylosing spondylitis), trauma or

taphonomic alterations can lead to an incorrect identification of human remains as non-human, or viceversa (Haglund and Sorg, 1997; see Chapter 7 of this thesis).

However, macroscopic analysis is a non-destructive, cost and time-effective method, can be highly reliable and a valid alternative to microscopic and biomolecular analysis (Christensen, Passalacqua and Bartelink, 2014).

The use of X-ray imaging is a non-destructive but more standardized method to distinguish between human and non-human bone fragments. For this purpose, radiography was used to measure the cortical thickness of long bones (Croker, Clement and Donlon, 2009). Through radiography, the sharp transition between cortical and trabecular bone in non-human species can be seen, as well as the cortical spicules that extend from the cortical bone to the medullary canal (Brogdon, 1998). Chilvarquer *et al.* (1987) looked at the trabeculae pattern in human and non-human long bones, and concluded that in human long bones the trabecular bone follows a circular oblong pattern, showing homogeneous but sparse distribution, while in non-human long bones the trabecula is more homogeneous and dense. Heat treatment and diagenesis can cause drastic changes to the trabecula, both in human and non-human bones. In burnt bones, the trabecular bone can change in shape (from plate-like to rod-like or vice versa), in thickness and spacing. The trabecular thickness and spacing tend to decrease because of the bone dehydration and shrinkage, respectively. The banding pattern of collagen fibrils degrades, which means that it can no longer function as an energy absorbing medium (Fantner *et al.*, 2004). Since trabecular parameters such as transverse organization, macroporosity and apical activity are related to age at death, the changes caused by heating can lead to misinterpretations (Boschin, Zanolli, Bernardini, Princivalle and Tuniz, 2015). Bone diagenesis in soil is another cause for collagen loss, which creates pathways that facilitate microbial invasion. Factors such as humidity, pH and temperature have an influence on the extent of the changes: for example, a neutral pH promotes microbial activity, while extreme pH or high temperatures accelerate the physico-chemical deterioration of the bone (Barrios Mello *et al.*, 2017).

Computed tomography and micro-computed tomography proved to be valuable methods for the human/non-human bone identification, although in this field further research is needed (Franklin and Marks, 2013). The research using CT or micro-CT for human/nonhuman bone differentiation has mainly focused on evolution and primates (Copes *et al.*, 2016). Rerolle *et al.* (2013) used CT to determine if the corticomedullary index (CMI), defined by the ratio of the diameter of the medullary cavity to the total diameter of bone, could be used to distinguish between human and non-human long bones. Measurement were taken on CT-scans of human, pig, dog, and sheep femora, tibiae and fibulae. However, the origin identification based on the CMI resulted effective for only 22.6% of the

samples used; it was concluded that the calculation of the CMI is not an effective method for determining the human or non-human origin of bone remains. In his review of the bone alterations caused by the burning process (in particular coloration, weight reduction, shrinkage, deformation, fragmentation and DNA degradation), Imaizumi (2015) explored the application of micro-CT to burnt bone identification. The images produced allowed to see the detailed structure of both cortical and spongy bone (the latter by using virtual slicing), and to look at the histological structures with intensely focused virtual slicing. The use of micro-CT led to the identification of the bones analysed, and to a positive distinction between human and non-human bone, as the histological differences between the species could be clearly seen (Fig. 3.1-3.2).
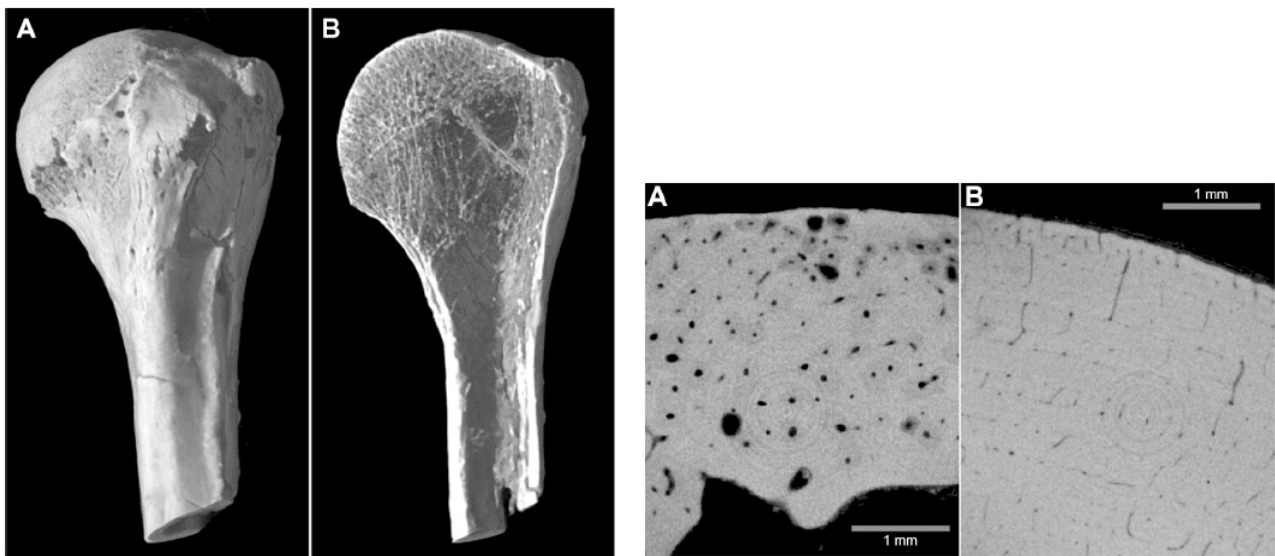
Fig. 3.1-3.2. Left: 3D images of cremated human humerus, proximal epiphysis, before and after virtual slicing. Right: compact bone structure of human tibia and bovine metacarpal (Imaizumi, 2015)

3.3. Microscopic and biomolecular methods

The observation of morphological differences for the differentiation between human and non-human bone is a time-saving, non-destructive procedure, but there are cases where no diagnostic feature is visible, or where the human and non-human bones share many similarities and the differences cannot be detected macroscopically. In these cases, the use of microscopic and biomolecular methods is recommended, although they are generally more expensive and time consuming (Apps, Vesely, Alys and Blythe, 2014).

In this section, histological, immunological and biomolecular procedures are presented, as they are the most widely accepted microscopic and biomolecular methods used for the human/non-human bone differentiation (Franklin and Mars, 2013); other methods that have been explored but still need further investigation are briefly mentioned in the last subsection.

3.3.1 Histological analysis

As briefly seen in Chapter 2, growth rate, size, weight, and hormones activity of human and non-human species determine the appearance and organization of their bone cells; the structural and organizational differences at the histological level provide the basis for the differentiation between human and non-human bone (Gosman, 2012).

Histology is the study of tissues and cells microstructure, as seen through a microscope. In bio-anthropology, it is used to determine the material in case of fragments, to assess age, to diagnose diseases, and to distinguish between human and non-human bone tissue (Christensen, Passalacqua and Bartelink, 2014). For histological analyses, thin bone sections 50-100 μm (micrometres) thick are used, which are embedded in stabilizing resin when too small or weathered; the thin slides obtained, that transmit light and have no overlapping structures, are mounted on a glass microscope slide and analysed through light microscopy, with tissue staining or polarized light (Mulhern and Ubelaker, 2012). The histological assessment of age is based on the observation of the age-related changes in the cortical bone microstructure that are due to the bone remodelling process. The most common criteria for histological age estimation are: osteon (intact and fragmentary) population density, number of primary vascular canals, amount of un-remodelled lamellar bone, amount of

remodelled bone, average size of secondary osteons, and average size of Haversian canals (Streeter, 2012). Long bones are commonly used for histological age estimation; when these are not available, ribs and clavicles are used. The use of ribs and clavicles is preferred, as these bones are less subject to non-age related remodelling (which affects weight bearing bones such as femur or tibia), and have a relatively small area that allows to sample the entire cross-sectional cortex and reduce sampling errors related to spatial variability (Mnich, Skrzat and Szostek, 2017). In fact, bone remodelling can vary depending on the bone, the specific area of the bone, and other factors such as age, sex, physical activity, ancestry, nutritional status and health status (Streeter, 2012). Since bone remodelling is less visible in juvenile bones, growth and modelling phases, which are more evident, are preferred for age estimation of juvenile individuals (Maggiano, 2012).

Histopathology is the study of microscopic changes in tissues, both soft and hard, caused by disease, trauma, or drug abuse. In forensics, histopathology is an important tool for the assessment of mechanism and cause of death; firearms and explosives injuries, stab wounds, asphyxiation, starvation, hypothermia, embolism, substance inhalation, and infections are among the causes of death that can be identified by the histopathological analysis of tissues (Dettmeyer, 2018).

As a general rule, human and non-human primates bone exhibits a Haversian system, while non-human, non-primate bone has plexiform or fibrolamellar bone (Vigorita, 2008). However, there are some exceptions. In humans, plexiform bone can be found in foetal bones and in bones where there is osteonal formation in response to injury or inflammation (periostitis). In large mammals the bone surfaces near muscle attachment sites can show Haversian bone; Haversian and plexiform bone can often coexist within the cortical bone of long bones and ribs, where plexiform bone appears near the periosteal surface and Haversian bone appears near the endosteal surface (Hillier and Bell, 2007). In fact, the compact bone internal structure can differ between individuals of the same species, between different bones of the same individual, and in different areas of the same bone, because of sex and age differences or type of mechanical stress (Mulhern, 2016). Furthermore, both in human and non-human bone, pathological conditions can affect the histological appearance of cortical bone. For example, in humans hyperparathyroidism causes an increase of bone remodelling, resulting in an increased number of Haversian systems; diabetes mellitus causes the opposite process, a decrease in the number of Haversian systems, because of a depression in remodelling rates (Stout, 1998). With Paget's disease, there is an increase in bone resorption, and the new bone formation is more rapid and disorganized. Other pathological conditions that cause histological changes to human bones are osteoporosis, osteomalacia, osteogenesis imperfecta, acromegaly, and paralysis (Hillier and Bell, 2007). The microscopic appearance of bone tissue can also change in non-human bones, because of

metabolic disorders, infections, hormonal disturbances, developmental anomalies, and trauma (Zachary, 2017).

To avoid misidentification of a bone fragment, the presence of osteon banding, generally considered as not present in human bone but common in non-human mammalian bone, was used to safely identify a bone fragment as human. The presence of distinct rows of five or more osteons was considered a strong indicator of non-human bone (Gilchrist, Vooght and Soames, 2011). However, a very recent research carried out on adult male bones by Andronowski, Pratt and Cooper (2017), who used SR micro-CT (Synchroton radiation-based micro-CT scanning), with high resolution 3D visualization of bone microarchitecture, proved that osteon banding can be present in human bone and therefore is not diagnostic of non-human bone. Multiple osteon bands were seen in temporal, parietal, and occipital bones; this is due to the minimal direct mechanical loading on the cranial bones of a human adult (particularly in comparison to long bones), where lamellar opposition is continued and remodelling is slowed. Linear arrangements of primary osteons into bands are also present in the bones of human juveniles (from infancy to adolescence), because the remodelling process is not as continuous as in adult bones (Cuijpers, 2009).

Quantitative microscopy, a method where quantitative measurements are taken on image data, has been used to calculate, among others, cortical bone thickness (Croker, Clement and Donlon, 2009), osteon area and circularity (Dominguez and Crowder, 2012), and Haversian system and canal diameter (Dettmeyer, 2011). The mean human osteon circularity is generally lower than the non-human one. However, osteon circularity can be different among the bones of the same individuals (both human and non-human), particularly between long bones and ribs, because of biomechanical differences (Crescimanno and Stout, 2012). The calculation of the Haversian system and canal diameter is considered the most successful among the quantitative microscopic techniques, because the diameters are very different between human and non-human species, in particular rat, hare badger, raccoon, dog, cat and deer (Benedix, 2004).

3.3.2 Immunological analysis

Immunological analysis can determine the human or non-human origin of a bone fragment and the specific species in case of non-human bone, by measuring the interspecies interactions of antigens and antibodies (Christensen, Passalacqua and Bartelink, 2014). A successful study was carried out by Ubelaker, Lowenstein and Hood (2004), who used a protein radioimmunoassay (pRIA) to determine the origin of bone fragments. Protein is extracted from the sample and combined with rabbit antisera (blood serums containing antibodies against specific antigens), which have been exposed to sera of selected species. The antibodies of the selected species are combined with the protein extracted and the rabbit antisera to observe the antibody-antigen reactions. Radioactive antibodies are then combined with the sample to detect the strongest, species-specific, antibody-antigen reaction. This method allows to safely identify human and non-human bone fragments, and requires a sample of only 200mg or less (Mulhern, 2016). The limitations of this method are the limited number of species available for comparison, and the possible misidentification due to diagenetic alteration of proteins in archaeological and poorly preserved bone remains (Potter, Reuther, Lowenstein and Scheuenstuhl, 2010).

Another immunological technique tested for the distinction between human and non-human bone is ELISA (enzyme-linked immunosorbent assay), a plate-based assay technique used to detect and measure substances such as peptides, proteins, antibodies, and hormones (Porwit, Mc Cullough and Erber, 2011). ELISA is commonly used to diagnose, among others, HIV, Lyme disease, syphilis, chicken pox, Zika virus, and coeliac disease; it is also used to detect food allergens (Gates, 2003). The method uses various antigen-antibody combinations, with an enzyme-labeled antigen or antibody. The enzyme activity is detected and measured by adding a substrate that changes colour when modified by the enzyme; the light absorption of the product formed after the substrate is added is measured and converted to numeric values (Wild, 2013). Proteins such as albumin have been identified in 3000 years old human bones, including cremated ones. Albumin's prolonged preservation is probably due to its encapsulation into the bone hydroxyapatite crystals (Cattaneo, Gelsthorpe and Sokol, 1994). Since albumin is extremely species-specific, it can be used for the identification of the human or non-human origin of fragmented remains, both forensic and archaeological. Cattaneo *et al.* (1999) performed ELISA on samples of human and non-human, burnt and unburnt, cortical bone, using albumin as target protein. Albumin was detected in all the unburnt bones, but only in five out of eleven human individuals exposed to high temperatures (800 to 1200°C).

3.3.3 Genetic Analysis

Mitochondrial DNA (mtDNA) is used for degraded and fragmented bone analysis, because it contains a higher copy number within cells than the nuclear DNA; furthermore, it is unique between species and can be used to safely distinguish human from non-human bone (Pereira, Carneiro and van Asch, 2010). The primary skeletal sources of mitochondrial DNA are bone marrow and dentin (Lee, 2007). Genetic species identification is used not only to differentiate human remains from non-human ones, but also to investigate the illegal hunting and trade of animals, and the presence of animal tissues in human murder cases (Savolainen and Lundeberg, 1999).

The species determination is possible because of the fragmentation of DNA sequences at unique genetic points: each genetic sample yields a different number of fragment lengths that correspond to the different locations of the genes between species (Dawnay *et al.,* 2007). Most studies involving genetic analysis for human/non-human bone identification focused on using different primers (initial short strand of DNA used as basis for replication) associated with genes at different locations between species (Nicklas and Buel, 2006). The origin determination is based on the comparison of the sample to be identified to a control sample from a known species (Hiroshige *et al.,* 2009).

The most commonly used mitochondrial loci for species differentiation are cytochrome *b* (cyt *b*, one of the 11 proteins in complex III, part of the mitochondrial respiratory chain), and the displacement loop (D-loop, or control region); the 12S and 16S ribosomal RNA (rRNA) genes are also used for species identification (Shewale *et al.,* 2007; Tobe and Linacre, 2008).

The hypervariable regions 1 and 2 (HV1 and HV2) in mtDNA have been successfully amplified and used for the identification of human skeletal remains from the Vietnam war and the differentiation between human and swine fragmented bones (Imaizumi, Saitoh, Sekiguchi and Yoshino, 2002).

Cytochrome *c* oxidase I, a protein key in aerobic metabolism, has also been identified as potential marker for species differentiation; this protein is species-diagnostic, but misidentification can occur because few data from reference species exist (especially in comparison with cyt *b*), and a low percentage match can be obtained (Dawnay *et al.,* 2007).

Bellis *et al*. (2003) found that the TP53 gene, which is located on the short arm of chromosome 17 and encodes a tumour suppressor protein, can be used as a potential animal species identification tool.

Other studies focused on genes that are unique to humans, such as the genes related to language development. An example is FOXP2, a gene linked to the development of speech and language; it is present in similar forms in many non-human species (particularly in birds), and its mutation causes a speech disorder in humans (Lai *et al.,* 2001). Hiroshige *et al.* (2009) used this gene to distinguish human remains from those of non-human primates. Another gene that can be potentially used for the human/non-human differentiation is KIAA0319, a protein coding gene involved in neuronal migration during development of the cerebral neocortex; in humans, variations of this gene are associated with learning difficulties such as dyslexia (Dennis *et al.,* 2009).

Despite DNA analysis has become easier to perform and its costs have been reduced, there are still some limitations, including limited species-related sample data, potential non-sterile environments and DNA degradation (Apps, Vesely, Alys and Blythe, 2014). DNA and ancient DNA (aDNA) sequences can be difficult to analyse because of molecular damage and exogenous contamination. There are several guidelines to follow in order to obtain reliable results, such as the use of dedicated laboratories, biochemical preservation tests, multiple negative controls during extraction and amplification, screening for human DNA in non-human remains (or vice versa), and reproducibility of results (Malmström *et al.,* 2005). However, the results might not be correct even if all the guidelines are followed. This happens because the same haplotypes, combinations of markers or alleles, can be present in both the remains analysed and modern contaminants, and therefore the sequence obtained may not be authentic; the contaminations can be already present in the samples, or can be derived from pre-laboratory handling of the remains. The type of pre-treatment of the samples may also have an influence on the level of contamination. The most common treatment methods involve the use of brushes, UV light, hydrochloric acid, bleach, and silicone rubber; none of these methods can guarantee a complete elimination of contamination (Gilbert *et al.,* 2003).

As seen in Subsection 1.2.1, DNA cannot be amplified from bones burnt at high temperatures. When the skeletal remains are compromised, because of cremation or taphonomic changes, quantitative microscopy is considered more reliable than genetic analysis (Cattaneo *et al.*, 2009).

3.3.4 Zooarchaeology by Mass Spectrometry (ZooMS)

ZooMS, short for ZooArchaeology by Mass Spectrometry, is a relatively new biomolecular method of species differentiation and identification based on the use of mass spectrometry to fingerprint collagen (Buckley *et al.,* 2014). Mass spectrometry is a widely used technique in chemistry, biochemistry, pharmacy and medicine; it is used to identify a compound from the molecular or atomic mass(es) of its constituents. A mass spectrometer produces charged particles or ions from the chemical substances analysed, and then uses magnetic and electric fields to measure the mass of the charged particles (Gross, 2017). In ZooMS, bones are identified by differences in the mass of the peptides (Buckley *et al.,* 2010). The triple helical structure of collagen possesses enough amino acid sequence variation to be able to discriminate not only between human and non-human material, but also between closely related species, such as sheep and goat (Buckley, 2017).

Collagen (Type I collagen) is among the most abundant proteins in vertebrates, and it can survive for thousands (in some cases millions of years) in fragmentary bones; its long term survival is linked to the entrapment of its fibrils into the bone apatite (Nielsen-Marsh *et al.*, 2002). In fact, collagen persists in mineralised tissues, such as antler, teeth and bone; the more rapid loss of other proteins like haemoglobin and osteocalcin leads to a selective enrichment of collagen into the bone, which increases the ease of obtaining a collagen fingerprint (Covington *et al.,* 2008). It was proved that collagen resists also at high temperatures (Buckley, Collins, Thomas-Oates and Wilson, 2009). Species differentiation based on collagen analysis is more efficient than genetic analysis, because collagen degrades at a slower rate than DNA, it is much more stable, and it can be sampled directly from bone, which allows to avoid the risk of contamination during the amplification process usually carried out for DNA analysis. Furthermore, ZooMS is a quicker and much less expensive technique (Buckley *et al.,* 2014).

Despite its efficiency, ZooMS presents some limitations, related to the collagen's content preservation itself, which can be affected by several factors, such as pH and hydrology, and to the lack of an extensive reference database (Lebrasseur, Ryan and Abbona, 2018).

3.3.5 Other methods

Several alternative methods of human/non-human bone identification have been investigated, with variable success. Calcium/Phosphorus ratio in hydroxyapatite (the mineral content of bones) was investigated as a method of differentiation, but it was not effective, as the values obtained were similar between human and non-human species, especially in those cases where diet and environment were the same (Zimmerman, Meizel-Lambert, Schultz and Sigman, 2015). Raman spectroscopy and laser-induced breakdown spectroscopy (LIBS), both based on the detection of sample elemental composition, have successfully provided species-specific information with a minimally destructive procedure, but currently are not routinely used for the human/non-human bone differentiation (Vass, Madhavi, Synstelien and Collins, 2005; McLaughlin and Lednev, 2012). Scanning Electron Microscopy (SEM), which provides high-resolution images by using a focused electron beam, and Energy Dispersive X-ray Spectroscopy (EDX), a chemical microanalysis technique, were used by Ubelaker, Ward, Braz and Stewart (2002), resulting in a highly correct classification. Other two techniques that are not standardized yet but have obtained valid results are X-Ray fluorescence (XRF) and handheld XRF, both based on the determination of the elemental composition of materials (Christensen, Smith and Thomas, 2012; Zimmermann, Shultz and Sigman, 2014).

3.4 Concluding remarks

In this chapter, the main macroscopic and microscopic techniques used for the differentiation between human and non-human fragmented bones were described. There are benefits and limitations in each technique. Histological, immunological and biomolecular analyses are effective techniques, and their cost is no longer prohibitive; however, they involve sample alteration or destruction (which can lead to ethical issues), and in some cases may produce incorrect results (Mays *et al.*, 2013). Further research using non-standardized methods is needed. The use of non-destructive techniques, especially those involving the use of X-ray imaging, need to be further investigated. Furthermore, new macroscopic techniques, and bone features that have not been considered yet as a parameter for the human/non-human distinction, should be investigated. This latter was the aim of the research presented in this thesis, where the potential of non-destructive techniques, such as GIS and micro-CT, and of bone features never or rarely used in the past for the human/non-human origin identification was explored. It is important to investigate thoroughly the potential of non-destructive methods, in order to prevent bone damage and reduce analysis time.

Chapter 4: AIMS AND OBJECTIVES

The overall aim of the research presented in this thesis was to investigate new or rarely used features for the differentiation between human and non-human fragmented bones, using non-destructive methods. This was achieved through a thorough examination of human and non-human skeletons and the experimental use of non-destructive procedures, as some of the features and the methods used in this research have not yet found widespread application in the human-nonhuman bone differentiation.

The individual thesis objectives were as follows:

- Investigate cranial curvature, cranial sutures, rib curvature, occipital condyles, linea aspera, nutrient foramina and cross-sectional shape as features on which to base the identification of the human or non-human origin of bone fragments;
- Investigate the scientific validity of GIS (Geographic Information System) software, morphological examination and Micro-Computed Tomography in the human-nonhuman bone fragments differentiation;
- Identify the non-human species living in the United Kingdom whose bones have the most human-like characteristics, in order to take into account the presence of their remains in case of uncertain origin identification of bone fragments;
- Evaluate whether fragmented bones can be differentiated using non-destructive methods. This is currently debated and not widely accepted, as destructive procedures are considered more reliable;
- Expedite the process of human-nonhuman origin identification of bone fragments.

Fig. 4.1 provides a summary of the parameters and the methods employed in this research in order to meet the aims and objectives. The materials and the methods used are described in detail in Chapter 5. The findings of this research are reported in Chapters 6-7 and Appendixes A and B.
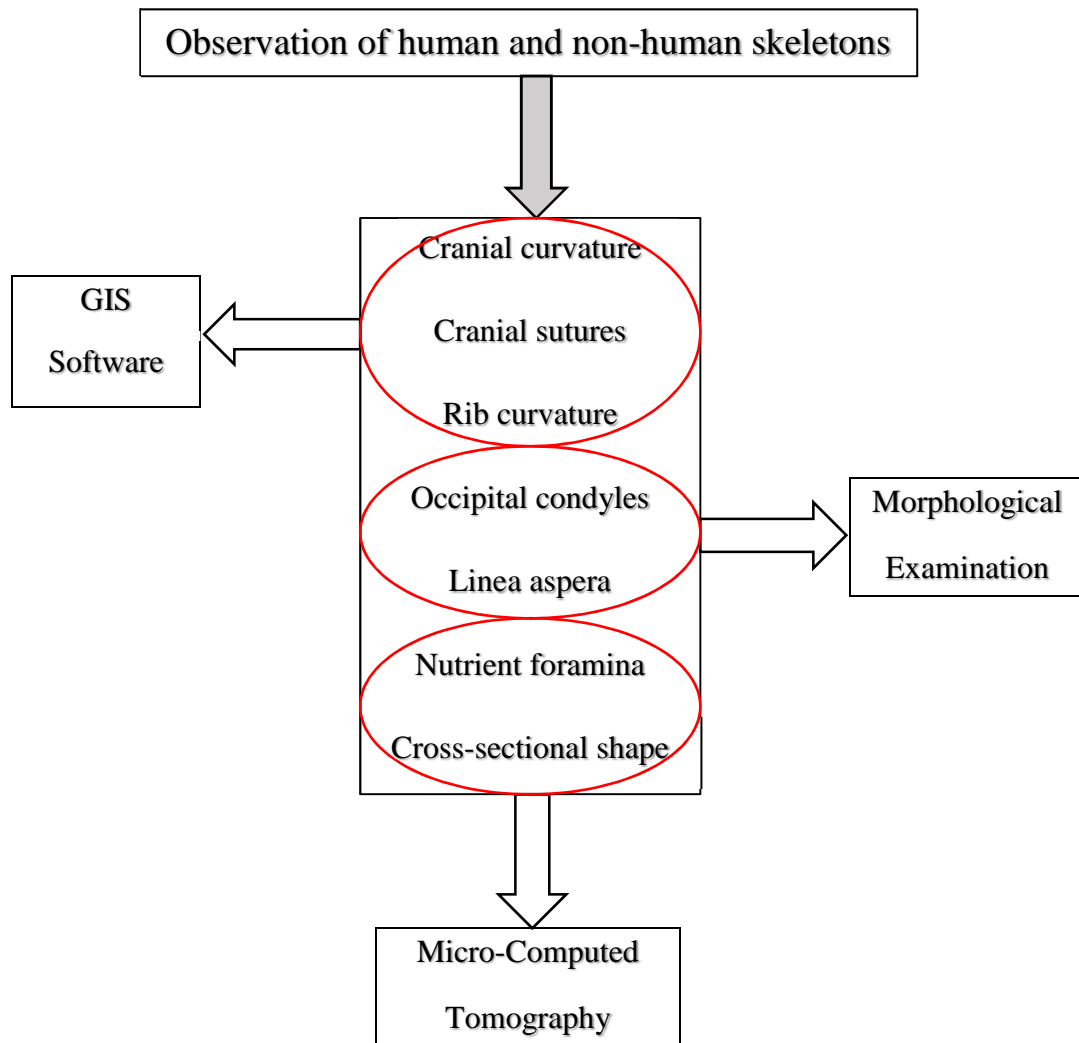
Fig. 4.1. Summary of features and procedures used in this thesis. After a preliminary assessment of human and non-human skeletons, cranial curvature, cranial sutures and rib curvature were analysed with a GIS software; occipital condyles and linea aspera were morphologically examined; nutrient foramina and cross-sectional shape of long bones were observed using micro-CT.

Chapter 5: MATERIALS AND METHODS

This chapter outlines the materials and the methods used. Section 5.2 (Materials) shows number and type of bones used for each part of the research, namely calculation of cranial curvature and suture pattern, calculation of rib curvature, analysis of occipital condyles, linea aspera, and nutrient foramina, and identification of limb bones cross-sectional shape. The analytical techniques, namely GIS software, morphological examination and micro-CT scanning, are outlined in section 5.3. The concluding remarks section (5.4) includes a diagram that summarizes the methods used and the materials on which they were applied.

5.1 Introduction

A preliminary analysis was carried out on human and non-human skeletons, in order to identify the non-human species present in the United Kingdom whose bones can be misidentified as human in a fragmentation scenario, and which specific bones and features should have been further investigated. The skeletal features observed for this research were chosen because their appearance can be similar in human and non-human bones; in a hypothetical fragmentation scenario where fragments showing these features (e.g. sutures, linea aspera, nutrient foramina) were found, their identification as human or non-human bone might be difficult. The skeletal areas and features investigated in this research have been rarely or never used in forensic anthropology for the purpose of differentiating human from non-human bone.

The non-human skeletons visualized were part of the reference collection of Oxford Archaeology (South OA, Oxford) and the displayed collection of the Grant Museum of Zoology, London; the human skeletons were part of the reference collection of the Cranfield Forensic Institute. The collection of human disarticulated skeletal material was donated to Cranfield University from the Medical Sciences Teaching Centre at the University of Oxford. The exact provenance of these human remains is unknown. The collection may have previously belonged to the Department of Physiology, Anatomy and Genetics (DPAG), which received the remains as donations by colleges from within the University of Oxford (Boston and Webb, 2012). The skeletons, probably of British and Indian individuals, were used as teaching material in the 19th century (Boulter, 2016).

More than 1000 bones were photographed and visually analysed; the specific species and the number of skeletons observed are shown in Table 5.1.

Species	Materials	Source
Common Pheasant (*Phasianus colchicus*)	1 adult (male) 1 adult (female) 1 juvenile	Oxford Archaeology
Wood Pigeon (*Columba Palumbus*) Feral Pigeon (*Columba Livia*)	1 adult 1 juvenile 1 adult 1 adult mounted skeleton	Oxford Archaeology Grant Museum of Zoology
Mute Swan (*Cygnus Olor*)	1 adult 1 adult mounted skeleton	Oxford Archaeology Grant Museum of Zoology
Chicken (*Gallus gallus*)	1 adult 1 juvenile 1 adult mounted skeleton	Oxford Archaeology Grant Museum of Zoology
Turkey (*Meleagris gallopavo*)	2 adults	Oxford Archaeology
Duck (*Anas platyrhynchos*)	2 adults	Oxford Archaeology
Goose (Anser anser)	2 adults	Oxford Archaeology
Cat (*Felis domesticus*)	2 adults 1 juvenile 1 foetal	Oxford Archaeology
Rabbit (*Oryctolagus cuniculus*) Hare (*Lepus europaeus*)	2 adults 1 juvenile 1 adult mounted skeleton 1 adult 1 juvenile	Oxford Archaeology Grant Museum of Zoology Oxford Archaeology
Brown Rat (*Rattus norvegicus*)	1 adult	Oxford Archaeology
Grey Squirrel (*Sciurus Carolinensis*)	2 adults	Oxford Archaeology
Badger (*Meles meles*)	1 adult 1 juvenile 1 adult mounted skeleton	Oxford Archaeology Grant Museum of Zoology

Fox (*Vulpes vulpes*)	1 adult 1 juvenile	Oxford Archaeology
Dog (*Canis lupus familiaris*)	3 adults 2 juveniles 1 neonatal 7 infant skulls 2 adult mounted skeletons 1 adult skull	Oxford Archaeology Grant Museum of Zoology
Cow (*Bos taurus*)	2 adults 2 juveniles	Oxford Archaeology
Horse (*Equus caballus*)	1 adult 1 foetal 1 young skull	Oxford Archaeology Grant Museum of Zoology
Sheep (*Ovis aries*) Goat (*Capra aegagrus hircus*)	2 adults (1 male, 1 female) 2 juveniles 1 juvenile skull 2 adults 1 juvenile 1 adult skull 1 juvenile skull	Oxford Archaeology Grant Museum of Zoology Oxford Archaeology Grant Museum of Zoology
Pig (*Sus scrofa domesticus*)	1 adult 1 foetal 1 juvenile mounted skeleton 1 adult skull	Oxford Archaeology Grant Museum of Zoology
Fallow Deer (*Dama dama*) Roe Deer (*Capreolus capreolus*) Red Deer (*Cervus elaphus*)	2 adults (1 male, 1 female) 1 juvenile 2 adults (1 male, 1 female) 1 adult	Oxford Archaeology
Brown Bear (*Ursus arctos*)	1 juvenile	Grant Museum of Zoology
Grey seal (*Halichoerus grypus*) Common seal (*Phoca vitulina*)	2 adult skulls 1 juvenile skull	Grant Museum of Zoology

South American Fur Seal (*Arctocephalus australis*)	1 adult skull	Grant Museum of Zoology
Leopard Seal (*Hydrurga leptonyx*)	1 adult skull	
Green Turtle (*Chelonia Mydas*)	1 adult skull 1 adult mounted skeleton	Grant Museum of Zoology
Hermanns's Tortoise (*Testudo Hermanni*)	1 adult mounted skeleton	
Loggerhead Turtle (*Caretta caretta*)	1 adult skull	
Mata Mata (*Chelus fimbriata*)	1 adult mounted skeleton	
Common Snapping Turtle (*Chelydra serpentina*)	1 adult mounted skeleton	
Human (*Homo sapiens*)	13 adult skulls/skull fragments 10 juvenile skull fragments 12 adult skeletons (bones not from same individuals) 2 juvenile partial skeletons (bones not from same individual)	Cranfield Forensic Institute

Table 5.1. Materials used for a preliminary analysis, divided by species. When known, the sex of the individuals is in brackets

Some non-human species were excluded because their bones are very different from the human ones (brown rat, grey squirrel, loggerhead turtle) or because they don't live in the United Kingdom (brown bear, South American fur seal, leopard seal, green turtle, Hermann's tortoise, mata mata, common snapping turtle). Interesting similarities were noticed between some human and mute swan long bones, but further analyses on this species could not be carried out, because of the difficulty of obtaining its bones.

5.1.1. Ethical considerations

The human remains analysed for this research were treated with dignity and respect (Walker, 2008). No destructive analyses were carried out on human remains. The morphological examinations and the calculations with a GIS software did not require any destructive procedure; the hundreds of photos that were taken were not shared or published for non-scientific purposes. As for the analyses carried out using a micro-CT scanner, the human bones were not cut with a band saw (procedure used for some non-human remains, see Section 5.3).

The human bones used were more than one-hundred years old, but were not archaeological (with the exception of six cranial fragments, see Subsection 5.2.2). In England, the standards of research for archaeological human remains can be found in documents created by the Department for Digital, Culture, Media and Sport (DCMS), English Heritage, and other Institutions that carry out research on archaeological human remains, like the British Museum (De Witte, 2015).

For the research presented in this thesis, the regulations set out in the Human Tissue Act 2004 were followed. The Human Tissue Act 2004 is an act of the United Kingdom Parliament that covers England, Wales and Northern Ireland, regulated by the Human Tissue Authority (HTA, hta.gov.uk). The Act regulates activities concerning the removal, storage, use and disposal of human tissue, including bones, defined as "relevant material" (Human Tissue Act, Section 53).

5.2 Materials

5.2.1 Cranial curvature and sutures

Human and non-human skulls are made up of different plates of bone (45 in humans) that fuse before and after birth (White, Black and Folkens, 2011). The interlocking fibrous articulations that connect the bones of the skulls are called sutures (White and Folkens, 2005). The cranial sutures tend to obliterate with age; the reliability of the sutural degree of closure for age at death estimation is still debated, as it is influenced by other factors, such as sex and ancestry (Uhl, 2013; Ruengdit *et al.*, 2018). The use of cranial sutures as a morphological trait for ancestry assessment is another debated issue; the sutures are generally defined as "complex" for American Indians and Asians and "simple" for Whites and Blacks, but variations have been found within ancestral groups (Hefner, 2009; Maddux, Sporleder and Burns, 2015; Payne-James and Byard, 2015).

Sixteen human and non-human crania were employed for the measurement of cranial curvature and cranial sutures using a GIS software. The three non-human species chosen for the study are fox, cattle, and sheep. These species were chosen after a thorough visual observation of the skulls of several non-human species (see Section 5.1). The relatively small sample size was due to the availability of only four skulls for each non-human species.

During the macroscopic observation of the samples, it was noticed that the crania of fox, sheep and cattle may be problematic if found fragmented, because they share some characteristics with the human ones. For example, to the naked eye, the parietal bones of fox and calf have a curvature similar to the human one, and fox and sheep cranial sutures may resemble some of the human skull sutures.

As for the fox, generally its sutures tend to be more linear than the human ones, but in some cases their pattern may resemble the one observable in human skulls. In juvenile foxes, both the coronal (between the frontal and parietals) and the sagittal (between parietals) sutures may cause confusion in small fragments, because in many cases their pattern is similar to the one seen in human crania (Fig. 5.1-5.2). Adult male foxes can have a prominent sagittal crest (a ridge projecting along the midline of the cranium); in case a cranial fragment showing the sagittal crest is found, its identification as non-human would be straightforward, even if the sutures have a human-like appearance.

Fig. 5.1-5.2. Young fox skull (left) and human child cranium, posterior view (right). The coronal suture and some portions of the sagittal suture in foxes (arrow) may resemble human cranial sutures.

The cranial sutures of a calf may look very similar to the human ones; the sagittal suture is the one that most resembles a human suture. However, there are some sections of the cattle sagittal suture where the bone tends to be flat. Since there are no flat portions in the human cranium, in these cases the non-human origin of a fragment would be clear. In general, the cranial curvature may represent a problem only when a calf cranium is found, because in adult samples cranial bones tend to be flatter and much thicker.

After a macroscopic observation of both sheep and goat skulls, it was noticed that only sheep sutures are more indented and thus very similar to the human ones, while generally the sutures in goat skulls are more linear. To the naked eye, sheep seem to be the most problematic animal when it comes to cranial sutures that could lead to a misidentification of non-human skull fragments for human (Fig. 5.3-5.4).

Fig. 5.3-5.4. Sheep skull (left) and human skullcap, superior view (right). The sagittal suture of sheep can be extremely similar to the human sagittal suture, especially in the posterior portion, towards the occipital bone (arrow).

Bird crania were not considered, as they are much thinner than mammalian crania. Their identification as bird crania is not challenging, as the small brain case, the large eye orbits and their translucent structure are diagnostic features that would not be confusing even in case of fragmented samples. Fish and reptile crania are also very different from the mammalian ones, as they have many open areas and are very light; the crania of bigger reptiles, such as turtles, have robust muscle attachments, used to pull the head toward the shell for protection (Beisaw, 2013).

The facial area of the skull was excluded from the study because its bones can be easily recognised as human or non-human, even if fragmented. As regards the more robust facial bones, such as zygomatic, maxilla and mandible, the difference between human and non-human ones is very clear, therefore these bones may be easily identified even in a fragmentary state.

The skulls used, kept at the Cranfield Forensic Institute, were of different ages, although none of them was an old individual, since sutures were needed for a successful analysis (Table 5.2). As for foxes and calves, it was noticed that their cranial sutures begin to fuse or become more linear after 1 year of age; in humans, cranial sutures begin to obliterate between 25 and 49 years of age, but their

progress is variable (Steele and Bramblett, 2012). In all the skulls used the sutures were visible, although they were at different degrees of closure. Age-related morphological differences have been observed in human cranial sutures: the interdigitations appear sharp in juvenile skulls and blunt in adult skulls, because of a remodelling process that meets the functional demand of stabilization during growth into adulthood (Jayaprakash and Srinivasan, 2013). Despite the difference in sharpness of the interdigitations, the suture pattern in juvenile and adult human skulls does not change (Jayaprakash and Srinivasan, 2013; see Section 6.1 of this thesis). The sex of the non-human individuals used for the study was unknown; as for the human skulls, the sex was known for only two individuals (one male, one female), but the other two could not be sexed as one was a child and one was incomplete. All the human individuals were white.

Species	Number and age of individuals	Total of skulls used
Human (*Homo sapiens*)	2 adults, 35-40 years 1 juvenile, less than 20 years 1 child (6-9 years)	4
Fox (*Vulpes vulpes*)	2 young foxes, 2 months 2 adult foxes, 1 year	4
Calf (*Bos taurus*)	2 young calves, 3 weeks 2 old calves, 8 months	4
Sheep (*Ovis aries*)	1 lamb, less than 1 year 3 young sheep, more than 1 year	4

Table 5.2. Details of the skulls used for the study (N=16, with three repeats for each skull), with number and age of human and non-human individuals. The human skulls were aged with the Meindl & Lovejoy (1985) method[1].

---

[1] This method uses scores that represent the degrees of closure of sutures. In the original study, 7 vault sutural sites and 5 lateral-anterior sutural sites were selected. Four scores were assigned to each degree of sutural closure: 0 = open; 1 = minimal to moderate closure (up to 50%); 2 = significant closure; 3 = complete obliteration. The sums of the site scores, or composite scores, are related to mean ages, ranging from 30.5 to 51.5 for the vault sites and from 32.0 to 56.2 for the lateral-anterior sites. The age of a skull is given by the comparison of the composite scores obtained (one for the vault and one for the lateral-anterior portion) to the corresponding mean age (Meindl and Lovejoy, 1985).

Newborn individuals were not considered because during the macroscopic observation it was noticed that human skulls are significantly different from non-human ones, in texture, shape and curvature, therefore a human newborn skull can be hardly confused with a non-human one. Furthermore, full access to newborn samples was difficult, both for human and non-human individuals.

The analyses were focused on the ectocranial sagittal suture (interfrontal/sagittal for animals) and on the curvature of the parietals. The ectocranial pattern of a suture differs from the endocranial one of the same suture, as the endocranial usually does not have a recognizable design, while the ectocranial has a characteristic pattern (Chandra Sekharan, 1985; Hershkovitz, 2004). Indeed, the endocranial pattern of a suture matches the ectocranial one in infants of 1-2 years, but as the age progresses the endocranial pattern becomes linear and less complicated while the ectocranial one takes on its distinctive pattern (Jayaprakash and Srinivasan, 2013).

The study focused on the sagittal area of the skull because GIS software are designed to read topographic maps, therefore the 3D models used for the analyses must resemble a landscape image. The software needs 2D vector data to run curvature calculation and suture mapping; a curved surface (as the cranial one would be if the whole neurocranium or more than one suture were considered) would produce incorrect data.

5.2.2 Additional cranial fragments for GIS method test

Six archaeological human parietal bone fragments, kept at the Cranfield Forensic Institute, were used to test the curvature calculation and the suture mapping method with GIS. The sex of the individuals was not known; their specific age was not known, but in all cranial fragments the sutures were still clearly visible. The fragments showed coronal, sagittal and lambdoid suture; the largest fragment measured 10 cm and the smallest 6 cm (Fig. 5.5-5.6). The choice to use archaeological material was due to the lack of availability of non-archaeological human parietal fragments (and vault fragments in general). Furthermore, only human fragments were used because non-human cranial fragments were not available.

Fig. 5.5-5.6. Two human cranial bone fragments used for the test

5.2.3 Rib curvature

Pig ribs were used for the shaft curvature calculation and its comparison with the human one. Pig was chosen because of the apparent similarity between its ribs curvature and the one seen in humans, and because its ribs are widely used for human consumption, therefore they are likely to be found in a forensic or archaeological scenario.

A total of eight ribs was used; four were pig ribs (provided by a butcher) and four were human ribs, kept at the Cranfield Forensic Institute (Table 5.3).

Species	Number and side of ribs	Total of ribs used
Human (*Homo Sapiens*)	3rd left 6th right 7th right 10th left (four adult, unsexed individuals)	4
Pig (*Sus scrofa domesticus*)	13-14th left 13-14th right (two unsexed individuals, less than 1 year old -typical slaughter age-)	4

Table 5.3. Details of the ribs used for the study (N=8, with three repeats for each rib).

Different ribs of four different human individuals were used in order to take into account as much variability as possible; human 1st, 2nd, 11th and 12th ribs were not considered as they are more characteristic and easier to identify. As for the pig, the 13th and 14th ribs were the only ones that could be obtained. The limited availability of pig ribs was the main reason why the total number of ribs used was small (N=8). This part of the research carried out on human and pig ribs was used to test the applicability of the curvature calculation method with GIS; a higher number of ribs would certainly produce more reliable results. In a study with a bigger sample size, the variability in the curvature among the ribs within the same species could be better measured. In humans, the curvature of the ribs decreases towards the distal portion of the rib cage (Baker, Dupras and Tocheri, 2005); furthermore, the shaft curvature increases slightly in adult individuals (García-Martínez, Recheis, and Bastir, 2015).

Only the central portion of the shaft was considered for the analysis, to simulate what would be a realistic scenario with fragmented rib shafts. More precisely, the shaft area enclosed between the rib angle and the wider/flatter area close to the costal cartilage was considered (Fig. 5.7). The head and the sternal end were not considered, as these show clear differences in human and pig ribs. The heads have peculiar shapes that allow to identify them as human or porcine (or non-human in general; Hillson, 2003); the pigs' sternal ends are more flared, wide and rounded than the human ones. Therefore, if the shaft is fragmented but even a portion of the head or sternal end is found, the

identification of the human or non-human origin of the rib would not rely on the calculation of the shaft curvature.

Fig. 5.7. Human 6th rib. The two black lines enclose the area of the shaft considered for the analysis. H=head; S=sternal end.

5.2.4 Occipital condyles

The occipital condyles are two projections on either sides of the foramen magnum, on the inferior part of the occipital bone (Kavitha *et al.*, 2013). The condyles articulate with the superior facets of the atlas (first vertebra), and make the movements of the head on the neck (pitch, roll, and yaw) relatively smooth (Arcoverde *et al.*, 2014).

The occipital condyles of 23 non-human species were observed (Table 5.4). The sex in most cases was unknown; although there are some minor sex differences, such as length, width, and height of the condyles and bicondylar breadth (all higher in males), both in human and non-human species (Elbroch, 2006; Casanova, 2012; de Oliviera *et al.,* 2013; Kumar & Nagar, 2015), the main characteristics of the condyles do not change. The skulls used for this study are part of the Oxford Archaeology, the Grant Museum of Zoology, and the Cranfield Forensic Institute collections. The sample size depended on the availability of skulls for each species.

Common Pheasant (*Phasianus colchicus*)	Wood-Feral Pigeon (*Columba Palumbus*; *Columba Livia*)	Chicken (*Gallus gallus*)	Turkey (*Meleagris gallopavo*)	Duck (*Anas platyrhynchos*)	Goose (Anser anser)
3	4	3	2	2	2
Cat (*Felis domesticus*)	**Rabbit-Hare** (*Oryctolagus cuniculus*; *Lepus europaeus*)	**Badger** (*Meles meles*)	**Fox** (*Vulpes vulpes*)	**Dog** (*Canis lupus familiaris*)	**Cow** (*Bos taurus*)
3	6	3	7	11	8
Horse (*Equus caballus*)	**Sheep-Goat** (*Ovis aries*; *Capra aegagrus hircus*)	**Pig** (*Sus scrofa domesticus*)	**Fallow-Roe-Red Deer** (*Dama dama*; *Capreolus capreolus*; *Cervus elaphus*)	**Grey-Common seal** (*Halichoerus grypus*; *Phoca vitulina*)	**Human** (*Homo sapiens*)
3	11-5	3	3-2-1	2-1	11
Total of skulls used 96					

Table 5.4. Species considered in the study and corresponding number of skulls used.

Human individuals under 5-7 years old were not considered for this study, as the *pars basilaris* and *pars lateralis*, which form the occipital bone along with the *pars squama*, are not completely fused until that age (Scheuer and Black, 2004). In foetal, perinatal and very young individuals the occipital condyles are not fully formed, as they are still divided between the *pars lateralis* and the *pars basilaris*. Indeed, in those rare cases where a human perinatal skull is found, the occipital bone parts are found separate and can be well distinguished, as they have a characteristic shape (Schaefer, Black and Schaefer, 2009). Even when foetal non-human skulls show human-like occipital condyles in appearance (as may happen with pigs or some dog breeds), their non-human origin would be clear. The non-human condyles would be fully formed, while the human ones are not complete until

approximately 7 years of age; therefore, if human-like but small occipital condyles are found, a human origin can be excluded.

5.2.5 Linea aspera

The *linea aspera* is a rough crest located along the posterior aspect of the femoral shaft, functioning as attachment for the leg extensors, flexors and adductors (Kulkarni, 2012). In humans, the linea aspera is very pronounced, while in other non-human animals is typically less prominent; this is because the muscles attached to the linea aspera are those mainly used in bipedalism (Adams, Crabtree and Santucci, 2008; Moore, Milz and Knothe Tate, 2014).

A complete femur showing the linea aspera can be safely identified as human or non-human; however, when it comes to fragmented femoral shafts where only a little portion of the linea aspera is visible, the shape of this latter is no longer clear. Some species may share specific characteristics with the human skeleton, such as sharpness or outline of the muscle markings that lie on the posterior femoral shaft. The potential similarities between some non-human species and humans may make the identification of femoral fragments challenging. Femur is one of the strongest bones in the skeleton and survives better than other bones; therefore, since incomplete or fragmented femora are found frequently, it is important to use methods that allow to safely identify them as human or non-human (Domínguez-Rodrigo and Barba, 2007; Lyman, 2013).

The femoral shafts of 21 non-human species were used for this study. Table 5.5 shows the number of femora considered, divided by species. The femora were part of the Oxford Archaeology, the Grant Museum of Zoology, and the Cranfield Forensic Institute collections.

Common Pheasant (*Phasianus colchicus*)	Wood-Feral Pigeon (*Columba Palumbus*; *Columba Livia*)	Chicken (*Gallus gallus*)	Turkey (*Meleagris gallopavo*)	Duck (*Anas platyrhynchos*)	Goose (Anser anser)
6	8	16	4	8	4
Cat (*Felis domesticus*)	**Rabbit-Hare** (*Oryctolagus cuniculus*; *Lepus europaeus*)	**Badger** (*Meles meles*)	**Fox** (*Vulpes vulpes*)	**Dog** (*Canis lupus familiaris*)	**Cow** (*Bos taurus*)
8	13	6	4	18	8
Horse (*Equus caballus*)	**Sheep-Goat** (*Ovis aries*; *Capra aegagrus hircus*)	**Pig** (*Sus scrofa domesticus*)	**Fallow-Roe-Red Deer** (*Dama dama*; *Capreolus capreolus*; *Cervus elaphus*)	**Human** (*Homo sapiens*)	
5	24	18	11-8-2	26	
Total of femora used					
197					

Table 5.5. Species considered in the study and corresponding number of femora used.

The human femora used were from adult or young adult individuals, and the non-human ones were from both adult and juvenile individuals. Human femora aged less than three years do not have a visible linea aspera (Moore, 2014), while juvenile mammals and birds have a visible linea aspera as non-human animals tend to grow much faster than humans and reach maturity at an early age (Deisboeck and Kresh, 2006). Foetal non-human femora were not used as it was noticed that at this age the linea aspera is not or barely visible.

The sex of most of the bones was unknown. The main difference between male and female individuals, both human and non-human, is the prominence of the muscle marking, which is usually less prominent in females (Guharaj, 2003); however, if the female individuals were particularly

athletic or engaged in physically demanding activities, their linea aspera and muscle markings in general would be more developed (Byers, 2017). Therefore, the unkown sex of the bones used did not represent a limitation, given the low levels of sex dimorphism in linea aspera (Polguj *et al.,* 2013) and the fact that the prominence was not among the features considered in this study.

5.2.6 Nutrient Foramina

Nutrient foramina are openings through which the blood vessels enter the bone. On long bones, nutrient arteries and peripheral nerves reach the marrow cavity from the outer surface through the nutrient foramina, which in most cases can be distinguished from any other cavity by the presence of a vascular groove (Beisaw, 2013). The blood carried by the nutrient arteries into the bone shaft is essential for the growth, nutrition and repair of the bones (Marenzana and Arnett, 2013). Indeed, a nutrient foramen is the site of the original center of ossification of a long bone, as the vessels passing through them are derived from those that supplied blood to the initial ossifying cartilage (Rao and Kothapalli, 2014). For this reason, the growing end of a long bone is indicated by the direction of the main nutrient foramen.

The blood vessels entering through the foramina are also vital for bone metabolism, the lifelong remodelling process where new bone tissue is produced in response to the wear and tear caused by mechanical loading and locomotion (Klein-Nulend and Bacabac, 2012). Therefore, the extent of blood flow and hence the individual (human or non-human) activity level can be inferred from the area of the nutrient canal (Seymour *et al.,* 2012; Ward, Pasterkamp, Yeung and Borst, 2000).

The non-human species included in this study - chicken, duck, sheep, pig, and deer - were selected because the shafts of their long bones share similar characteristics with the human ones, making their identification potentially challenging if they were found in a fragmentary state.

The study sample comprised a total of 384 human and non-human limb bones: left and right humeri, radii, ulnae, femora and tibiae, or tibiotarsi for birds (Table 5.6).

	Human	**Sheep**	**Deer**	**Pig**	**Chicken**	**Duck**
Humerus	22 (2, 1L,1R)	11 (2, 1L,1R)	10 (2, 1L,1R)	10 (2, 1L,1R)	10 (2, 1L,1R)	4 (2, 1L,1R)
Radius	26 (2, 1L,1R)	10 (2, 1L,1R)	10 (3, 1L,2R)	9 (1 L)	10 (2, 1L,1R)	4 (2, 1L,1R)
Ulna	23 (2, 1L,1R)	9 (2, 1L,1R)	9 (3, 1L,2R)	9 (1 L)	10 (2, 1L,1R)	4 (2, 1L,1R)
Femur	26 (2, 1L,1R)	8 (2, 1L,1R)	9 (2, 1L,1R)	14 (2, 1L,1R)	10 (2, 1L,1R)	4 (2, 1L,1R)
Tibia/ Tibiotarsus	33 (3, 2L,1R)	27 (2, 1L,1R)	9 (2, 1L,1R)	10 (2, 1L,1R)	10 (2, 1L,1R)	4 (2, 1L,1R)
Fibula	10			10		
Tot	**140**	**65**	**47**	**62**	**50**	**20**
Total of limb bones used 384						

Table 5.6. Number of bones considered for this study, divided per species and long bone. In brackets the number of bones scanned is shown, where L=left and R=right. An additional deer radius and ulna were scanned to counterproof the results of the first two scans, as the foramina on these bones were extremely small and difficult to see. Only one pig radius and ulna were available for scanning. An additional human left tibia was scanned; the first left tibia scanned showed tibial periostitis, but it was decided to scan also a healthy one, for more consistent results.

The individuals considered for the study were both juvenile and adult, in most cases of unknown sexes, and of modern date (19th-20th century and contemporary for some non-human species); most of them had no detectable pathology affecting the shaft, although some of the samples showed osteoarthritis at different degrees of severity. The human bones and part of the non-human ones employed for this research derived from the Cranfield Forensic Institute collection; most of the non-human bones were obtained from butchers and from the collections of Oxford Archaeology and the Grant Museum of Zoology.

Table 5.7 shows number and age of the bones used for the morphological examination of nutrient foramina:

	Human *Homo sapiens*	Sheep *Ovis aries*	Deer *Dama d.; Capreolus c.*	Pig *Sus scrofa domesticus*	Chicken *Gallus gallus*	Duck *Cairina moschata*
Humerus	**20** +20 yrs	**9** 3 mths, 3 yrs, 3.5 yrs	**8** -4 mths, 5.5 yrs,+5yrs	**8** foetal, 1 yr, 3 yrs, 3.5 yrs	**8** 8 wks, 5 mths, 2 yrs	**2** 5 mths
Radius	**24** +20 yrs	**8** 3 yrs, +3.5yrs	**7** -4 mths, +5 yrs	**8** foetal, 1 yr, 3 yrs, 3.5 yrs	**8** 8 wks, 5 mths, 2 yrs	**2** 5 mths
Ulna	**21** +20 yrs	**7** 3 yrs, +3.5yrs	**6** -4 mths, +5 yrs	**8** foetal, 1 yr, 3 yrs, 3.5 yrs	**8** 8 wks, 5 mths, 2 yrs	**2** 5 mths
Femur	**24** +20 yrs	**6** 3 yrs, +3.5yrs	**7** -4 mths, -1 yr, +5 yrs	**12** foetal, 1 yr, -2 yrs, 3 yrs, 3.5 yrs	**8** 8 wks, 5 mths, 2 yrs	**2** 5 mths
Tibia/ Tibiotarsus	**30** +20 yrs	**25** 3 yrs, 3.5, 5 yrs	**7** -4 mths, -1 yr, +5 yrs	**8** foetal, 1 yr, 3 yrs, 3.5 yrs	**8** 8 wks, 5 mths, 2 yrs	**2** 5 mths
Fibula	**10** +20 yrs			**10** foetal, 1 yr, -2 yrs, 3 yrs, 3.5 yrs		
Total	129	55	35	54	40	10
Total limb bones observed 323						

Table 5.7. Number and age of the limb bones used for the morphological examination of foramina.

Table 5.8 shows number and age of the bones scanned:

	Human	Sheep	Deer	Pig	Chicken	Duck
Humerus	2 + 20 yrs	2 - 3 mths, + 3 yrs	2 + 1 yr, + 5.5 yrs	2 3.5 yrs	2 5/6 mths	2 5 mths
Radius	2 + 20 yrs	2 + 4 mths, + 3.5 yrs	3 + 4 yrs	1 3.5 yrs	2 5/6 mths	2 5 mths
Ulna	2 + 20 yrs	2 - 3 yrs, + 3.5 yrs	3 + 4 yrs	1 3.5 yrs	2 5/6 mths	2 5 mths
Femur	2 + 20 yrs	2 - 3 yrs, 3.5 yrs	2 - 1yr, + 5 yrs	2 - 1 yr	2 5/6 mths	2 5 mths
Tibia/ Tibiotarsus	3 + 20 yrs	2 3 yrs	2 - 1 yr, + 4 yrs	2 - 1 yr, 2 yrs	2 5/6 mths	2 5 mths
Total	11	10	12	8	10	10
Total limb bones scanned: 61						

Table 5.8. Number and age of the bones used for micro-CT.

Fibulae were not included, as the non-human species considered in this study have an extremely gracile fibula (chicken and duck) or have a bony prominence on the proximal lateral tibia, with no shaft (sheep and deer). Among the species considered, only pig has a fibula, but this bone was not further analysed as it is very different from the human one; human and pig fibula share a medial location of the nutrient foramen, but even in a fragmentary state they cannot be misidentified, because of their peculiar shape (Fig. 5.8-5.9).
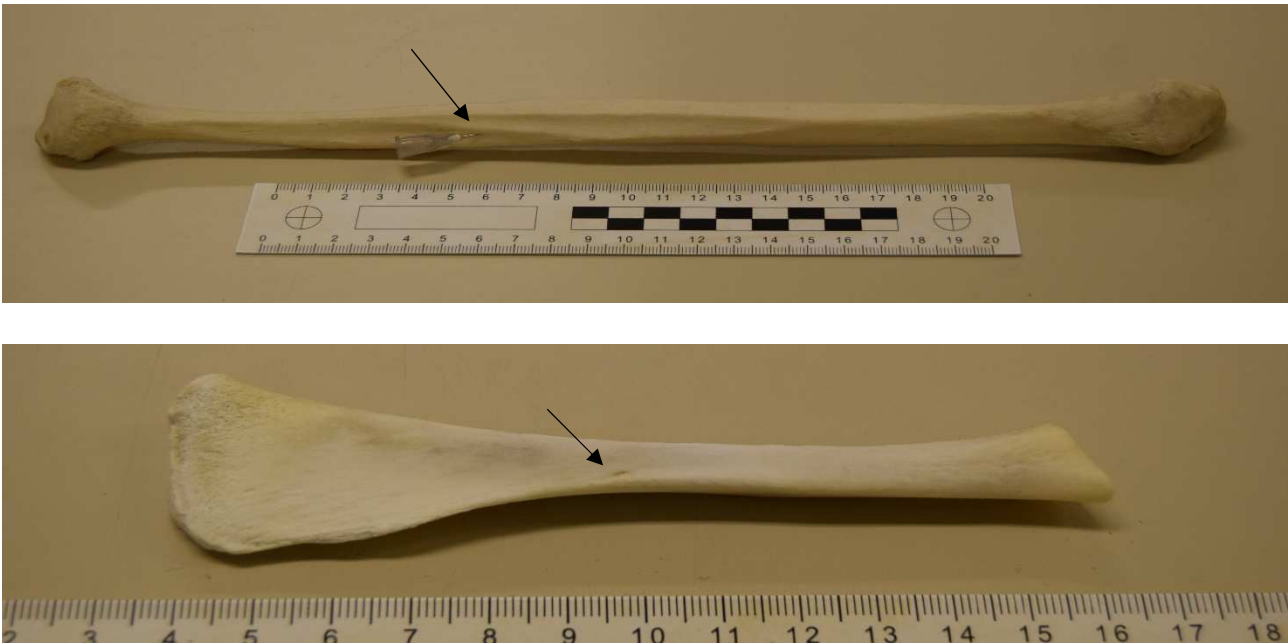
Fig. 5.8-9. Human (top) and pig fibulae. The nutrient foramina are indicated by arrows (a 27G needle was inserted into the human foramen to detect its direction, see section 5.3.2).

5.2.7 Cross-sectional shape

Fragmented long bone shafts can be particularly difficult to identify, especially when diagnostic anatomical landmarks and epiphyses are not visible. The shafts of the limb bones are among the most commonly found bones, because their dense cortex allows a better preservation (Croker, Clement and Donlon, 2009).

Previous studies that considered long bones cross-sectional shape were mainly focused on primate bones (Ruff, 1990; Carlson *et al.*, 2006; Ruff and Larsen, 2014), human skeletal adaptation (Stock and Pfeiffer, 2001; Holt, 2003; Ruff, 2003), and population comparison (Ogilvie and Hilton, 2011; Stock *et al.*, 2011), but not on the human-nonhuman bone differentiation (see Chapter 7 of this thesis).

The non-human species chosen for this study were the same ones observed in the nutrient foramina research - chicken, duck, sheep, pig, and deer – because of the similarities of their limb bone shafts with the human ones and the high frequency with which their bone remains can be found.

The bones used for scanning, a total of 58, were the same used for the study focused on the nutrient foramina: left and right humeri, radii, ulnae, femora and tibiae/tibiotarsi (Table 5.9). Fibulae were not

scanned, for the same reasons they were excluded from the foramina study (section 5.2.6). The sample size for each species was relatively small, as the main aim of this study was to explore the potential of the micro-CT scanning for the detection of human and non-human bone cross-sectional shapes; the high cost of the procedure was another factor that affected the choice of the sample size.

	Human	Sheep	Deer	Pig	Chicken	Duck
Humerus	**2**	**2**	**2**	**2**	**2**	**2**
	1 L, 1 R	1 L, 1 R	1 L, 1 R	1 L, 1 R	1 L, 1 R	1 L, 1 R
Radius	**2**	**2**	**2**	**1**	**2**	**2**
	1 L, 1 R	1 L, 1 R	1 L, 1 R	1 L	1 L, 1 R	1 L, 1 R
Ulna	**2**	**2**	**2**	**1**	**2**	**2**
	1 L, 1 R	1 L, 1 R	1 L, 1 R	1 L	1 L, 1 R	1 L, 1 R
Femur	**2**	**2**	**2**	**2**	**2**	**2**
	1 L, 1 R	1 L, 1 R	1 L, 1 R	1 L, 1 R	1 L, 1 R	1 L, 1 R
Tibia/ Tibiotarsus	**2**	**2**	**2**	**2**	**2**	**2**
	1 L, 1 R	1 L, 1 R	1 L, 1 R	1 L, 1 R	1 L, 1 R	1 L, 1 R
Total	10	10	10	8	10	10
Total limb bones scanned: 58						

Table 5.9. Number of bones scanned, divided per species and long bone. L=left and R=right. The additional deer radius and ulna and human tibia scanned to study nutrient foramina were not considered. Only one pig radius and ulna were available for scanning.

None of the long bones used showed weathering or erosion of cortical bone (Fig. 5.10-5.11).

Fig. 5.10-5.11. Sheep right humerus (top), postero-lateral view, and human left ulna. As the two bones in the photos above, the bones scanned showed no cortical weathering or erosion.

Antlers and horns were excluded from the study, despite they might resemble mammalian long bones if found fragmented. Antlers have a very thick cortex with a wood-grainlike appearance and a very dense spongy bone; horns have both the exterior and interior surface much more porous than a long bone (Beisaw, 2013; Fig. 12).

Fig. 5.12. Sheep horns

5.2.8 Location of the skeletal features considered

Figures 5.13-5.15 show the location of the bone features considered for this research, on human, non-human mammal and avian skeletons. Since nutrient foramina and cross-sectional shape cannot be shown, the location of the long bones is indicated.
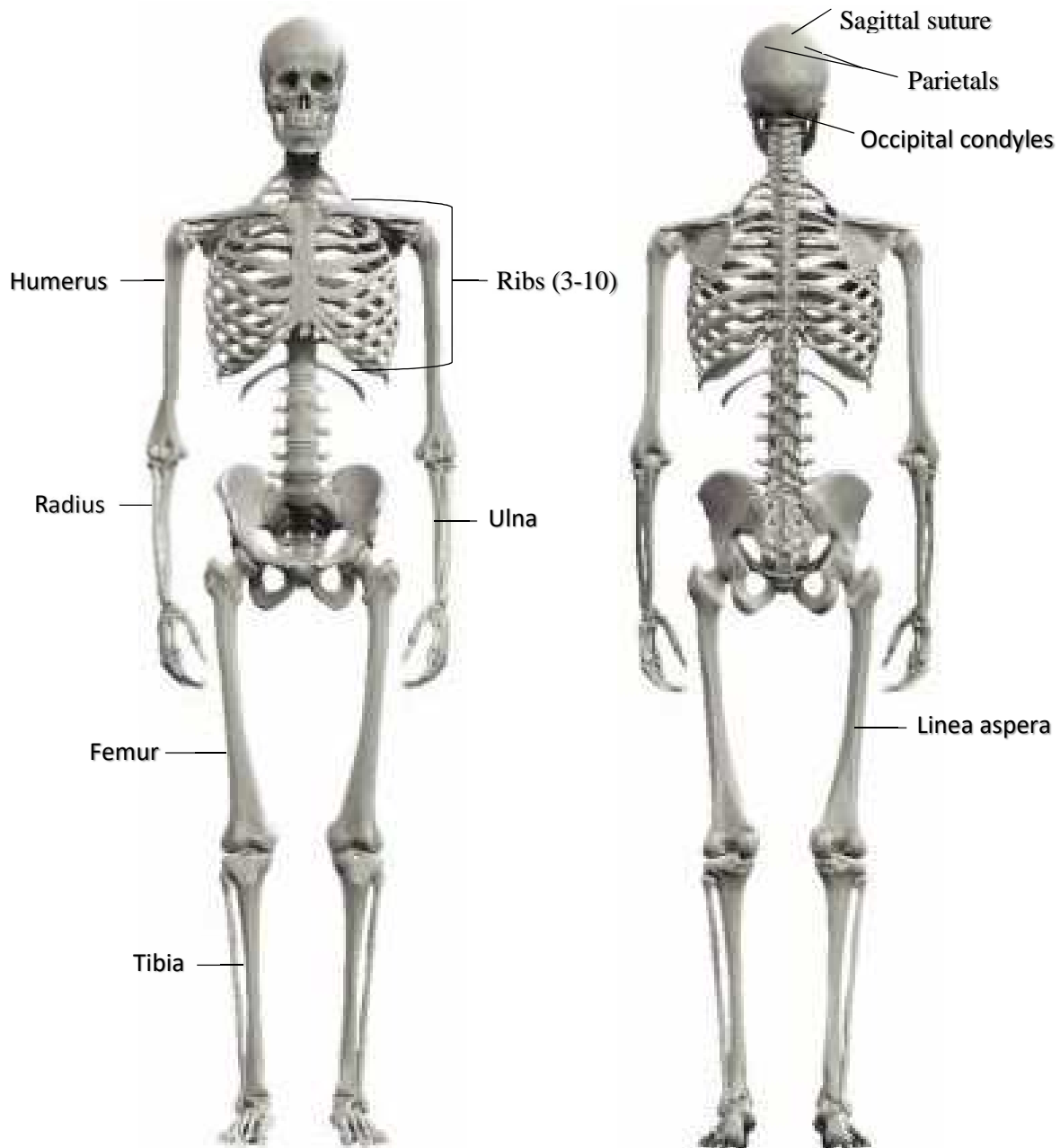
Fig. 5.13. Human skeleton, anterior and posterior view (http://psychic-vr-lab.com, modified).
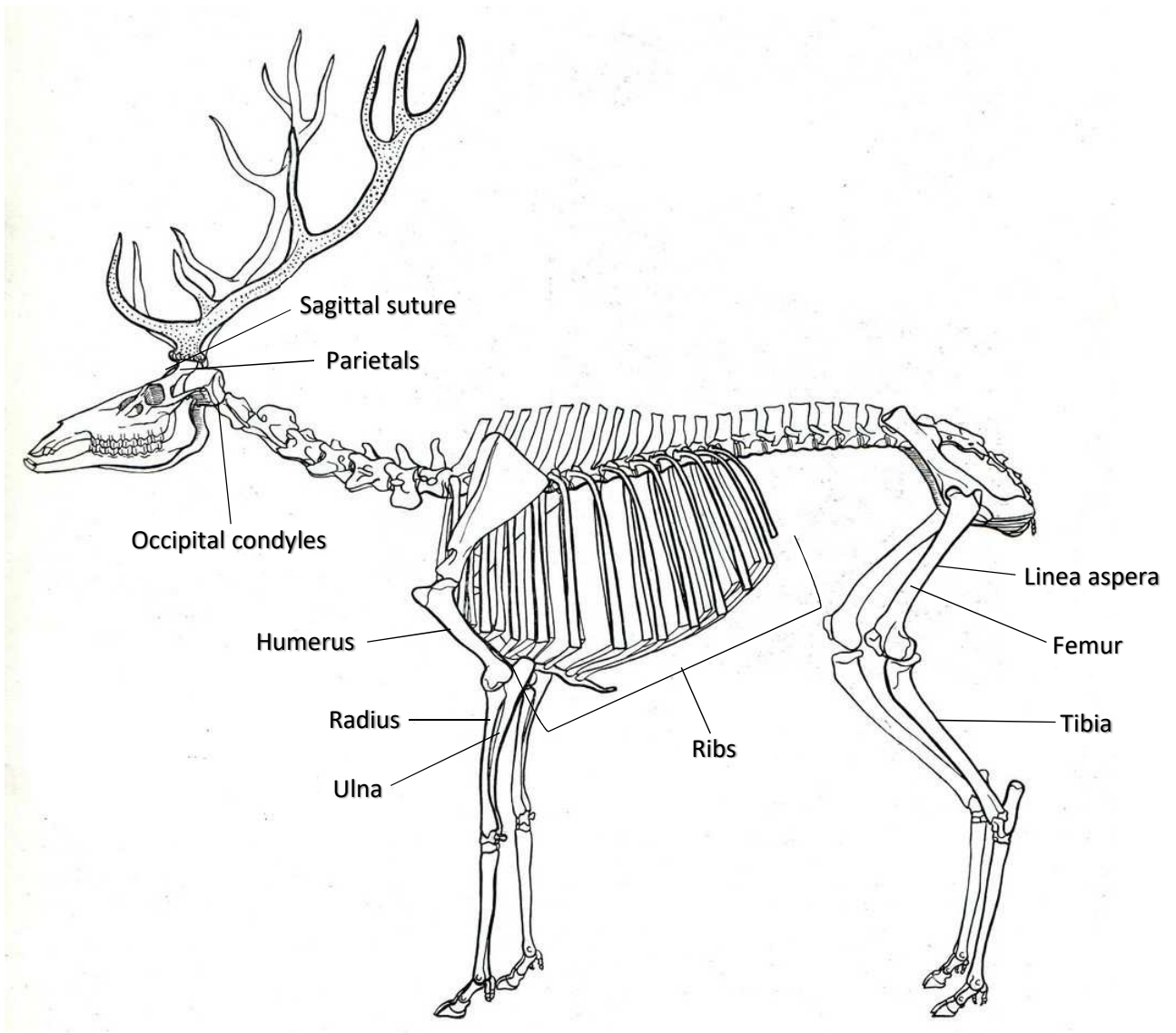
Fig. 5.14. Red deer skeleton (Lydekker and Sclater, 2011, modified).
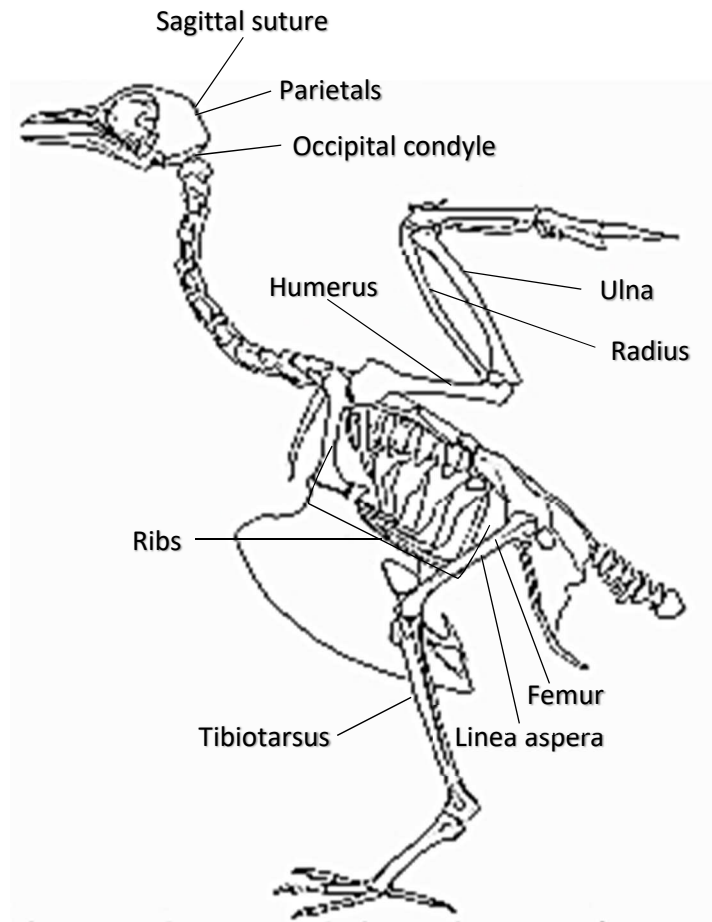
Fig. 5.15. Avian skeleton (bafari.org, modified).

5.3 Methods

5.3.1 GIS (Geographic Information System)

A GIS software was tentatively used to demonstrate its utility for the distinction between human and non-human cranial bone fragments and rib shafts. The software was used to identify the cranial sutures patterns and the curvature of human and non-human cranial bones and ribs.

A GIS software is a tool that helps visualising, generating, modifying and analysing geographic and spatial data (Lloyd, 2010). GIS is a valuable instrument to precisely identify the logical relationships between the position of objects; because of the geographical component of many data, the software can be used for multiple purposes, such as identifying problems like drugs distribution, monitoring climate change, keeping track of weather events, analysing crime patterns, understanding trends, or

analysing surfaces (esri, 2018). The information that can be put into GIS (a process called data capture) can include cartographic data, photographic data, digital data (for example, those collected from satellites or drones), or data in spreadsheets, such as population demographics (National Geographic, 2017).

The use of GIS in Archaeology is widespread, particularly to understand the human actions on past landscapes and to predict the location of archaeological sites, based on known patterns in data (Conolly and Lake, 2006). In Forensics, GIS is usually used to locate and recover remains, or to map the scenes (Manhein, Listi and Leitner, 2006; Walter and Schultz, 2013).

GIS was chosen for this research because the bone, in this specific case the cranial vault, can be treated as a topographical landscape, and some of its features can be read as in a map. The basic idea of this research was to consider the parietals area of the cranium as a surface whose curvature could be quantitatively calculated, and the sutures as rivers whose pattern could be mapped and compared. Promising results were achieved in this unique application of GIS to anthropology by Bolton (2013), who successfully attempted to quantify the pubic symphysis surface as a geographical landscape, by visualizing the peaks and valleys of the surface as a mountain-range, in order to find age-correlated changes in slope, aspect and volume.

A GIS software needs a 3D or 2D model to run its analysis and calculations. At a first stage, a 3D model of each skull was needed. Some scanning attempts were made with a Nikon Metrology MMDx50 handheld laser scanner, but it produced low image resolutions; the sutures were not completely scanned, and appeared as shapeless voids on the crania.

Photogrammetry was then chosen to create 3D models of the skulls. Photogrammetry is a viable and affordable alternative to laser scanning. It is a technique used to convert 2D images into 3D models with XYZ coordinates, through photographs. The basic principle used is the triangulation, where the location of an object is calculated by the intersection of lines in space (Robinson, 2007).

Multiple photographs must be taken all around the object, at an average interval of 20° one from the other, at three or four different angles. The object should be clear and well lit, on a uniform and light (possibly white) background, whose presence should not interfere with the image; a non-uniform background would lead to an "unclean" 3D image. The quality of the pictures should be the highest possible (Konecny, 2014).

For this research, the skulls were placed on a white surface and turned of 20° degrees for each picture, which was taken from a fixed point with a digital camera on a tripod. When the rotation of the skull was complete, the tripod was moved to a higher angle and the entire process was repeated. Pictures

were taken from four angles. On average, 100-120 photos for each skull were taken. The photos were uploaded on a laptop and optimised by improving their sharpness and brightness, and by cutting redundant background.

Agisoft PhotoScan software was used to build the 3D models. After uploading the photos, they were aligned, and a dense cloud, a mesh and a texture were built (Fig. 5.16). The 3D models obtained were then cleaned and cut, in order to select the parietals (for curvature calculation) and the interfrontal/sagittal suture area of the crania.
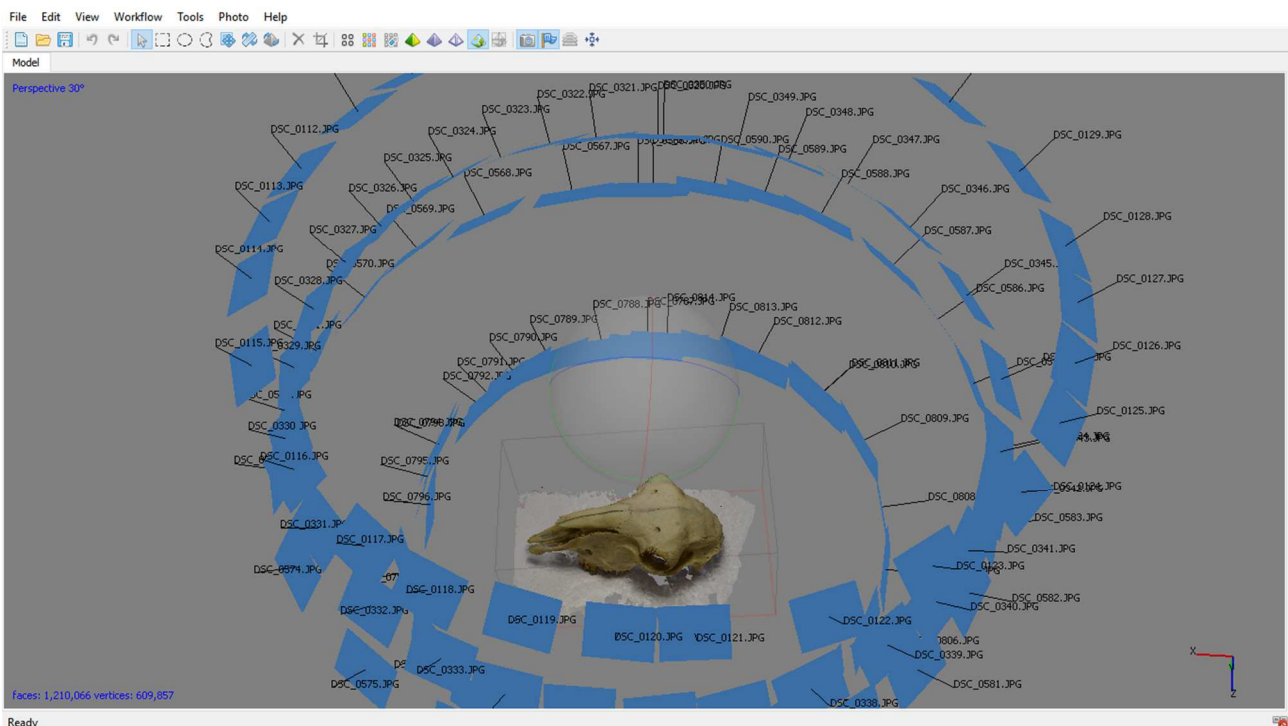
Fig. 5.16. 3D image of a sheep skull created with Agisoft Photoscan. The blue squares around the image represent the photos taken.

The model files were first exported in VRML file format in Agisoft Photoscan; Meshlab was used to export the VRML files in XYZ files, which could be correctly read by the GIS software.

In this research, ArcGIS 10.3.1. software was used to calculate the curvature and map the sutures. Since before this study a GIS software had not yet been used for cranial bone sutures and curvature analysis, the researcher had to explore all the applicable software features in order to find those suitable for the calculation of curvature and suture pattern analysis.

As for curvature, ArcScene (a viewing application of ArcGIS) was first used to create a TIN (Triangulate Irregular Network), which is a 3D representation of the elevation values of a surface, using the 3D XYZ files obtained from Meshlab. After a TIN was created, slope and aspect (the direction of slope) were calculated. The main aim was to compare the slope of the cranial bone surface of the different species considered, assuming that higher slope values corresponded to a more pronounced curvature. However, these calculations were not considered satisfactory since the curvature of the samples was only inferred from slope measurements but not directly calculated.

The only way to calculate the curvature was to use the Curvature feature in ArcScene. At first, this feature was considered too obvious and simple, but after a through exploration of most of the ArcGIS features, it was realized that the Curvature one was the most suitable for the aim of the study. In ArcScene, the curvature is one of the spatial analyst tools; for the calculation, the symbology was modified (stretched-hillshade effect, to improve the visual contrast), the colour ramp was left to default black to white, and the Z-factor (elevation) was set to 1. The output data obtained included a raster image of the bone showing shades of the colour ramp corresponding to specific ranges of curvature values (set to 5 classes), and classification statistics (count, minimum, maximum, sum, mean, standard deviation). Since the same results were obtained using the same settings, a set number of three repeats for each skull was considered satisfactory.

As for sutures, the process turned out to be much more complex than expected. As already mentioned, the initial idea was to consider the sutures as rivers whose network could be extracted. Therefore, the hydrologic analysis functions in ArcScene seemed to be the most appropriate to use. However, cranial sutures unlike rivers have no depth and are read by GIS as simple lines; for this reason, the hydrologic features were not able to run appropriate analyses.

ArcMap (another component of ArcGIS) was also explored for suture mapping. DEM (Digital Elevation Model) files were generated in Agisoft Photoscan in order to highlight elevations and sutures, but the images produced failed to highlight the sutures, which were not even visible (again, for lack of depth), so they could not be properly read by ArcMap.

After many failed attempts made both in ArcScene and ArcMap, only the Contour feature in ArcScene proved to be useful for the suture mapping. Since sutures are read as lines by the GIS software, all those software features that require depth as a prerequisite for river mapping cannot be used. The cranial surface can still be treated as a topographic map by generating contour lines, which highlight the shape and the elevation of the terrain.

Like Curvature, the Contour feature in ArcGIS is a spatial analyst tool. The settings were as follows: contour interval (distance between contour lines) = 1; features symbol = river, green; in layer properties – symbology – quantities – graduated colours, fields value = contour, and normalization = shape length (to highlight the suture pattern instead of the single lines). Classification statistics were part of the output data, but these were not used for further analysis because they were related to the entire sagittal/parietal surface selected, not the suture alone. It was not possible to isolate the sagittal suture, as GIS did not recognize it as a river or any kind of separate surface; for this reason, only the visual, qualitative part of the data obtained was used for the study.

Both the Curvature and the Contour functions required the input of 2D raster data. The VRML 3D files obtained from Agisoft Photoscan were imported in ArcScene and converted in JPG format; the position and illumination of each file were then adjusted, in order to show as clearly as possible both curvature and sutures.

This study was preliminary, and the method was tested on a specific suture and area of the cranium; if proven successful, it may be repeated on other sutures and/or other cranial areas.

The human and pig rib shaft curvature was calculated following the same procedure used for crania. The ribs were photographed both in superior and inferior view, in order to verify whether there was a view from which the curvature could be detected with more precision.

5.3.2 Morphological examination

The occipital condyles and the foramen magnum of 96 skulls of 24 species, including human, were morphologically examined, photographed, and compared. In particular, the observation was focused on foramen magnum shape, occipital condyles shape, condyles texture, condyles borders, and whether the condyles meet inferiorly (Fig. 5.17); where seen, other characteristics of each pair of condyles were considered. These specific features were chosen because it was noticed that they appeared analogous among the individuals of the same species (regardless of sex; see Section 5.2.4), and that a differentiation between human and non-human could be done using them as criteria. The features chosen did not require a quantitative method. A qualitative method was used because those quantitative data that could be obtained by measuring the condyles, such as length or width, change with age and between sexes, in both human and non-human skulls. Furthermore, in many cases where the condyles are fragmented, such measurements would be of no use as not applicable.

The basicranium, which includes foramen magnum and occipital condyles, is likely to survive and to be found, even if fragmented, as it is protected by a large mass of soft tissue made up of muscles, tendons and ligaments (Gapert, Black and Last, 2009). The features chosen and used for this research were completely or partially detectable even in case of fragmentation of the occipital condyles area (see Results in Chapter 6). Furthermore, in those cases where one or two of the features considered were not visible (for example, the foramen magnum or the complete shape of the condyle), the remaining ones could help identifying the origin of the fragment.
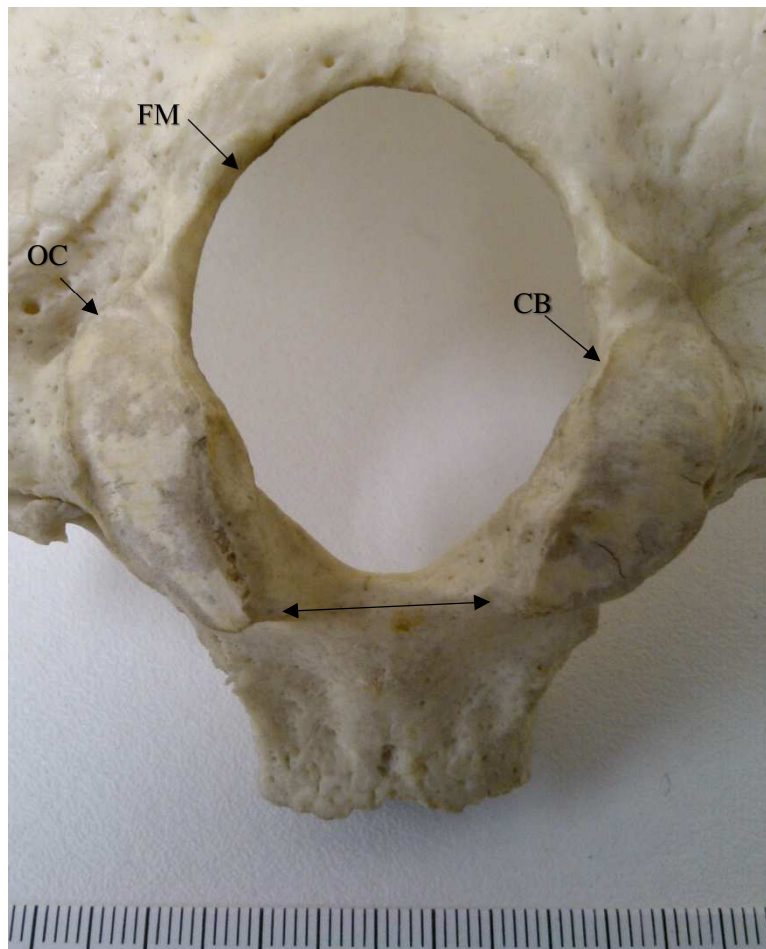
Fig. 5.17. Parts of the occipital bone considered in this study.

FM= foramen magnum; OC= occipital condyles; CB= condyles borders; the two-point arrow indicates the area where the condyles meet in certain species. The occipital in this picture is human.

A similar analysis was carried out on linea aspera. 197 femoral posterior shafts of human and 21 non-human species were analysed and photographed. The linea aspera of each species was observed and described in detail, looking for example at its main shape, the location and outline of the single lips that form the linea aspera, or at the possible presence of foramina. A comparison between the human linea aspera and each non-human one was made, in order to facilitate femoral bone identification in a fragmentation scenario, particularly in those cases where a non-human linea aspera appeared particularly similar to the human one.

In the study focused on nutrient foramina, three features (location, appearance, direction) were examined, while for shape and angle of foramina, micro-CT scanning was used (see section 5.3.3). 384 bones were observed to identify the location, appearance and direction of the primary nutrient foramen, where the main artery runs, as each long bone might have subsidiary, smaller nutrient foramina (Bostrom, Yang and Koutras, 2000). Location and direction were explored as identification parameters in other studies (Dongchoon, 2013; Hughes, 1952; Johnson, Beckett and Marquez-Grant, 2017); the present study is the first in the field where the appearance of the nutrient foramina is considered as a potential parameter for the identification of fragmented bones.

As for the location, the section of the shaft where the foramen is located was considered (e.g. proximal, medial, etc.), and when possible, the presence of close features such as muscle markings was taken into account and recorded. The foraminal index (Hughes, 1952), which is usually used to give a percentage value to the nutrient foramen location (in terms of distance from the epiphyses) was not used in this study, because it would be of no use in a forensic (or bioarchaeological) situation where bone fragments are found.

To define the appearance of the foramina, features such as shape, vascular groove characteristics and orientation were observed, using a magnifying lens. The direction of the foramina was detected with a 27G x 3/4 in hypodermic needle (Campos, Pellico, Alias and Fernandez-Valencia, 1987; Fig. 5.18).

Fig. 5.18. Sheep radius. The hypodermic needle was used to detect the direction of the foramen. The proximal epiphysis is on the right.

5.3.3 Micro Computed Tomography

Micro Computed Tomography (micro-CT) was employed in this study because it is a high resolution imaging method that allows to carry out a precise non-destructive analysis of very small features such as nutrient foramina, and of the cross-sectional shape without sectioning the bones. Furthermore, it is a rapid technique that permits to scan a sample in a short time, within 40 minutes to 12 hours. Micro-CT is a high-resolution X-ray based imaging modality that enables the acquisition of digital images and the processing of 3D images of small samples (Gantt, Grine and Martin, 2007). An X-ray generator emits X-rays that pass through the sample and are recorded by a detector, which produces a projection image; the sample is rotated and the procedure is repeated, until the rotation is completed (Sisniega, Vaquero and Desco, 2014; Fig. 5.19). X-rays are generated by a microfocus X-ray tube that emits a beam of electrons accelerated by a voltage of up to 240 kV, which are focused onto a tungsten or similar metal target (du Plessis, Broeckhoven, Guelpa and le Roux, 2017). The X-rays are directed through the sample and are collected by a 2D X-ray detector as a projection image, or radiograph; during the process, hundreds or thousands of 2D projection images, acquired from different angles by rotating the sample, are recorded. After scanning, a 3D data set is produced with the projection images, by using filtered back-projection algorithms (Lin and Miller, 2002). The 3D volumes allow for the multidirectional examination of an area of interest and for advanced measurements, for example dimensional or volumetric (Singhal, Grande and Zhou, 2013).
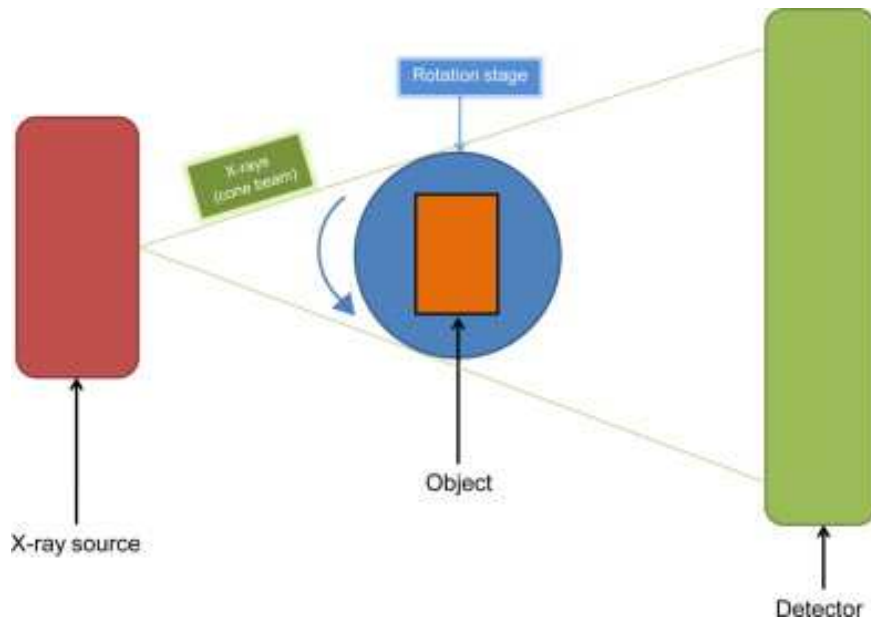
Fig. 5.19. Micro-Computed Tomography principle (Hindelang, Zurbach and Roggo, 2015).

Micro-CT is used in a variety of fields, such as dental research, anatomical imaging, materials analysis, pharmaceutical research, comparative anatomy (mainly human-primates) and in vivo animal and plant testing (Stock, 2011). It is used in palaeoanthropology (for fossil reconstruction) and biological/forensic anthropology, particularly for age and cortical thickness estimation, pathology diagnosis and individual identification (Wu and Schepartz, 2009; Franklin, Swift and Flavel, 2016).

Out of 384 limb bones, 61 were selected for micro CT-scanning, ensuring that all the species considered in this study and both adult and juvenile individuals were included. The bones were scanned with a Nikon Metris X-tek XT H 225 micro-CT scanner, at the Cranfield Forensic Institute. The micro-CT scanner utilizes a proprietary 225 kV microfocus X-ray source, with 3 µm focal spot size, which gives high image visibility of detail. It offers a large inspection volume, as it is able to accommodate small to medium sizes samples weighing up to 15 kg. Despite the large inspection volume of the micro-CT scanner that allowed to accommodate even the largest non-human bones, these were cut with a band saw, in order to sample the area that had the primary nutrient foramen; the bones were cut only to reduce the number of scans, given the high costs of the procedure. The bones that were cut and the complete small bones were scanned in bundles, with individual bones wrapped in plastic bags to allow for digital separation of the data for each bone (Fig. 5.20-5.21). The settings, which were kept for the scanning of all the samples, were as follows: 500 ms exposure time, 100 kV,

50 uA (microA), system set to optimize projections (usually 1571), with two frames per projection, voxel size 0.137 mm.
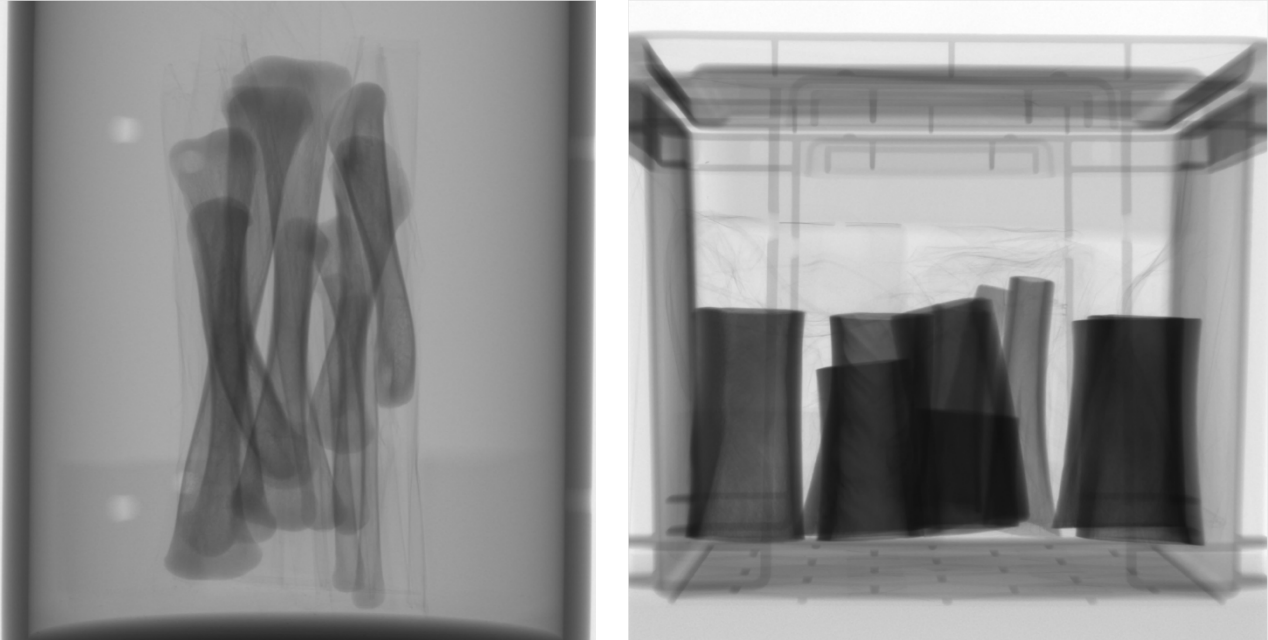
Fig. 5.20-5.21. Bundle of complete chicken bones in a cylindric plastic container (5.20); cut pig and deer bones in a squared plastic container (5.21). Foam sheets were used to keep the bones still during the scanning

The micro-CT images were then processed with CT Pro software and manipulated with VG Studio Max software (v. 2.1; Fig. 5.22-5.23), in order to detect the shape of the nutrient canal entrance and calculate the angle at which the canal enters in the bone. To isolate the section of the bone showing the nutrient foramen, the region of interest was extracted; the object was oriented using simple registration, to specify the coordinate system. Surface determination and extraction were carried out in order to detect the shape of the canal entrance on the YZ plane (proximal-distal/distal proximal view, depending on the direction) and on the XY plane (exterior-interior view), and to calculate the angle on the XZ plane (side view).
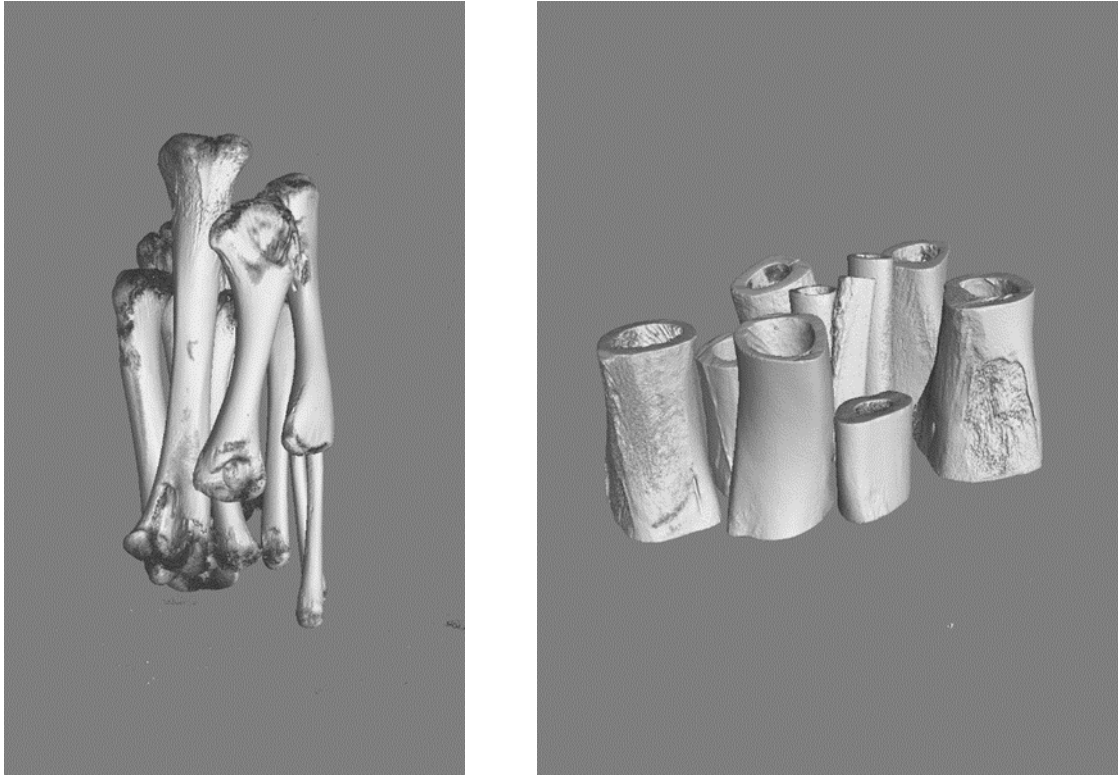
Fig. 5.22-5.23. 3D reconstruction of the chicken bones bundle (left) and the pig and deer cut bones (right) seen in images 5.20 and 5.21, before being processed.

In the study focused on the cross-sectional shape, 58 human and non-human limb bones were scanned. The scanning procedure was the same used for nutrient foramina, including the scanner settings. The micro-CT images were manipulated with VG Studio Max software to detect the cross-sectional shape of the shafts, at the 50% of the bone length (mid-shaft). To isolate the section of the bone showing the cross-sectional shape, the region of interest was extracted; the object was oriented using simple registration; surface determination and extraction were carried out in order to detect the shape at the mid-shaft on the YZ plane (proximal-distal view).

A qualitative approach was employed for the comparison between human and non-human cross-sectional shape of long bones, as no quantitative data would have been consistent with the aims and objectives of this research. Initially it was thought that the cortical thickness of limb bones could be calculated. However, it was decided to exclude this feature because it can considerably vary according to bone section and side, is not homogeneous and is not applicable to some bones, such as non-human ulnae, which have a reduced medullary canal. Furthermore, physical activity makes the cortical thickness too variable to be used as a parameter to distinguish human from non-human bones,

especially in a fragmentation context (Warden *et al*., 2014). Other quantifiable cross-sectional measurements would be useful only in the field of evolutionary anatomy. Some examples are the second moment of area, used to characterize the resistance of a bone to bending around an axis; cortical area, used to estimate the ability of a bone to withstand axial compression; ratio of the second moments of area in the maximum and minimum direction, used to quantify the circularity or ellipticity of the cross-section (Young, 1989; Lieberman, Polk and Demes, 2004; Marelli and Simons, 2014). The above mentioned quantitative data would not be useful in the identification of the human or non-human origin of a fragmented bone; the cross-sectional shape was the only feature considered as recognizable in a bone fragment and therefore helpful to identify its origin.

5.4 Concluding remarks

In this chapter, the materials and the methods used for the research were described. Some of the bone features considered, such as cranial sutures, occipital condyles and nutrient foramina, are not commonly used in bioanthropology for the differentiation between human and non-human fragments. As for the techniques used, morphological examination and micro-CT have found widespread use in bioanthropology, although micro-CT is not regularly used for the human/non-human distinction; in this research, GIS software found a relatively new application in bioanthropology, since it is commonly used in other fields, such as geography, engineering and archaeology.

The following diagram (Fig. 5.24) summarizes the contents of this chapter, showing the methods used, the bone features to which they were applied, and the number of bones used for each feature.
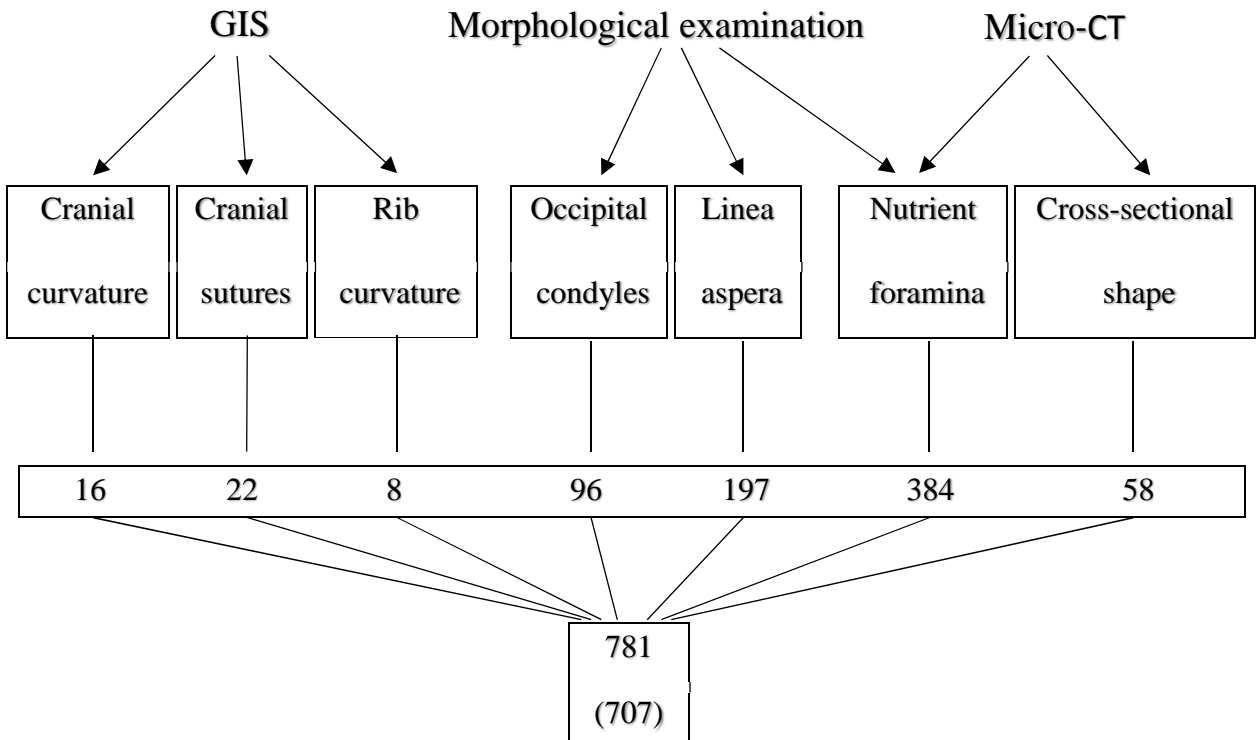
Fig. 5.24. Summary diagram of materials and methods. The total number of bones used for this research is 707. 781 is the total number of bones that includes the ones for which more than one feature was observed: the 16 skulls used both for cranial curvature and sutures are double counted, and the 58 limb bones counted for the cross-sectional shape study were the same scanned in the nutrient foramina study.

Therefore: 781 - 16 - 58 = 707.

Chapter 6: RESULTS

This chapter presents the results of the thesis. Initially, the results relating to the analysis of cranial and rib curvature and cranial sutures with a GIS software are presented (section 6.1). This is followed by the results of the morphological examination of occipital condyles and linea aspera (sections 6.2 and 6.3 respectively). In the occipital condyles section (6.2), the characteristics of the occipital condyles in each species considered (including humans) are observed, then a detailed comparison of human condyles with those of the most challenging non-human species considered follows; a table that summarizes the main characteristics of human and non-human condyles concludes the section. In section 6.3., the observation of the linea aspera in each species considered is followed by a closer analysis of the similarities and the differences between human and non-human linea aspera. The results relating to the examination and the micro-CT analysis of nutrient foramina are presented in section 6.4. Section 6.5 presents the results of the micro-CT analysis of the limb bones cross-sectional shape of mammals (including humans) and birds; the shapes are compared and then considered in a hypothetical fragmentation scenario. The last section of this chapter (6.6) shows the results of a blind test carried out on of bone fragments whose human or non-human origin was not known.

6.1 Cranial curvature, sutures and rib curvature

6.1.1 Cranial curvature

The curvature calculation process with ArcGIS generated numeric values and classification statistics (count, minimum, maximum, sum, mean, standard deviation; see Appendix A). The mathematically derived values describe the shape of the surfaces on a cell-by-cell basis; more specifically, they describe the degree to which a surface is convex (positive values) or concave (negative values) at that cell.

For each species, the four mean values were compared in SPSS, in order to group them for further calculations and to show the degree of variation between individuals of the same species (Table 6.1):

Species	N	Mean	Std. Deviation
Fox	4	11	117.45
Calf	4	32	110.45
Sheep	4	-22	69.91
Human	4	11	119.46

Table 6.1. Mean values comparison, divided by species

As the means comparison and the high values of standard deviation show, there is a high variability among skulls of the same species.

A Student's t-test for independent samples (unpaired) was performed, in order to determine whether there is a statistically significant difference between the means of sheep, calf and fox cranial curvature and the means related to human curvature.

The independent t-test requires that the dependent variable is approximately normally distributed within each group. A Shapiro-Wilks test of normality was performed for each group; in all four groups the data were normally distributed (sheep, $p = 0.99$; calf, $p = 0.89$; fox, $p = 0.50$; human, $p = 0.32$).

The independent t-test assumes the variances of the two groups are equal. The assumption of homogeneity of variance was assessed using Levene's test of Equality of Variances. The group

variances could be treated as equal (sheep, σ^2 = 3665.50; calf, σ^2 = 9149.59; fox, σ^2 = 10345.24; human, σ^2 = 10703.36).

The null hypothesis for the independent t-test is that the population means from the two unrelated groups are equal: H$_0$: u1 = u2; the alternative hypothesis is that the population means are not equal: Ha: u1 ≠ u2. The independent t-test calculates the size of the mean difference and a p-value, or probability of type I error (an erroneous rejection of a true null hypothesis).

An independent t-test was run on the data with a 95% confidence interval (CI) for the mean difference. The results were as follows:

- Sheep – Human cranial curvature: t (6) = 0.485, p = 0.644, with a difference of 33.60 (95% CI, -135.73 to 202.94); the absolute value of the calculated t is smaller than the critical value (0.485<2.447), so the means are not significantly different;
- Calf – Human cranial curvature: t (6) = 0.251, p = 0.809, with a difference of 20.46 (95% CI, -178.58 to 219.51); the absolute value of the calculated t is smaller than the critical value (0.251<2.447), so the means are not significantly different;
- Fox – Human cranial curvature: t (6) = 0.0053, p = 0.995, with a difference of 0.44 (95% CI, -204.51 to 205.40); the absolute value of the calculated t is smaller than the critical value (0.0053<2.447), so the means are not significantly different.

In all cases, the null hypothesis was not rejected, and the probability of type I error was high, as p>0.05. The cranial curvature in fox and human skulls appeared as equal (t = 0.0053, p = 0.995), which means that the fragmented parietals of these two species could not be distinguished on the basis of their curvature. As for calf and sheep, their cranial curvature appeared as different from the human one, but the difference was not statistically significant.

The test was repeated using four human parietal bone fragments (6 to 10 cm), from four different individuals. A test involving both human and non-human fragments would have been ideal, in order to test the curvature comparison method with GIS on actual fragments (instead of hypothetical fragments, as done in this study); however, it was not possible to obtain non-human cranial fragments. The only possible solution was to compare the values of the human fragments with the non-human values obtained in the original study.

The variability among the human parietal fragments used for the test was much lower than the one seen in human skulls in the original study, being SD = 6.01, M = 1.84 (compared to SD = 119.46, M= 11). The normal distribution of the data was tested with a Shapiro-Wilks test (p = 0.27). A Levene's test of Equality of Variances was used to assess the homogeneity of variance; the population variance measured in the human fragments (σ^2 = 27.14) was different from the one measured in sheep, calf and fox groups at the 0.05 significance level. Since the group variances could not be treated as equal, when running the t-test the option "Equal variances not assumed" was used. The results of the independent t-test were as follows:

- Sheep – Human cranial curvature: t (6) = 0.586, p = 0.578, with a difference of 20.58 (95% CI, -65.25 to 106.43); the absolute value of the calculated t is smaller than the critical value (0.586<2.447), so the means are not significantly different;
- Calf – Human cranial curvature: t (6) = 0.605, p = 0.567, with a difference of 33.48 (95% CI, -101.85 to 168.81); the absolute value of the calculated t is smaller than the critical value (0.605<2.447), so the means are not significantly different;
- Fox – Human cranial curvature: t (6) = 0.213, p = 0.837, with a difference of 12.57 (95% CI, -131.30 to 156.44); the absolute value of the calculated t is smaller than the critical value (0.213<2.447), so the means are not significantly different.

As in the first test, in all cases the null hypothesis was not rejected, and the probability of type I error was high, as p>0.05. The difference between human and non-human curvature values was not statistically significant.

6.1.2 Sutures

Figures 6.1-6.16 represent the output of the contour lines creation in ArcGIS. The images were cut in order to highlight the sagittal suture (in dark blue). The contour interval applied was 1; at first, a bigger contour interval was applied, but the sutures were not visible and could not be distinguished from the rest of the surface.
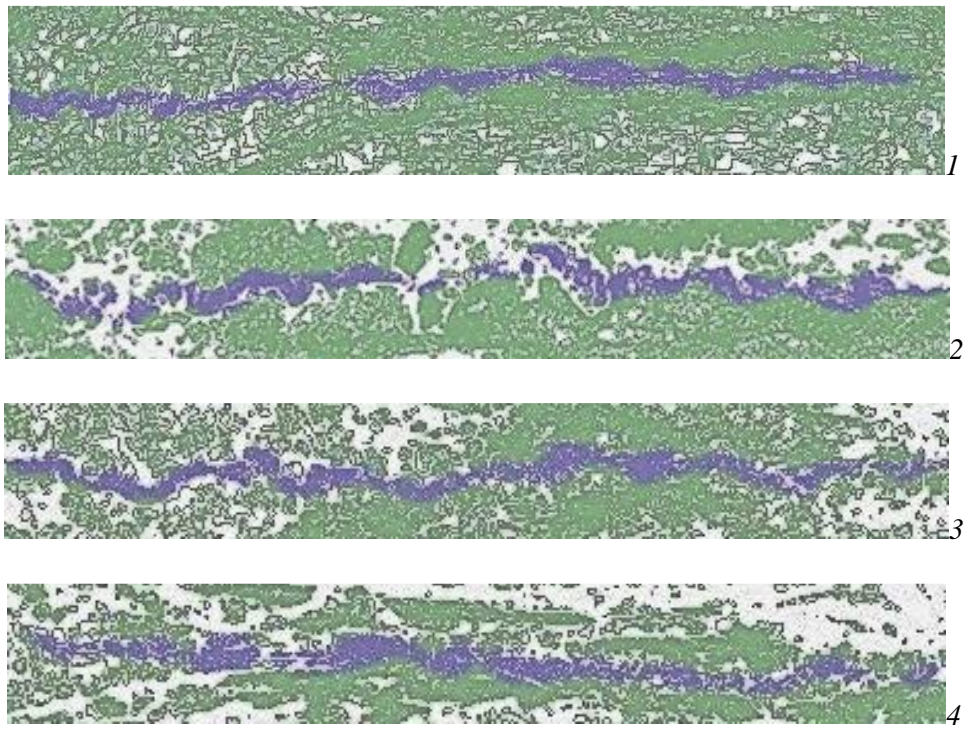
Fig. 6.1-6.4. Fox sagittal suture (in dark blue)
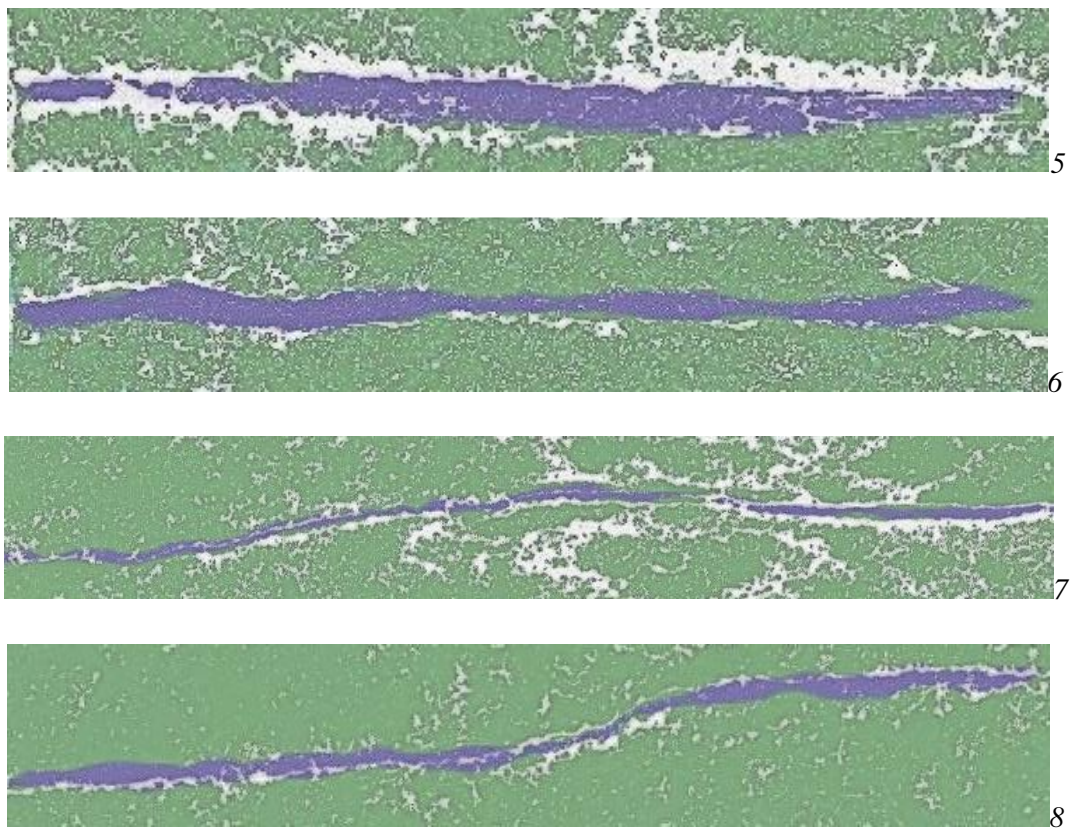
Fig. 6-5-6.8. Calf sagittal suture (in dark blue)
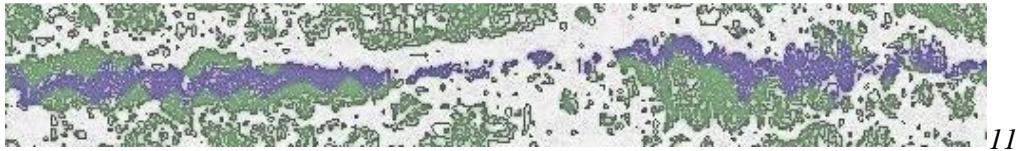
Fig. 6.9-6.12. Sheep sagittal suture (in dark blue)
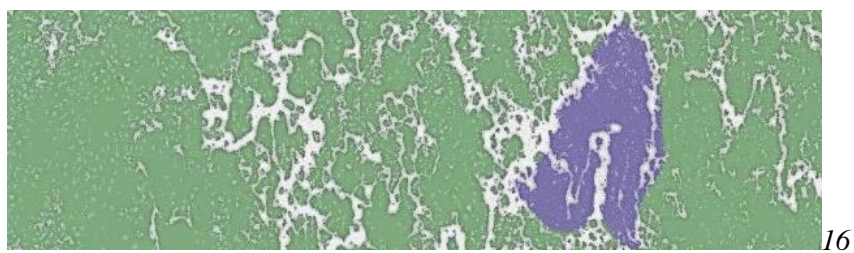
Fig. 6.13-6.16. Human sagittal suture (in dark blue)

The suture patterns were clearly visible in all images, except for no. 6.15 and 6.16 (the last two), which show two human adults with the sagittal suture partially obliterated. Since the partial or total closure of a cranial suture prevents the creation of contour lines, this method may not fully work with older individuals.

As for the fox, the sagittal crest may interfere with the sagittal suture and partially cover it; however, in most of the images the difference between the two can still be seen (the crest is much more linear than the suture); the suture can also be seen on the frontal area of the neurocranium, where the crest is absent.

Calf sutures are clearly the less similar to the human ones, as their pattern is mostly linear.

Young foxes seem to have more indented sutures than adult ones, and this can make them more similar to humans; the two adult foxes (Fig. 6.1 and 6.4) show a more linear pattern, therefore their cranial bones may be less problematic if found fragmented, as they would clearly appear non-human.

Among the non-human species considered in this study, sheep seems to be the one with the most human-like sutures; the pattern looks particularly similar on the posterior part of the sagittal suture, towards the lambdoid suture.

However, when the suture patterns produced by ArcScene were highlighted and compared, the differences among the species (and the intra-species similarities) became clearer. Each species showed a specific sagittal suture pattern: undulated in foxes (young individuals), linear in calves, closely denticulated in sheep (undulated in some cases), and largely denticulated in humans (Table 6.2).

Species	Sagittal suture pattern	
Fox		Undulated
Calf		Linear
Sheep		Closely denticulated
Human		Largely denticulated

Table 6.2. Sagittal suture pattern, divided by species

This method was tested on six fragments of human crania showing the sagittal suture (Fig. 6.17).
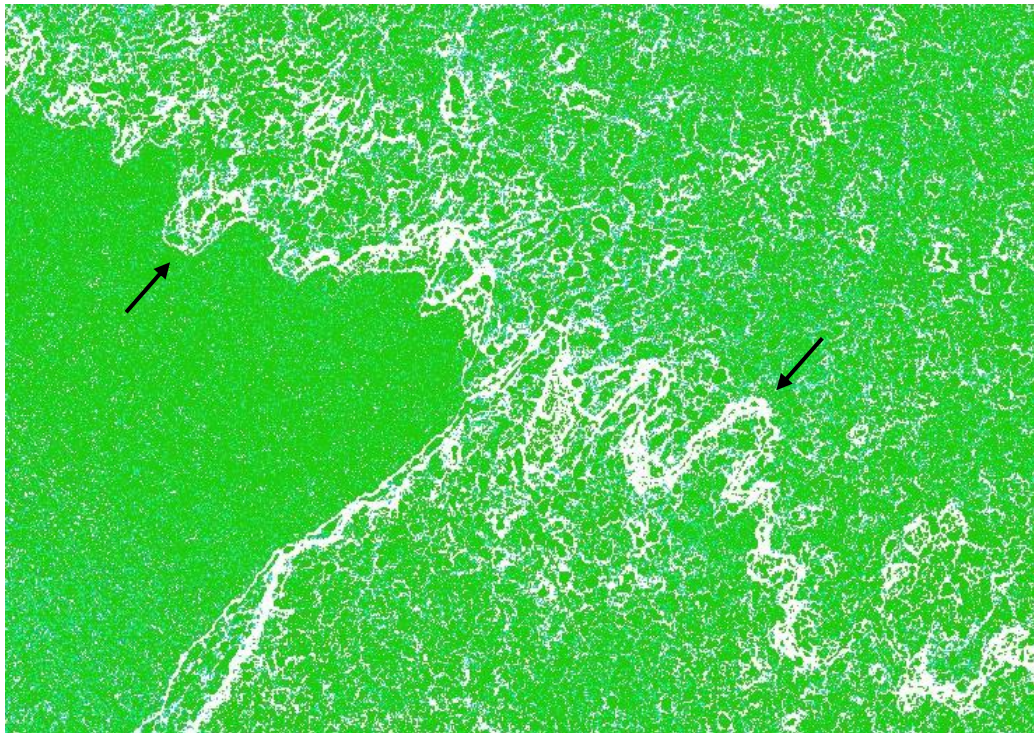
Fig. 6.17. Sagittal suture of a human cranial fragment, as seen using the GIS method

The image above shows two cranial fragments that belonged to the same individual and that were temporarily reattached in order to test the contour lines method with ArcGIS. In the left half of the image (indicated by the upwards arrow), only one side of the suture is visible, while on the right half (downwards arrow) the two reattached fragments show the complete suture pattern. When only one side of the suture is available, the suture pattern cannot be securely identified with the contour lines, because in a 2D raster image the ectocranial and the endocranial sutures tend to overlap, as shown in Fig. 6.18:
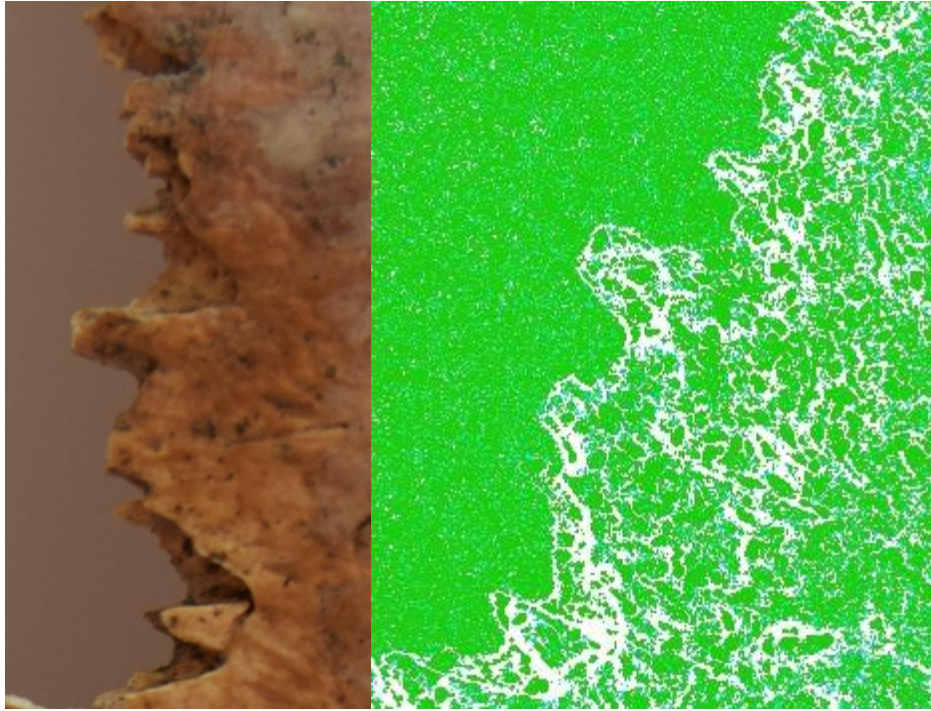
Fig. 6.18. 2 cm suture fragment (left) and the same fragment as seen in ArcGIS (right).

The complete suture shown in the right half of Fig. 6.17 was highlighted and compared with the human pattern shown in Table 6.2 (Fig. 6.19-20):

Fig. 6.19. Suture pattern of cranial fragment tested

Fig. 6.20. Human sagittal suture pattern

The suture of the cranial fragment follows the same largely denticulated pattern seen in the other human crania considered in this study.

6.1.3 Rib curvature

As in the cranial curvature calculation process, the curvature feature in ArcGIS generated numeric values representing the degree of concavity/convexity of a surface, and classification statistics (see Appendix B). The means obtained were compared in order to look at the rib curvature variability within the same species, in superior view, inferior view and in both (Table 6.3-6.4):

View	N	Mean	Std. Deviation
Superior	4	-7	8.19
Inferior	4	-6	1.36
Superior and Inferior	8	-6	5.50

Table 6.3. Comparison of mean values of human rib curvature

View	N	Mean	Std. Deviation
Superior	4	2	6.96
Inferior	4	1	2.06
Superior and Inferior	8	1	4.76

Table 6.4. Comparison of mean values of pig rib curvature

As the low values of standard deviation show, there is low variability in the rib curvature of the same species, in particular when the curvature is measured in inferior view.

The same procedure seen in the comparison of parietal curvatures was followed. A Student's t-test for independent samples (unpaired) was performed, in order to determine whether there is a statistically significant difference between the means of human and pig rib shaft curvature, in superior, inferior, and combined views.

Since the independent t-test requires that the dependent variable is approximately normally distributed within each group, a Shapiro-Wilks test of normality was performed; in all six groups the data were normally distributed (human superior, $p = 0.86$; human inferior, $p = 0.99$; human superior and inferior, $p = 0.89$; pig superior, $p = 1.0$; pig inferior, $p = 0.65$; pig superior and inferior, $p = 0.88$).

The independent t-test assumes the variances of the two groups are equal. The assumption of homogeneity of variance was assessed using Levene's test of Equality of Variances. The group variances could be treated as equal (human superior, $\sigma^2 = 50.23$; human inferior, $\sigma^2 = 1.39$; human superior and inferior, $\sigma^2 = 26.47$; pig superior, $\sigma^2 = 36.34$; pig inferior, $\sigma^2 = 3.20$; pig superior and inferior, $\sigma^2 = 19.85$).

An independent t-test was run on the data with a 95% confidence interval (CI) for the mean difference. The results were as follows:

- Human superior view – Pig superior view: t (6) = 1.679, p = 0.144, with a difference of 9.02 (95% CI, -4.12 to 22.16); the absolute value of the calculated t is smaller than the critical value (1.679<2.447), so the means are not significantly different;
- Human inferior view – Pig inferior view: t (6) = 5.511, p = 0.001, with a difference of 6.83 (95% CI, 3.79 to 9.86); the difference is very statistically significant; the absolute value of the calculated t exceeds the critical value (5.511>2.447), so the means are significantly different;
- Human superior-inferior view – Pig superior-inferior view: t (14) = 3.080, p = 0.008, with a difference of 7.92 (95% CI, 2.40 to 13.44); the difference is very statistically significant; the absolute value of the calculated t exceeds the critical value (3.080>2.145), so the means are significantly different.

In the comparison between human and pig rib shaft curvature in superior view, the null hypothesis (H_0: u1 = u2) was not rejected and the probability of type I error was higher than 0.05. In the comparison between rib curvatures in inferior and combined views, the null hypothesis was rejected and the probability of type I error was very low (lower than 0.05). Therefore, in this cases the alternative hypothesis (Ha: u1 ≠ u2) must be accepted, as the population means are not equal. If the rib shaft curvature is calculated from the inferior point of view, or if both superior and inferior views are considered, a human rib would appear different from a pig one (or viceversa); the method tested can be potentially useful for the differentiation between human and pig fragmented rib shafts.

6.2 Occipital Condyles

Bird crania have particular characteristics that make them very different from any human bone, thus they cannot be misidentified as human even when found fragmented. Occipital condyles were observed in pheasant, pigeon, chicken, turkey, duck, and goose skulls. Below the condyles of these six bird species are described, although they can be easily recognized and thus excluded from further comparative analyses.

Pheasant *(Phasianus colchicus*; N = 3*)*. Both juvenile and adult individuals have a unique cranium, which is too different from the human one. It is very light, and the bone has a smooth and glossy texture. It has only one bean-shaped, pointing upwards, bulbous and remarkably elevated occipital facet.

Pigeon *(Columba palumbus, Columba livia*; N = 4*)*. As in pheasants, its occipital condyle is single, bean-shaped with the two lateral extremities pointing upwards, bulbous and elevated (Fig. 6.21). The surrounding bone appears extremely light, airy and translucent, therefore even fragments of a pigeon skull could not be misidentified for a non-bird animal.

Domestic fowl/Chicken *(Gallus gallus*; N = 3*)*. The occipital condyle is similar to the pheasant and pigeon one (single, bean-shaped, pointing upwards, bulbous and elevated); the only difference is the presence of two foramina on both sides and a pit immediately below it. The foramen magnum is drop-shaped.

Turkey *(Meleagris gallopavo*; N = 2*)*. Although its skull is larger, it has the exact same characteristics as the chicken.

Duck *(Anas platyrhynchos*; N = 2*)* **and Goose** *(Anser anser*; N = 2*)*. The crania of these two species share the same characteristics. The occipital condyles are very similar to those of the other birds observed. The foramen magnum resembles the chicken one, although it is more oval and pear-shaped.

Fig. 6.21. Pigeon skull, ventral view. A single, bean-shaped occipital condyle (arrow) is present in all the bird species observed.

Unlike birds, several mammal crania may share some characteristics with the human ones, making the origin assessment of some cranial fragments potentially challenging. The mammal species observed for the comparison of occipital condyles are cat, rabbit/hare, badger, fox, dog, cow, horse, sheep/goat, pig, deer, and seal.

Cat *(Felis domesticus*; N = 3*).* Its occipital bone is very robust, with a rough surface. The foramen magnum is rhomboidal, slightly more curved on the inferior half, with an upward oriented nutrient foramen just above it. On its sides, there are two comma-shaped condyles, bulbous, smooth and not joined inferiorly. The condyles are remarkably elevated, but their borders flatten on the inferior portion (Fig. 6.22).

Rabbit *(Oryctolagus cuniculus*; N = 6*)* **and Hare** *(Lepus europaeus*; N = 6*).* The foramen magnum is rhomboidal, with slightly convex superior portions. The two occipital facets appear like slightly

twisted comma and do not join inferiorly. As in the cat, the condyles have strongly elevated borders, which flatten inferiorly (Fig. 6.23).
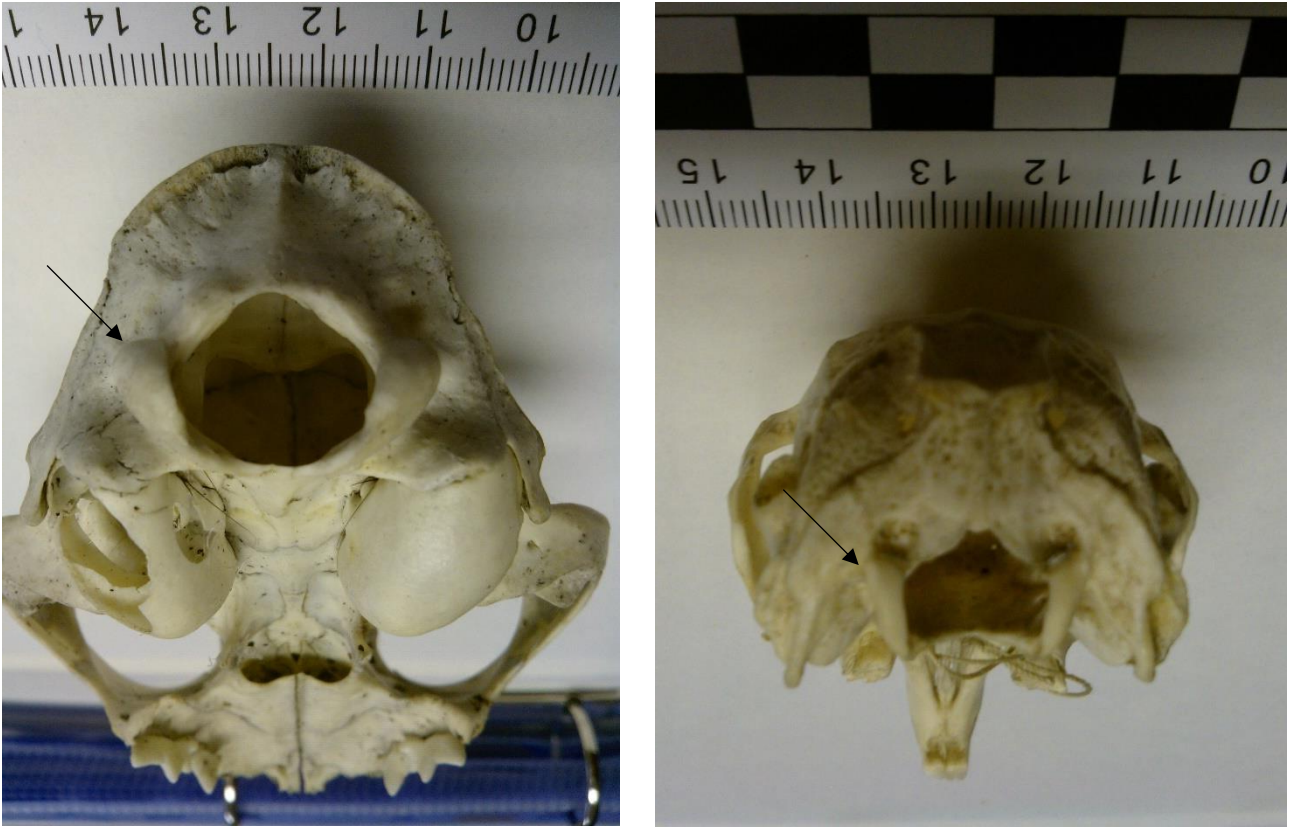
Fig. 6.22-6.23. Cat and Rabbit skull, posterior view (arrow indicates the condyles)

Badger *(Meles meles*; N = 3*)*. The shape of the foramen magnum resembles a rounded isosceles triangle, with protruding and sharp edges. The occipital condyles are bulbous and drop-shaped, not remarkably elevated like in other non-human mammals; they have a lateral-medial orientation. Inferiorly, the condyles narrow, flatten and join (Fig. 6.24-6.25).
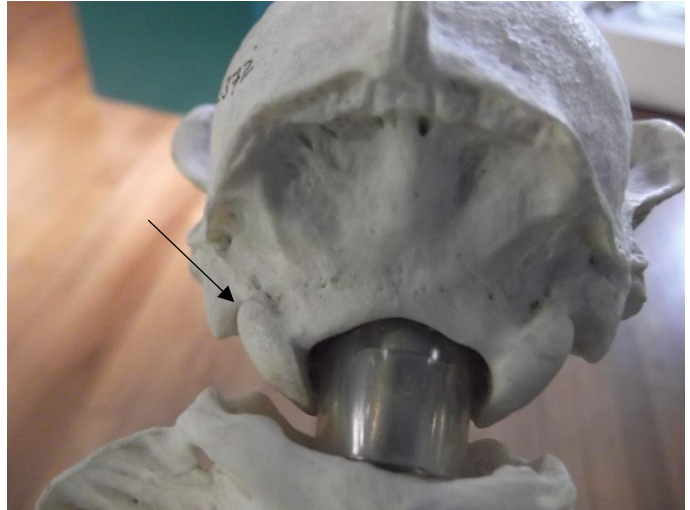
Fig. 6.24-6.25. Badger skulls, posterior view. Fig. 6.24 clearly shows the foramen magnum; fig. 6.25 shows the occipital condyles (arrow).

Fox *(Vulpes vulpes*; N = 7*).* Its foramen magnum has a rounded rhomboidal shape, with elevated and protruding edges. The smooth occipital facets are bean-shaped and remarkably elevated. As seen in badgers, the condyles narrow and flatten inferiorly; they can unite or not (variability among various fox skulls was noticed). There are also two foramina behind each condyle (Fig. 6.26).
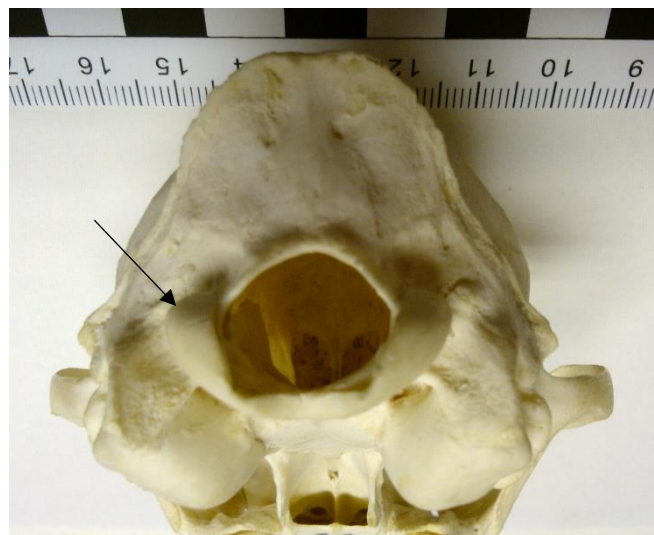
Fig. 6.26. Fox skull, posterior view

Dog *(Canis lupus familiaris*; N = 11*)*. Dog skulls can be very different from each other, because of the high number of existing breeds. Dog skulls of several breeds, whose number depended on the Oxford Archaeology and Grant Museum of Zoology availability, were observed. It was noticed that the overall shape of the condyles and the foramen magnum remains the same. The foramen magnum has an irregular shape, which resembles a pentagon with the three inferior faces slightly convex and the two superior ones concave; the uppermost part tends to be more pointed. The occipital condyles can be comma-shaped or bulbous rectangles, which flatten inferiorly, but do not join. Their lateral borders are very elevated, while their medial ones are barely visible (Fig. 6.27). Juvenile dog skulls of some breeds may have condyles that strictly resemble the human ones; however, as already stated in Chapter 5, even if human-like they are fully formed and then too small to be human (Fig. 6.28).
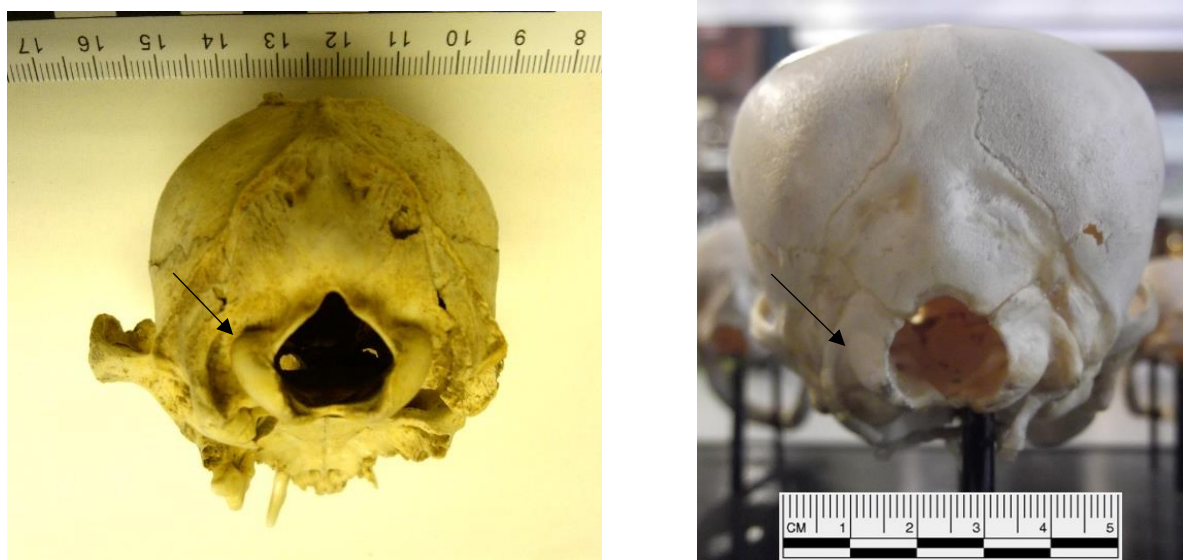
Fig. 6.27-6.28. Adult and juvenile dog skulls, posterior view

Cow *(Bos Taurus*; N = 8*)*. The complete occipital condyles of an adult cow skull are too big to be misidentified as human (Fig. 6.29). If a cow skull fragment with a complete condyle is found, its origin assessment would not be challenging. Identification problems may arise if a fragmented cow condyle or a fragmented calf skull are found. The foramen magnum is nearly perfectly rounded. As for the occipital condyles texture, they tend to be smooth to rough; usually rough condyles can be found in adult individuals. Their shape is irregular: in posterior view, the condyles resemble the flippers of a pinball, slightly curved and with sharp edges (Fig. 6.29); in ventral view, their shape is similar to an hourglass silhouette (Fig. 6.30). Their borders are neat and strongly elevated, with a

thickness of 2-3 mm, which raises to 4 mm in the central portion. Inferiorly, the condyles flatten, although not completely (as seen in other species), and are distinctly separated.
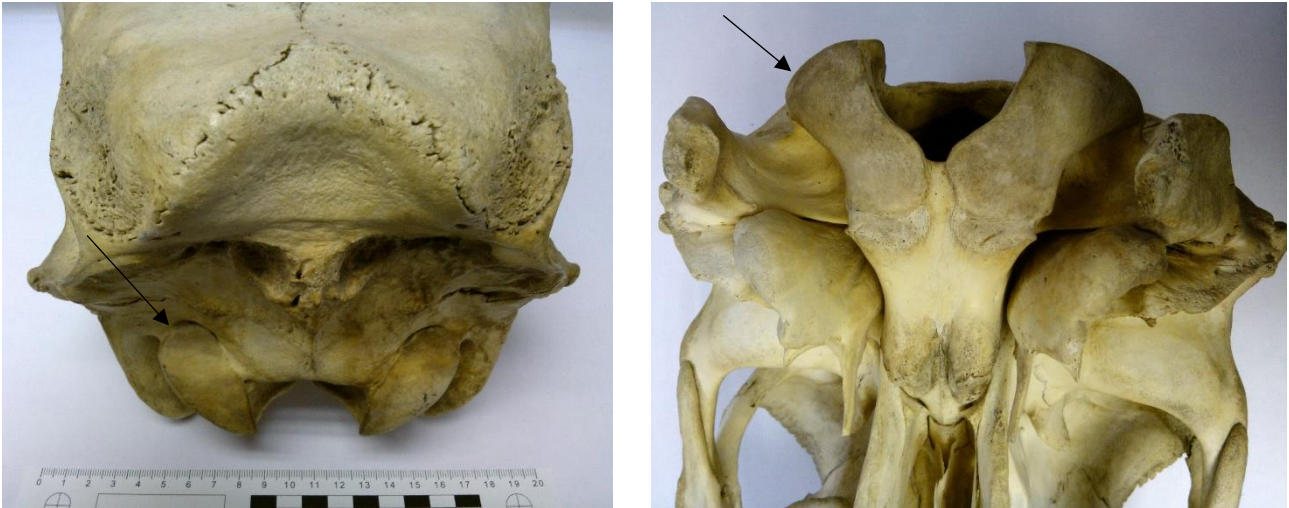
Figure 6.29-6.30. Cow skull, posterior and ventral view

Horse *(Equus caballus*; N = 3*).* The foramen magnum has a slightly flattened oval shape. Its superior border is bulbous, with foramina and ridges that run parallel towards the centre, in a V scheme. As in cows, the occipital facets have an irregular shape. In posterior view, their shape is similar to the one seen in cows, but more bulbous and much less oblique than cows, as their position is nearly parallel to the foramen magnum (Fig. 6.31). In ventral view, their shape resembles an overturned isosceles triangle with a rounded tip. The condyles do not meet inferiorly (Fig. 6.32).
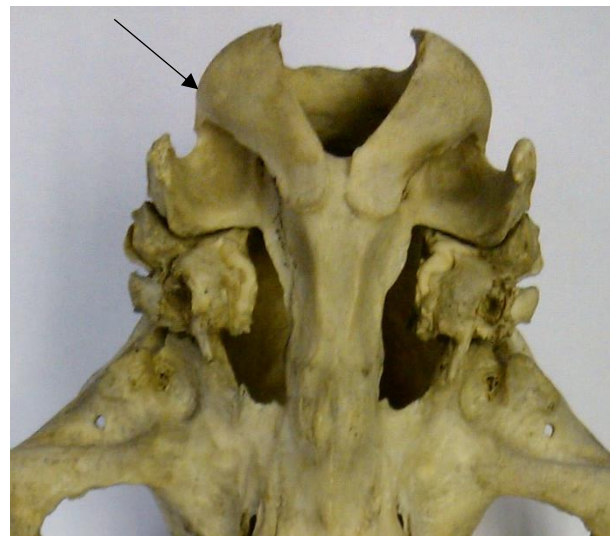
Fig. 6.31-6.32. Horse skull, posterior and ventral view

Sheep *(Ovis aries*; N = 11*)* **and Goat** *(Capra aegagrus hircus*; N = 5*).* The foramen magnum can have a mushroom shape or a rounded rhomboid one, with the two superior faces slightly convex, as seen in cows. In one sheep it was a perfect hexagon, with rounded angles. In goats, the foramen magnum shape resembles a reversed acorn. The occipital condyles are bulbous and comma-shaped (in goats they are much wider than in sheep), and do not meet inferiorly. Their borders are only slightly elevated (<1mm; Fig. 6.33-6.34).
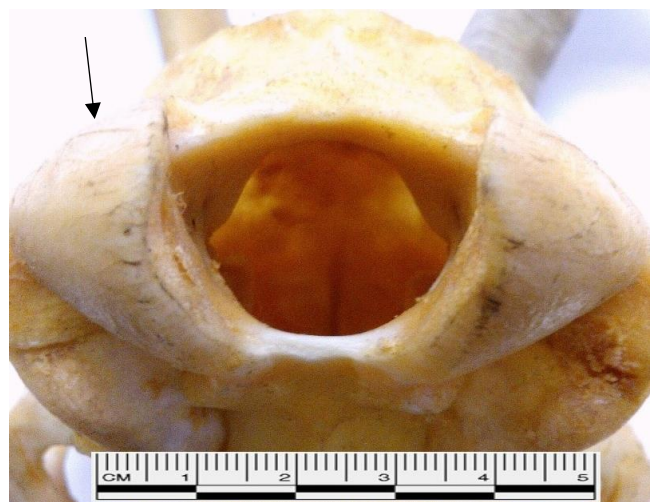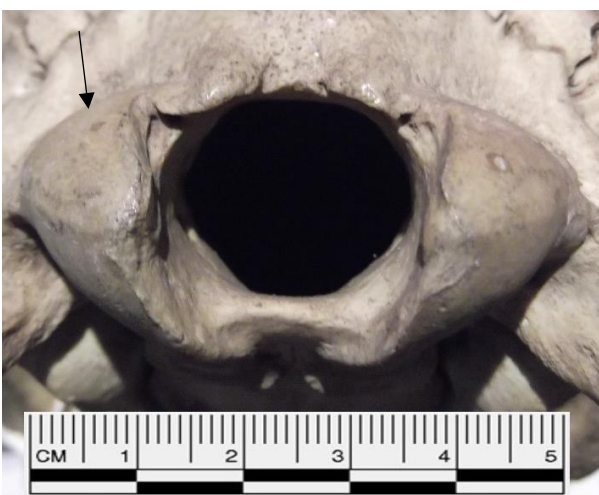
Fig. 6.33-6.34. Sheep and Goat skulls, posterior view

Pig *(Sus scrofa domesticus*; N = 3*)*. Its foramen magnum has an equilateral triangle shape, with rounded edges and a domed rim. Pig skulls have very raised occipital condyles, which have a rough texture. It was noticed that some individuals have much smoother muscle markings and condyles, probably because of sex differences. In posterior view, condyles are drop-shaped, with the tip pointing downwards (Fig. 6.35); postero-inferiorly, they are comma-shaped, and do not meet inferiorly (Fig. 6.36). In infant pigs, condyles are bean shaped.
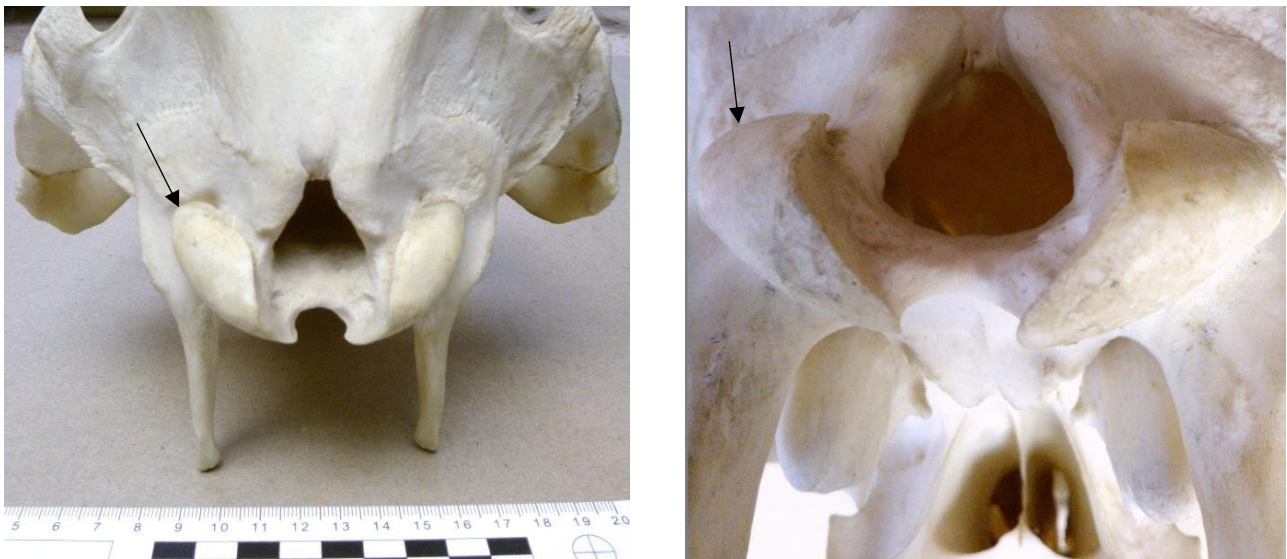
Fig.6.35-6.36. Pig skull, posterior and postero-inferior view

Deer *(Dama dama*, N = 3; *Capreolus capreolus*, N = 2; *Cervus elaphus*, N = 1*)*. The foramen magnum has an oval shape, slightly flattened horizontally. The occipital condyles are smooth, and their borders are almost completely flat. Posteriorly, they are eye-shaped, while ventrally/inferiorly their shape resembles a bulbous twisted comma; the condyles do not meet inferiorly (Fig. 6.37-6.38). On the anterior end of the condyles there are very strong muscular attachments for the *rectus capitis* muscles, which sustain and move the neck, and are particularly strong in male individuals, because of the antlers.
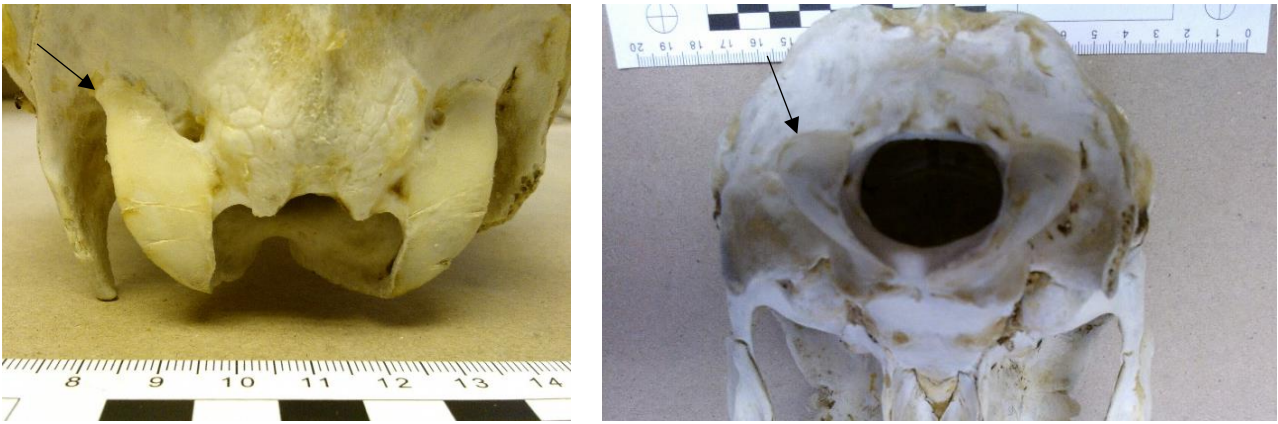
Fig. 6.37-6.38. Deer skull, posterior and ventral view.

Seal. Several types of seals were observed, however most of the attention was focused on common seal (*Phoca vitulina*; N = 1) and grey seal (*Halichoerus grypus*; N = 2), which are the two common types living in the United Kingdom (the ones living in Arctic and Antarctic were first observed but then excluded). In grey seal, the foramen magnum is a rounded rhomboid. The occipital condyles have an elongated bean shape. Inferiorly the condyles do not meet, although they are very close to each other (Fig. 6.39). In common seal, the foramen magnum has a rhomboidal shape, horizontally flattened and with rounded edges. The condyles have an elongated bean shape with bulbous edges; inferiorly, condyles do not meet and tend to narrow (Fig. 6.40).
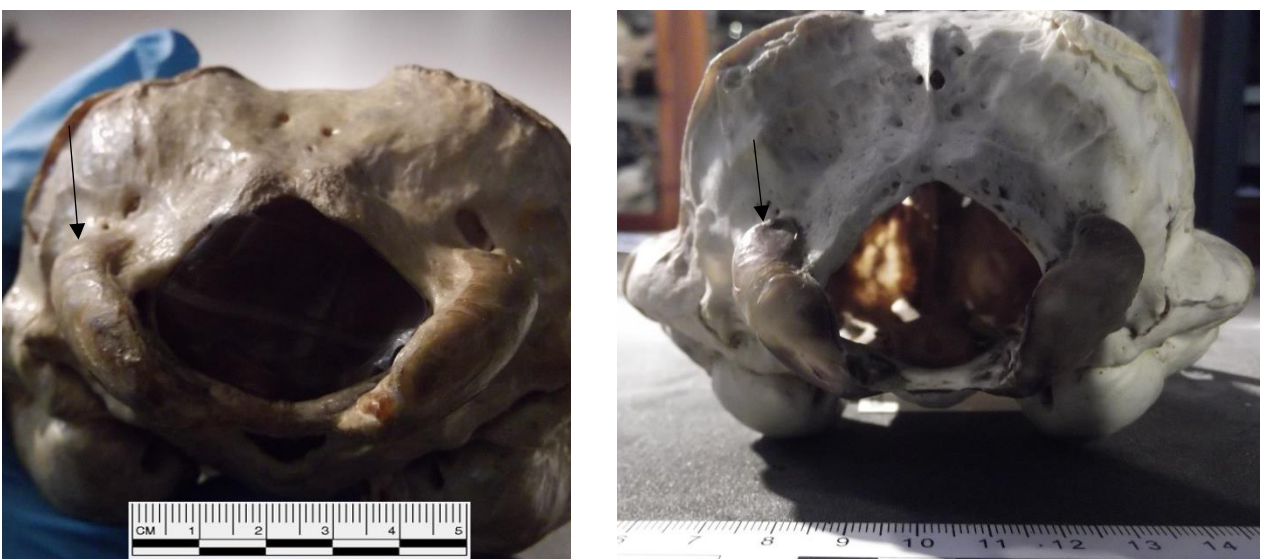
Fig. 6.39-6.40. Grey seal and Common seal skulls, posterior view

Human *(Homo sapiens*; N = 11*)*. The foramen magnum has an oval shape, or a very rounded rhomboidal one (Fig. 6.41). Generally, the occipital condyles are bean-shaped, although in some cases they can be circular, eight-like, triangular, S-like or kidney-shaped. There may also be individuals with deformed or two-portioned condyles (Kalthur, Padmashali, Gupta and Dsouza, 2014). In all cases, condyles have a smooth surface and do not meet inferiorly.

Fig. 6.41. Human occipital bone, inferior view

The following table (Table 6.5) summarizes the data obtained with the morphological examination of the human and non-human occipital bone. For each species the foramen magnum shape, occipital condyles shape, condyles texture and borders are shown. The last column says if the occipital condyles meet/do not meet inferiorly.

Species	F.M. shape	O.C. shape	O.C. texture	O.C. borders	O.C. meet inf.
Pheasant	/	bean-shaped, pointing up	smooth, glossy bulbous	elevated	single condyle
Pigeon	/	bean-shaped, pointing up	translucent, bulbous	elevated	single condyle
Chicken	drop-shaped	bean-shaped, pointing up	smooth, bulbous	elevated	single condyle
Turkey	drop-shaped	bean-shaped, pointing up	smooth, bulbous	elevated	single condyle
Duck-Goose	oval drop/ pear-shaped	bean-shaped, pointing up	smooth, bulbous	elevated	single condyle
Cat	rhomboidal	comma-shaped	smooth, bulbous	elevated, flattened inf.	no
Rabbit/Hare	rhomboidal	twisted comma-shaped	smooth	elevated, flattened inf.	no
Badger	isosceles triangle-shaped	drop-shaped, narrowed inf.	bulbous	flat	yes
Fox	rounded rhomboidal	bean-shaped, narrowed inf.	smooth	elevated	yes/no
Dog	irregular, pentagonal	comma-shaped/rectangular	bulbous	elevated laterally	no
Cow	rounded	flipper-like post., hourglass-like inf.	smooth/rough	sharp, very elevated	no
Horse	slightly flattened oval	flipper-like post., isosc. triangle inf.	bulbous	bulbous	no
Sheep/Goat	mushroom/rhombus/ hexagon/acorn-like	comma-shaped	bulbous	slightly elevated	no

Pig	rounded equilateral triangle-shape	drop-shaped post., comma-shaped post-inf.	rough	elevated	no
Deer	oval	eye-shaped post., bulbous twisted comma-shaped inf	smooth	flat	no
Seal	rounded rhomboidal	elongated bean-shape	smooth	bulbous	no (very close)
Human	oval/ very rounded rhomboidal	bean-shaped (rarely circular, eight-like, triangular, S-like, kidney-shaped)	smooth	bulbous	no

Table 6.5. Characteristics of the occipital condyles, divided by species

The data summarized in the table above can be further narrowed down, in order to clearly see which non-human species share specific characteristics with humans. In the table below (Table 6.6), each column shows the characteristics of human foramen magnum/condyles, and the non-human species that have those same characteristics (birds were excluded).

Oval/ very rounded rhomboidal foramen magnum	Bean-shaped occipital condyles	Smooth textured condyles	Bulbous occipital condyles borders	Occipital condyles do not meet inferiorly
Deer (oval) Fox Seal (rounded rhomboid)	Fox Infant pigs	Rabbit/Hare Fox Cow Deer Seal	Horse Seal	Cat Rabbit/Hare Fox Dog Cow Horse Sheep/Goat Pig Deer Seal

Table 6.6. Characteristics of human condyles and the non-human species where they can be seen

As in human skulls, the deer skull has an oval foramen magnum, and its occipital condyles are smooth and do not meet inferiorly. However, these three similarities are not enough to consider deer as a challenging species, if occipital fragments were found. Indeed, only in a situation where just the foramen magnum were found the presence of deer remains could be considered, but the finding of the foramen magnum alone is rare, if not impossible. Furthermore, two condyles that do not meet inferiorly cannot be used as the only feature for the identification of a fragment, as many species have this characteristic; if two condyles that do not meet inferiorly are found, other characteristics such as shape and borders must be considered in order to understand the human or non-human origin of the fragment. Accordingly, as shown in the table above, cat, dog, sheep, goat and adult pigs can be excluded from the list of species that can be challenging if occipital remains are found, as their condyles share only one characteristic with the human ones, namely that they do not meet inferiorly. This characteristic alone is not enough for the origin assessment of an occipital bone fragment.

As for the fox, it seems to be a more challenging species, as its foramen magnum has a rounded-rhomboid shape, and its occipital condyles are bean-shaped, smooth and do not meet inferiorly, as in humans (although there are some cases among foxes where the condyles do meet). Unlike human,

fox occipital condyles show very elevated borders; this characteristic may help to quickly assess the non-human origin of a fragmented occipital condyle. The only possible scenario where a fox condyle may be very challenging is one where the borders have been completely eroded and then are not more visible. However, this scenario is extremely specific and unlikely to happen, as the erosion process cannot exclusively involve the condyles borders and leave the condyle surface undamaged.

Unexpectedly, seal occipital area appears to be the most similar to the human one, as its characteristics are almost the same as seen in humans. Indeed, as in humans the grey/common seal has a foramen magnum with a rounded rhomboidal shape, and smooth occipital condyles with bulbous borders that do not meet inferiorly (although they can be very close to each other). Nonetheless, its condyles have an elongated bean-shape, while the human ones are bean-shaped; the difference can be clearly seen if two pictures are compared. Theoretically, a challenging scenario would be one where common/grey seal fragmented occipital condyles are found, therefore their complete shape cannot be seen. However, if better observed, seal occipital condyles can be easily distinguished from the human ones, even if found in a fragmentary state. As can be seen in the pictures above (Fig. 6.39-6.40), overall seal condyles are more powerful and robust than the human ones (Fig. 6.41), and the basis on which they rest is much more elevated. The occipital bone itself is more bulky in seal skulls, therefore if condyles are found with a portion of occipital bone their non-human origin can be easily assessed (despite the similarities between human and seal foramen magnum rim). Furthermore, in seal skulls the superior part of the occipital condyles lies far from the foramen magnum, while in human ones the medial edge of the condyles lies on the foramen rim. Conversely, in human skulls the inferior portion of the condyles is far from the foramen magnum, while in the seal ones the medial edge of the condyles lies on the foramen rim.

As already mentioned earlier, foetal/infant pig skulls have bean-shaped occipital condyles. However, other than this pig occipital condyles and foramen magnum do not share any characteristic with the human ones. Although condyles in infant pigs may closely resemble the human ones, they would be too small and fully formed to be human, as in humans the occipital condyles are not completely formed until 5-7 years of age.

As regards rabbit/hare, cow and horse, they share only one, non-relevant characteristic with human occipital condyles (besides the inferior non-union). Indeed, rabbit/hare and cow condyles tend to have the same texture of the human ones, while in horse skulls only the condyles borders are human-like. These similarities are not enough to make the occipital condyles of these species challenging if found in a fragmentary state.

The following table (Table 6.7) contains the main foramen magnum and occipital condyles shapes encountered, along with the condyles texture and borders characteristics. This table and table 6.5 can be used when the origin of fragmented and/or isolated occipital condyles needs to be identified. The underlined entries correspond to the foramen magnum and occipital condyles types seen in human crania; if during the observation of fragmented condyles all the underlined entries are ticked, the fragment might be safely identified as human. The variations shown in table 6.5 should also be considered.

Foramen magnum shape	drop	pear	rhombus	isosc. triangle	rounded rhombus		
	pentagon	rounded	flat oval	equil. triangle	oval		
Condyles shape	bean	comma	drop	flipper-like	hourglass	isosc. triangle	eye
Condyles texture	smooth	rough	bulbous				
Condyles borders	flat	bulbous	slightly elevated (<1mm)	elevated	very elevated (>2-3mm)	elevated laterally	elevated, flattened inferiorly	sharp
Condyles meet inferiorly	yes	no	single condyle				

Table 6.7. Main shapes and characteristics of human and non-human occipital condyles. The underlined entries correspond to a possible human origin

6.3 Linea aspera

Human *(Homo sapiens*; N = 26*).* In the human femur, the linea aspera is flanked by two lips, the *labium mediale* and the *labium laterale,* which originate as medial and lateral ridges proximally, and continue as medial and lateral supracondylar ridges distally (Fig. 6.42). Proximally, the medial ridge diverges into the spiral line (origin of the *vastus medialis* muscle) and the pectineal line (insertion of the *pectineus* muscle), while the lateral ridge runs up to the base of the greater trochanter as gluteal tuberosity (attachment for the *gluteus maximus* muscle) (Polguj *et al.*, 2013). Distally, the medial and lateral supracondylar ridges enclose the popliteal surface, a triangular area where the popliteal artery passes (Martini, Timmons and Tallitsch, 2012) (Fig. 6.43).
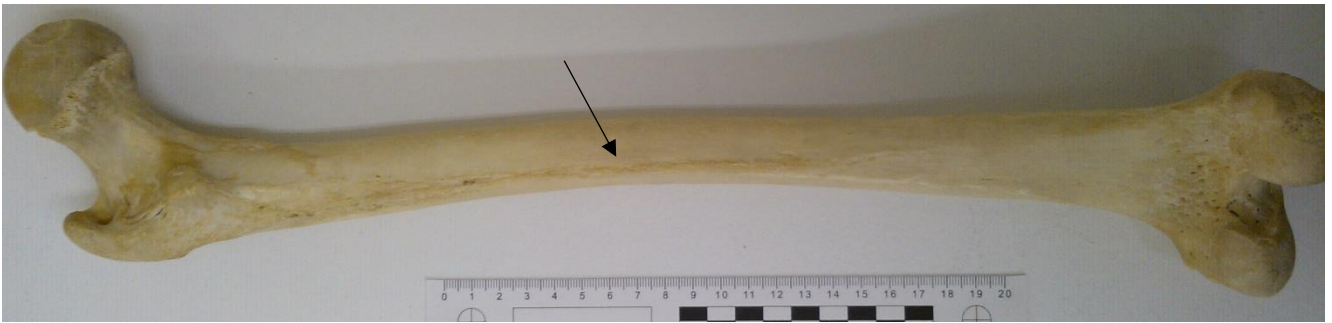
Fig. 6.42. Human left femur, posterior view. The arrow indicates the linea aspera
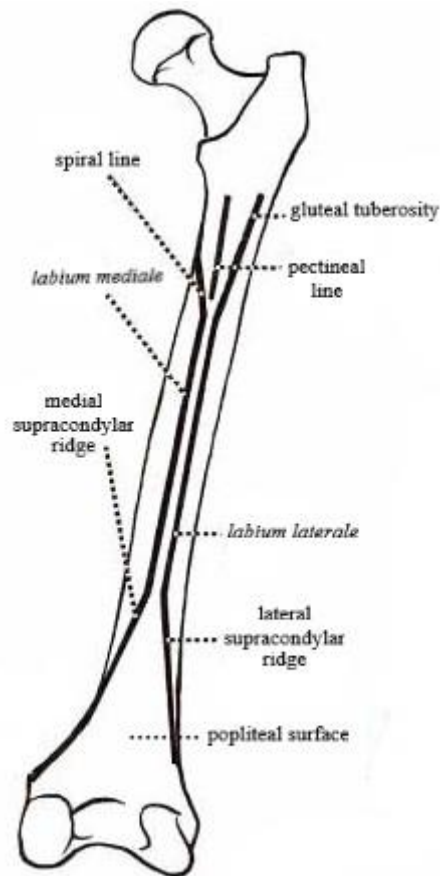
Fig. 6.43. Schematic representation of the linea aspera (O'Rahilly, Muller, Carpenter and Swenson, 2008; image modified)

Pheasant *(Phasianus colchicus*; N = 6*)*. Overall, the femur is glossy (Beisaw, 2013) and very smooth. The linea aspera is double, with an X-like structure, with two lines that meet in the distal half of the shaft, alongside the nutrient foramen (Fig. 6.44). The medial line goes from the lesser trochanter to the medial condyle, while the lateral one goes from the posterior distal portion of the greater trochanter to the lateral condyle. The area enclosed between the two lines is very smooth.
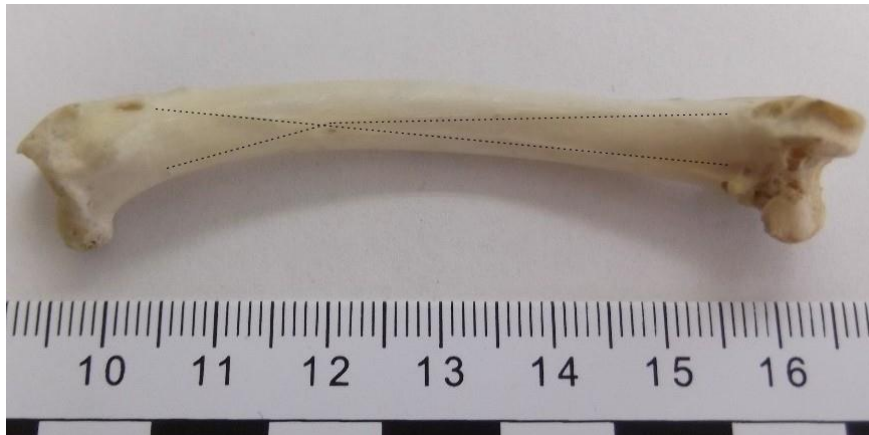
Figure 6.44. Pheasant left femur, posterior view. The dashed line highlights the linea aspera

Pigeon *(Columba palumbus, Columba livia*; N = 8*)*. The long bones in pigeons are all very smooth, glossy and translucent. As in pheasant, the linea aspera is double and X-like, but the lines meet in the proximal half, enclosing the nutrient foramen (Fig. 6.45).

Fig. 6.45. Pigeon right femur, posterior view. The dashed line highlights the linea aspera

Chicken *(Gallus gallus*; N = 16*)*. As in other birds, the linea aspera is double and X-like, although it is sharper and rough. The medial line is sharper and longer than the lateral one, as it extends for the whole length of the shaft; the lateral line starts from the mid-shaft and ends increasingly flattening at the lateral condyle (Fig. 6.46).

108

Fig. 6.46. Chicken right femur, posterior view. The dashed line highlights the linea aspera

Turkey *(Meleagris gallopavo*; N = 4*).* Its linea aspera has the same appearance as the chicken linea aspera (Fig. 6.47).
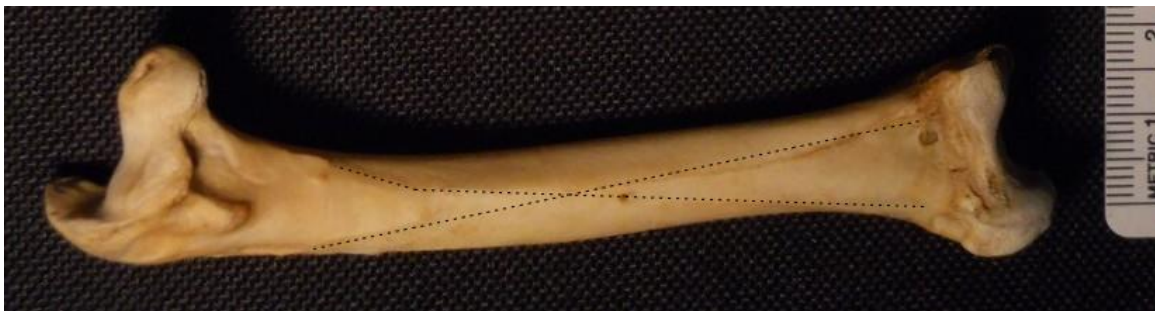
Fig. 6.47. Turkey left femur, posterior view (Avli 167, archaeol. https://hiveminer.com).

The dashed line highlights the linea aspera

Duck *(Anas platyrhynchos*; N = 8*).* The linea aspera is double, and its X-like structure is evenly divided between the proximal and the distal part of the shaft, with the nutrient foramen at the exact centre of the posterior shaft. As in the chicken, the medial line is sharper. The area enclosed between the two lines is rougher than the rest of the femur (Fig. 6.48).

Fig. 6.48. Duck right femur, posterior view. The dashed line highlights the linea aspera

Goose *(Anser anser*; N = 4*).* Its linea aspera is double and V-like, formed by two lines that origin from the superior part of the shaft and meet at the centre of the distal shaft, where lays the nutrient foramen. The medial line is very sharp, while the lateral one is barely visible (Fig. 6.49).

Fig. 6.49. Goose right femur, posterior view. The dashed line highlights the linea aspera

Cat *(Felis domesticus*; N = 8*).* The linea aspera is double, although only on the superior shaft. Indeed, two lines start on the lesser trochanter and on the posterior portion of the greater trochanter respectively, and meet in the middle of the shaft, on the nutrient foramen. On the distal portion of the shaft, there is only a single line that ends on the medial condyle. Overall, the linea aspera has a Y-like shape (Fig. 6.50).

Fig. 6.50. Cat right femur, posterior view. The dashed line highlights the linea aspera

Rabbit *(Oryctolagus cuniculus*; N = 13*)* **and hare** *(Lepus europaeus*; N = 13*).* The whole femur has a very smooth texture, except for the linea aspera, which is made of two parallel lines that lie mainly in the proximal part of the shaft (Fig. 6.51).

Figure 6.51. Rabbit right femur, posterior view (utep.edu). The dashed line highlights the linea aspera

Badger *(Meles meles*; N = 6*).* Its femur and its other long bones are robust, as in all scavengers. The plateau linea aspera extends for most of the posterior shaft surface. A lateral line starts from the posterior portion of the greater trochanter and a medial one starts in the exact middle of the proximal shaft. The two lines run parallel to the middle shaft, where lies the nutrient foramen, then pull away from each other and reach the condyles (Fig. 6.52). The area enclosed between the lines is very rough.

111

Figure 6.52. Badger left femur, posterior view. The dashed line highlights the linea aspera

Fox *(Vulpes vulpes*; N = 4*).* The linea aspera is double, formed by two lines that start from the lateral and medial upper shaft respectively, and get closer at the nutrient foramen, which lies on the proximal half of the shaft. From the foramen, the two lines run parallel and very close to each other to the condyles. The area enclosed between the two lines is concave, especially on the distal part of the shaft, where a straight groove is formed (Fig. 6.53).

Figure 6.53. Fox right femur, posterior view. The dashed line highlights the linea aspera

Dog *(Canis lupus familiaris*; N = 18*).* As for the long bones, a few breeds were available for the study; this may give only partial results, as dog skeletons of different breeds can have different

characteristics. However, when the pictures of the femora observed were compared with those present in veterinary medicine books (Aspinall and Cappello, 2015; de Lahunta, 2013; Johnston and Tobias, 2018; Newton and Nunamaker, 1985), all breeds appeared to be the same when it comes to the linea aspera. The linea aspera is double, and follows the X-structure seen in other species: two lines (with the lateral one rougher than the medial one) meet at the nutrient foramen in the superior half of the shaft, then flare and reach the condyles. The area enclosed between the lines is very rough (Fig. 6.54).

Fig. 6.54. Dog left and right femur, posterior view. The dashed line highlights the linea aspera

Cow *(Bos Taurus*; N = 8*).* The linea aspera is double and encloses a very rough area, including the supracondyloid fossa on the lateral distal shaft. The lateral line of the linea aspera is longer than the medial one, extending from the inferior portion of the greater trochanter to the lateral condyle; the medial line starts on the proximal half of the shaft and proceeds diagonally to the popliteal surface, above the condyles (Fig. 6.55).

Fig. 6.55. Cow right femur, posterior view. The dashed line highlights the linea aspera

Horse *(Equus caballus*; N = 5*).* The horse posterior femur has extremely powerful muscle attachments. The double linea aspera has its origin on the lesser trochanter, where two lines (with the medial one much more large and rough) bifurcate and run diagonally with a medial-lateral orientation to the middle third of the femur. Here the two lines join again, forming an extended rough area lateral to the nutrient foramen (Fig. 6.56). The whole lateral line serves as attachment for the great adductor muscle (Stubbs, 1976).

Figure 6.56. Horse right femur, posterior view. The dashed line highlights the linea aspera

Sheep *(Ovis aries*; N = 24*)* **and Goat** *(Capra aegagrus hircus*; N = 24*).* The double linea aspera is made by two sharp lines that originate from the postero-inferior portions of the femoral head and of the greater trochanter respectively; the two lines run parallel from the proximal to the distal shaft (Fig. 6.57).
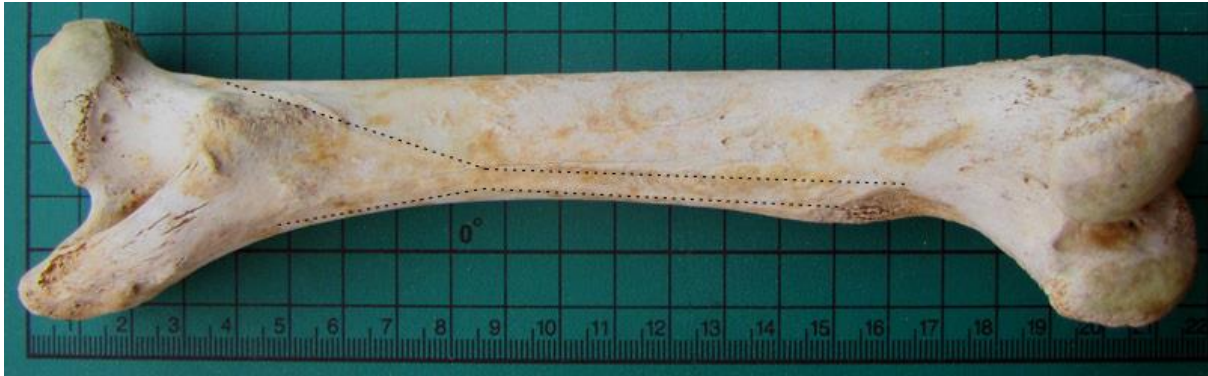
Figure 6.57. Sheep left femur, posterior view (Natural History Museum, London).
The dashed line highlights the linea aspera

Pig *(Sus scrofa domesticus*; N = 18*).* The linea aspera is double. The lateral line originates at the posterior surface of the greater trochanter, while the medial one originates at the lesser trochanter. The two lines follow a crooked X-like scheme, laterally oriented, ending at the distal third of the shaft. The medial line ends at the nutrient foramen (Fig. 6.58).

Figure 6.58. Pig left femur, posterior view. The dashed line highlights the linea aspera

Deer *(Dama dama*, N = 11; *Capreolus capreolus*, N = 8; *Cervus elaphus*, N = 2). Overall, the deer species have a smooth femur, being the linea aspera the only rough area. The double linea aspera has a lateral line that originates at the greater trochanter and a medial line that originates at the lesser trochanter. Slightly above the middle third of the shaft, the two lines get very close to each other, ending lightly flared in the distal third of the shaft. Three species of deer were observed. It was noticed that the linea aspera and the muscle markings may differ in roughness and sharpness between the species, but their general structure remains the same (Fig. 6.59-6.60).

Fig. 6.59-6.60. Fallow deer and Roe deer right femur, posterior view.

The dashed line highlights the linea aspera

In the table below (Table 6.8), the structure of the linea aspera in the species observed, including humans, is summarized:
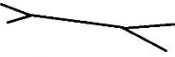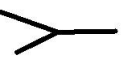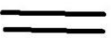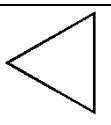
Species	Linea Aspera	
Human		Single
Pheasant		Double, X-like
Pigeon		Double, X-like
Chicken		Double, X-like
Turkey		Double, X-like
Duck		Double, X-like
Goose		Double, V-like
Cat		Double, Y-like
Rabbit/Hare		Double, two parallel lines
Badger		Plateau, bottleneck-like
Fox		Double, funnel-like
Dog		Double, X-like
Cow		Double, triangle-like
Horse		Double, D-like
Sheep/Goat		Double, funnel-like
Pig		Double, crooked X-like
Deer		Double, crooked narrow X-like

Table 6.8. Linea aspera shape, divided by species. The drawings represent the linea aspera as seen horizontally, where left is proximal and right is distal.

117

As for the main shape of the linea aspera, the drawings show a clear and strong resemblance between human and deer; in pheasant, pigeon, chicken, turkey and duck only the distal portion of the linea aspera resembles the human one, while in dogs the only human-like portion of the linea aspera is the proximal one.

Further observations on the characteristics of the linea aspera in each species and comparisons with the human femur may help to establish which non-human species should be taken into account in case of fragmented femoral remains and which ones can be definitively excluded.

- **Pheasant.** In the proximal half of the linea aspera (the one ending at the nutrient foramen), the lines are slightly sharp and do not have the roughness that can be seen and touched on human femur. The central portion is made by two parallel lines that enclose a smooth surface; the human linea aspera does not have parallel lines in any of its portions. As for the distal part, in pheasant femur the popliteal surface enclosed is convex, as the cross-sectional shape of the femoral shaft is mainly circular, while in human the popliteal surface is flat, therefore the two lines that enclose it cannot be confused with those of a pheasant even in a fragmentary state (Fig. 6.61).

Fig. 6.61. Pheasant-Human linea aspera comparison.

- Pigeon. The proximal lines of the linea aspera are barely visible. The central and inferior portions are rough, however if fragmented they would appear glossy and translucent, then non-human and easily identifiable as bird bone. Despite the similarities in the main structure of the linea aspera of pigeon and human, the glossy and translucent texture of the pigeon femur makes this species impossible to misidentify as human when it comes to femoral shaft fragments (Fig 6.62).

Fig. 6.62. Pigeon-Human linea aspera comparison

- Chicken/Turkey. On the proximal portion, the lateral line is barely visible, and the medial one has a zig-zagged outline that the human linea aspera does not have in any of its portions. The central portion is made of two very sharp parallel lines, again not seen in the human femur. On the distal portion, the main pattern is similar to the one seen in the human linea aspera; however, as in pheasant, the popliteal surface is convex, and the lines that enclose it are sharper than the ones seen in human femur at the same location (Fig. 6.63).

Fig. 6.63. Chicken-Human linea aspera comparison

- Duck. The proximal medial line shares several characteristics with the human linea aspera, including the main outline and the roughness. However, if fragmented, this portion can still be distinguished from the human one, as in duck the line is elevated, while in human it is relatively flat. Furthermore, the cross-sectional shape of the proximal portion of the femur can help to assess the non-human origin of a fragment showing the linea aspera, as it tends to be circular in duck and flattened posteriorly in human. As for the distal portion, as seen in the drawings the main scheme in duck may be similar to the human one, but the duck femur has a rougher and more rounded popliteal surface, which is moreover enclosed by sharper lines (Fig. 6.64). The only portion of the duck posterior femur that may be challenging if found fragmented is the central portion of the linea aspera, as laterally to it the nutrient foramen can be seen, as in humans; further observations on the nutrient foramina in long bones are made later in this chapter (section 6.4).

Fig. 6.64. Duck-Human linea aspera comparison

- Goose. The medial line is sharp, while the lateral one is a barely visible line that ends as a very narrow groove in proximity to the nutrient foramen; none of these characteristics is seen in human linea aspera (Fig. 6.65).

Fig. 6.65. Goose-Human linea aspera comparison

- Cat. As for the proximal half, the lateral line is barely visible and the medial one is too smooth to be misidentified as any of the portions of the human linea aspera. The distal line (starting from the nutrient foramen) is a narrow groove not seen in the posterior shaft of the human femur (Fig. 6.66).

Fig. 6.66. Cat-Human linea aspera compatison

- **Rabbit/Hare**. The lines that make the linea aspera are relatively smooth, as the rest of the femoral surface. They may look similar to the ones seen in the distal portion of the human femur; however, in rabbit and hare femur they do not enclose a flat popliteal surface. Furthermore, the main cross sectional shape of the rabbit/hare femur is circular, therefore the surface between the two lines is convex (Fig. 6.67).

Fig. 6.67. Rabbit-Human linea aspera comparison

- Badger. Its linea aspera is not made of lines, but is an extended area that covers most of the posterior femoral shaft; furthermore, its popliteal surface is much deeper than the human one (Fig. 6.68). There are no features in the badger posterior femoral shaft that may be misidentified as human if found fragmented.

Fig. 6.68. Badger-Human linea aspera comparison

- Fox. Proximally to the nutrient foramen, the lines are barely visible, while the rest of the linea aspera appears too different from the human one, as it forms a long, straight, shallow groove that is not seen on human femur (Fig. 6.69).

Fig.6.69. Fox-Human linea aspera comparison

- Dog. The proximal portion of the linea aspera appears as very similar to the human one, as its lateral line has the same roughness, position and outline of the human one, making potentially difficult the origin assessment of a femoral fragment showing this portion of the linea aspera. However, if better observed, it can be noticed that in dog femur the line is slightly hollow; this particular can make the proximal portion of the dog linea aspera distinguishable from the human one. As for the mid-distal portion, in dogs the linea aspera flares and becomes an extended rough area with sharp borders, while in human femur it remains a single line (Fig. 6.70).

Fig.6.70. Dog-Human linea aspera comparison

- **Cow.** The superior portion of the linea aspera and the whole medial line may look similar to the inferior ones seen on human femur, as they have the same outline and sharpness; however, in cow these lines do not enclose a popliteal surface, therefore the bone surface between them is convex and not flat as in humans. As for the inferior portion of the lateral line, it appears very different from anything on human femur, as it gets rougher and wider, and includes a massive supracondylar fossa (Fig. 6.71).

Fig. 6.71. Cow-Human linea aspera comparison

- **Horse**. The medial line of the linea aspera is too wide to be challenging in a fragmentation context. As for the lateral one, it may look a human-like rough line, but at a closer look it appears too sharp to be human, and its undulating pattern is different from the straight one seen on human femur (Fig. 6.72).

Fig.6.72. Horse-Human linea aspera comparison

- Sheep/Goat. Its linea aspera is made of two very sharp lines that do not look like any of the portions of the human linea aspera. Furthermore, the lines enclose a concave area, in particular on the mid-distal shaft. Along with the main scheme, these characteristics make sheep and goat posterior femoral shaft non-identifiable as human (Fig. 6.73).

Fig. 6.73. Sheep-Human linea aspera comparison

- Pig. The lines that form the linea aspera may be similar to the human ones in terms of roughness and main outline. However, while the human linea aspera is rough but relatively flat, in pig femur it is raised, being sharp on its proximal half and domed on the distal half (Fig. 6.74).

Fig. 6.74. Pig-Human linea aspera comparison

- Deer. Roughness and sharpness of the lines that make the linea aspera vary greatly between deer species and between male and female individuals. As it can be clearly seen in the drawings in Table 6.8, the main schemes of deer and human linea aspera are very similar. However, the degree of similarity between a deer and a human depends on the deer species and sex. For example, in roe deer (Fig. 6.75, up) the lines are too soft to look human; it should also be noted that the individual in Fig. 6.75 was a female. Conversely, in fallow deer (male individual; Fig. 6.75, middle) the superior portion of the linea aspera is too massive to look human. However, the central portion looks very similar to the human one (location, outline), and at this point of the femoral shaft human and deer tend to have a similar cross-sectional shape, rounded with a slight flattening or slight elevation at the linea aspera, which could represent a challenge in case femoral fragments were found. A possible solution to the problem can be found with a further and closer observation of the deer linea aspera. In fact, it was

noticed that on the central portion of it, the medial line is wider than the lateral one, which is thin and sharp; conversely, on human femur the central part of the linea aspera is made up of two equal lines or by a single, rough line. Further studies focusing on deer femora may be needed, as there are six deer species that live freely in the British countryside: Red deer, Sika deer, Roe deer, Reeves' muntjac deer, Fallow deer, and Chinese water deer (The British Deer Society, 2015).

Fig. 6.75. Deer-Human linea aspera comparison

The following table (Table 6.9) shows the main characteristics of the human linea aspera compared with the corresponding features that were seen only in non-human femora. This table, along with table 6.8, can be used to identify the human or non-human origin of a femoral fragment showing the linea aspera.

Linea aspera	
Human	**Non-human**
Shape: single/two equal lips with proximal and distal bifurcating lines	Shape: D, X, V, Y-like, two parallel lines, funnel-like, triangle, crooked X, bottleneck-like
Rough, but flat lines	Sharp, wide, or grooved lines
Straight lines	Undulating or zig-zagged lines
Narrow, deep groove might be present between the lines on mid-shaft	Wide, shallow groove or convex surface between the lines
Flat popliteal surface	Convex or deep popliteal surface

Table 6.9. Main characteristics of human and non-human linea aspera

6.4 Nutrient foramina

The primary nutrient foramina of human and non-human limb bones were analysed using morphological examination (for location, appearance and direction) and micro-CT (for foramina shapes and nutrient canal angle).

6.4.1 Location

The nutrient foramina locations, according to species and bones, are summarized in table 6.10 (below).

	Human	**Sheep**	**Deer**	**Pig**	**Chicken**	**Duck**
Humerus	A, D , ML	PO, D, LL	PO, D, LL	PO, D, LL or ML	L, PR	L, MS
Radius	PO, PR, ML	PO, PR, on attach. with ulna	PO, PR, LL	PO, PR	PO or M, MS	PO, MS
Ulna	M, PR	M, PR	M, D	M, PR	M, PR	M, PR
Femur	PO, PR, on linea aspera (or medial/ lateral to it)	A, PR	A, PR	PO, D or MS	PO, MS, on or lat to muscle marking	PO, MS, on or lat to muscle marking
Tibia/ Tibiotarsus	PO, PR (can be LL)	L, PR, PL	L, PR, PL	L, PR, PL	A, PR, ML	A, PR, ML

Table 6.10. Nutrient foramina locations. A= Anterior; PO= Posterior; PR= Proximal; D= Distal; M= Medial; L= Lateral; MS= Middle-shaft; ML= Medially Located; LL= Laterally Located; PL= Posteriorly Located

From the table above is clear that human humerus and radius do not share the nutrient foramen location with any other non-human long bone. Human humerus is the only bone where the main nutrient foramen has an anterior, distal and medially located position. The foramen in sheep, deer and

pig radius is on the posterior and proximal portion of the bone, as in the human radius, although the latter is the only bone where the foramen is medially located.

The nutrient foramen in the human ulna has the same location as in chicken, duck, sheep and pig ulnae. As for human femur and tibia, the foramen location is the same as in pig, deer and sheep radii. However, their differentiation (based on foramen location) would be difficult only in case of very young juvenile individuals that would still not have those features that might help distinguishing a radius from a femur, such as the linea aspera or the attachment to ulna.

6.4.2 Appearance

The appearance is what can be perceived by the naked eye, that is the morphology of the foramen itself and its vascular groove; the shape of the canal entrance alone can be better seen in the micro CT-scans. The vascular grooves, indentations through which the vessels flow across the bone and enter the nutrient foramen, can have specific characteristics that help distinguishing the foramina. Some foramina do not have any visible vascular groove; in these cases, the visible shape is that of the foramen alone. In some long bones/species, the nutrient foramina can show variations (Table 6.11).

For each foramen, shape, vascular groove details (if any) and orientation are shown (M-L= medial-lateral; L-M= lateral-medial; P-A= posterior-anterior).

	Human	Sheep	Deer	Pig	Chicken	Duck
H	U-shaped M-L	Drop-shaped No groove M-L	Drop-shaped No groove M-L	Pointed drop-shaped, deep No groove	Drop/Inverse drop-shaped or oval	Drop-shaped or oval
R	Drop/Inverse/ Pointed drop-shaped Small or no groove	Inverse rounded V-shaped Long narrowing groove or no groove	Drop/Inverse drop-shaped or dot Small or no groove	Inverse V-shaped Long shallow groove	Linear or drop-shaped or rounded	Linear Long narrow groove
U	Rounded V-shaped Long narrow groove	Inverse drop-shaped	Dot	Drop-shaped Very small round groove	Drop-shaped	Narrow drop-shaped Long groove
F	Drop/Pointed drop/Inverse drop-shaped	Pointed drop-shaped Small or no groove	Drop/Pointed drop-shaped Small narrow groove L-M	Pointed drop/ Drop-shaped or Inverse V with long deep groove	Inverse drop/ Drop-shaped or oval	Drop-shaped
T	Rounded V-shaped Long widening very deep groove	Rounded V-shaped Long straight /widening /narrowing groove P-A	Long pointed drop-shaped Deep groove	Pointed drop	Pointed drop-shaped Wide deep long groove	V-shaped Widening long groove

Table 6.11. Nutrient foramina appearance. H=humerus; R=radius; U=ulna; F=femur; T=tibia

As seen in the table above, in some human and non-human long bones the appearance of the primary nutrient foramen can vary. Fig. 6.76 shows the variations observed expressed in percentages:
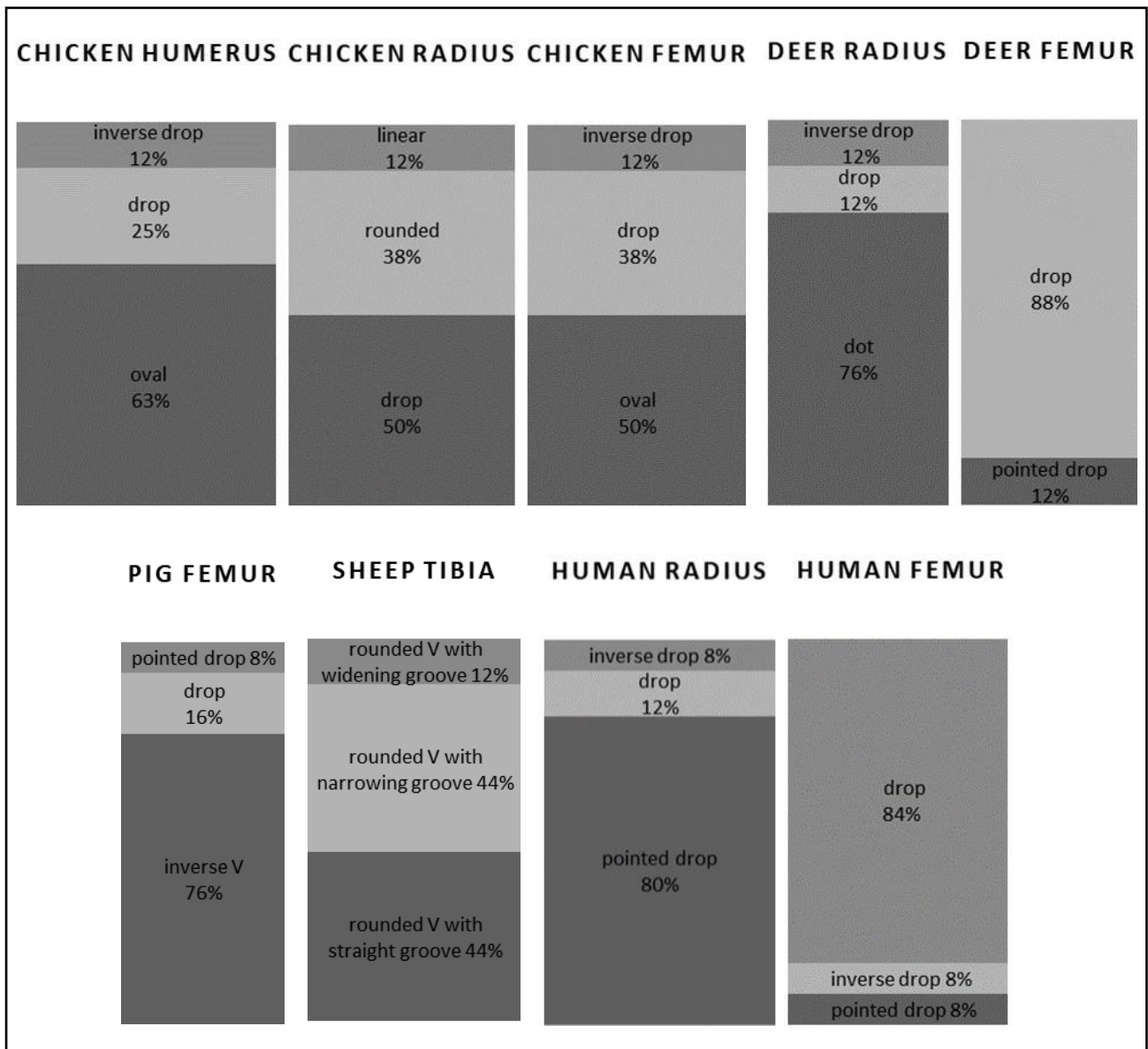
Fig. 6.76. Variations of nutrient foramen appearance in human and non-human long bones

Most of the bones present in Fig.6.76 showed a predominant nutrient foramen appearance and relatively little variation; chicken foramina and sheep tibia's groove showed more substantial variations.

For reference, the main shapes occurring in human bones are shown in the pictures below (Fig. 6.77 a-e):
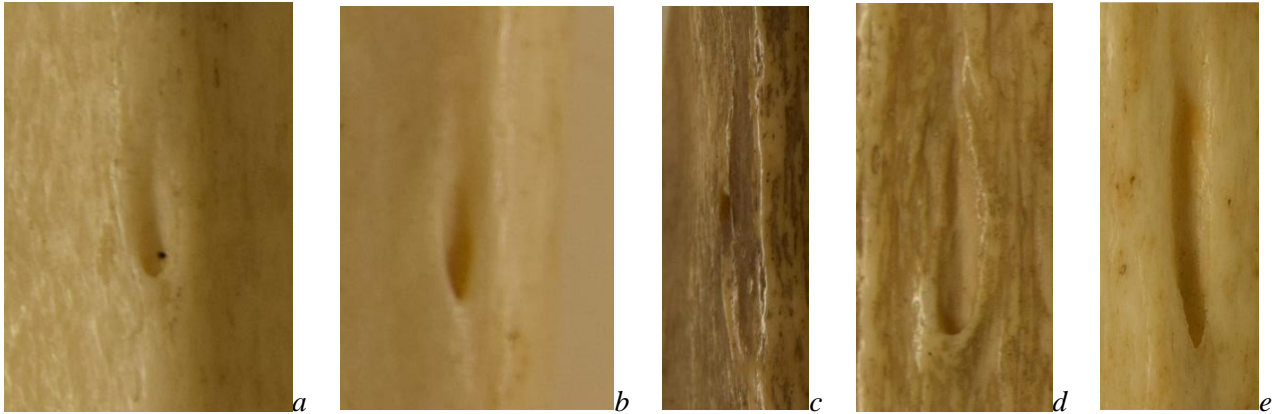
Fig. 6.77, a-e. Human nutrient foramina (not in scale). From left to right: a) U-shaped (humerus), b) pointed drop-shaped (radius), c) rounded V-shaped with long groove (ulna), d) drop-shaped (femur), e) rounded V-shaped with long widening deep groove (tibia). Length of foramina in mm (including groove): a= 4.5; b= 6.5; c= 14; d= 11.5; e= 19.

In some long bones of different non-human species, the nutrient foramina have the same appearance of human nutrient foramina, as shown in Table 6.12:

Appearance	Species	Bone
Drop-shaped	Human	Femur
	Pig	Femur
	Chicken	Humerus; radius; ulna; femur
	Duck	Humerus; femur
Drop/pointed drop-shaped with small or no groove	Human	Radius
	Sheep	Femur
	Deer	Radius
Rounded V-shaped with long widening groove	Human	Tibia
	Sheep	Tibia

Table 6.12. Nutrient foramina appearances that occur in multiple bones and species

The nutrient foramen appearance in the human humerus is unique (when compared to the species considered in this study), therefore its identification should be theoretically straight forward.

The human radius might share the foramen appearance with deer radius and sheep femur. In this study most of the deer radii observed (76%) had the foramen shaped as a small dot; if this is the case in reality as well, the deer radius might be an issue only in those few cases where the foramen is drop or inverse drop-shaped. The foramen on a sheep femur can be difficult to distinguish from that in a human radius, as the area where it is located is flat on both bones; in this case, using other parameters might help with the origin identification.

As for the human ulna, no other non-human ulnae or limb bones have the same appearance.

The nutrient foramen of the human femur has a common shape shared with many other non-human bones: chicken humerus, radius, ulna and femur; duck humerus and femur; pig femur and tibia; sheep ulna. The location of the foramen in the human femur (on, lateral or medial aspect to the linea aspera), might help in the identification process.

In the human tibia, the characteristics of the nutrient foramen are quite distinct from other tibiae. However, the foramen might appear similar to that of a sheep tibia. In this case, the vascular groove appearance can be the key for the differentiation; in human tibiae, the vascular groove is always widening, while in sheep tibiae it can show variations and a specific orientation.

6.4.3 Direction

Table 6.13 shows the direction in which the nutrient canal enters the long bones of each of the species considered, detected with a hypodermic needle. The directions are either P-D= Proximal-Distal or D-P= Distal-Proximal.

	Human	Sheep	Deer	Pig	Chicken	Duck
Humerus	P-D	P-D	P-D	P-D	P-D	P-D
Radius	D-P	D-P	D-P	D-P	P-D	P-D
Ulna	D-P	D-P	D-P	D-P	P-D	P-D
Femur	D-P	P-D	P-D	D-P	D-P	P-D
Tibia	P-D	P-D	P-D	P-D	P-D	P-D

Table 6.13. Nutrient foramina direction

In humeri and tibiae of all species considered, the nutrient canal runs proximally-distally. As for radii and ulnae, in human, sheep, deer and pig the canal runs in a distal-proximal direction, while it runs in a proximal-distal direction in chicken and duck. Human femora share the distal-proximal canal direction with pig and chicken.

6.4.4 Shape from micro-CT scans

Figures 6.78-6.80 show parts of the Micro Computed Tomography procedure used for the calculation of nutrient foramina angle and the detection of nutrient foramina shape (and the mid-shaft cross-sectional shape, see Section 6.5). The images show how single bones and bundles appeared in VG Studio Max software before being processed, in proximal-distal, exterior-interior, and lateral views.
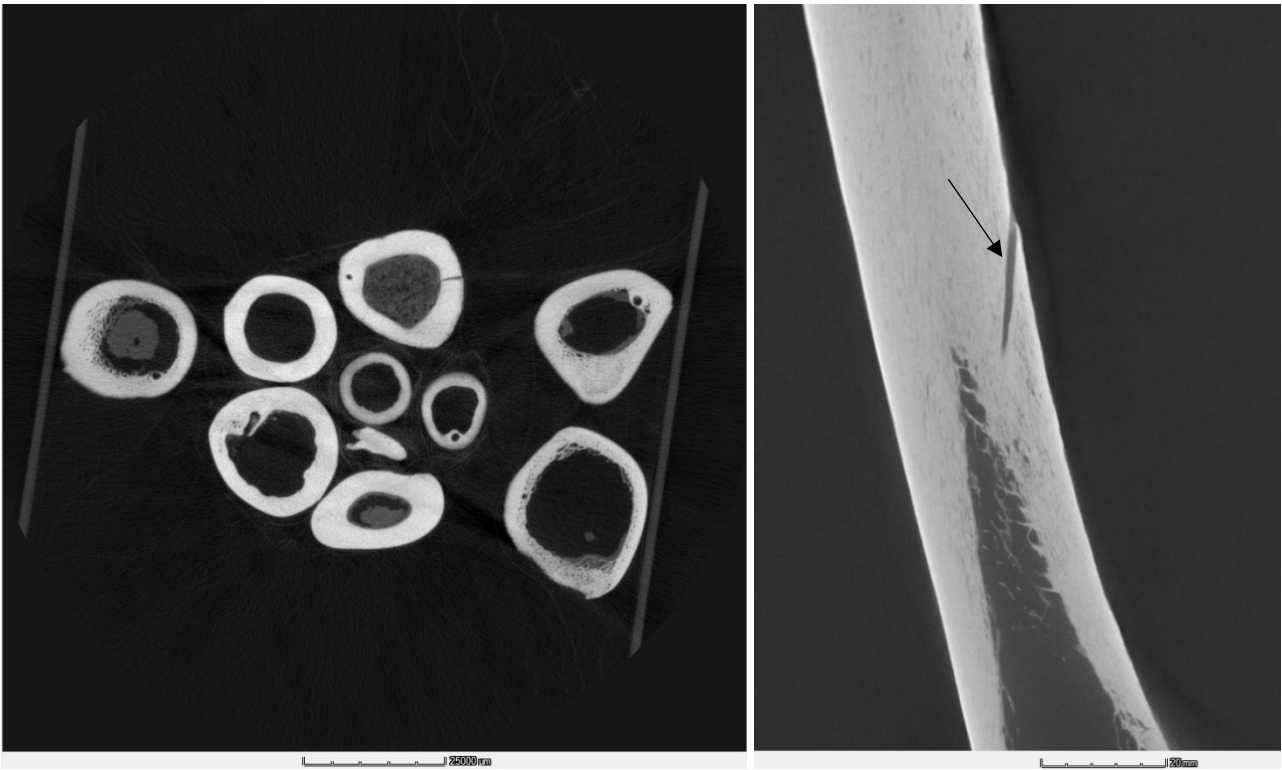
Fig. 6.78. Pig and deer cut bones in proximal-distal view (YZ plane)

Fig. 6.79. Human left femur, exterior-interior view (XY plane). The nutrient canal is clearly visible (arrow)
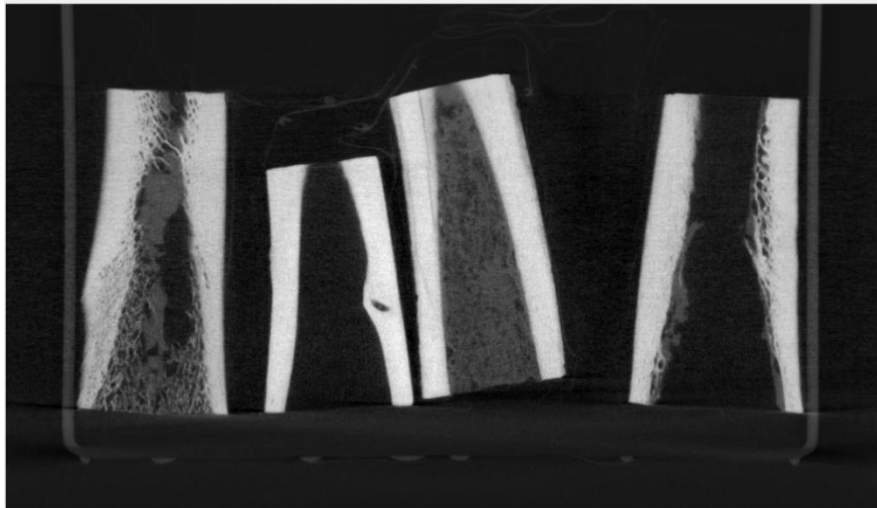
Fig. 6.80. Pig and deer cut bones in lateral view (XZ plane)

The different shapes of the nutrient foramina, divided by species and long bones, are shown in tables 6.14-6.15. Two points of view were considered: exterior-interior (XY plane) and proximal-distal/distal-proximal (YZ plane).
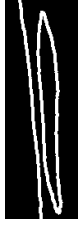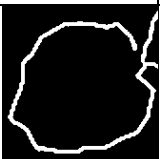
X Y	RH	LH	RR	LR	RU	LU	RF	LF	RT	LT
H U M A N										
S H E E P										
D E E R										
P I G										
C H I C K E N										
D U C K										

141

Table 6.14. Foramina shapes, XY plane (not in scale). RH= right humerus; LH=left humerus; RR= right radius; LR= left radius; RU= right ulna; LU= left ulna; RF= right femur; LF= left femur; RT= right tibia/tibiotarsus; LT= left tibia/tibiotarsus. Since the deer left radius foramen was too small and undetectable in the scans, two right radii were scanned. Pig right radius and right ulna were not available for scanning.

In the human humerus the foramen appears as drop-shaped; only one of the sheep humeri seems to share the same shape, although here the drop is more rounded. As for the human radius, the shape of the foramen is a long oval, shared with pig femur and tibia, and only in one case both for deer radius and sheep humerus.

The pointed oval shape in human ulna and the long, pointed, narrow drop shape in femur and tibia are not found on any other non-human bone considered in this study.

The human humerus is the only bone where the foramen shape as seen from the YZ plane corresponds to the one seen from the XY plane (Table 6.15). In the radius, ulna, femur and tibia the shape of the foramen as seen from its entrance (proximal or distal) does not correspond to the shape seen from the exterior-interior point of view. The shapes on the YZ plane vary even within the same species; as one can see from the images in the table below, in many cases right and left foramen shape of each bone are different.

Table 6.15. Foramina shapes, YZ plane

6.4.5 Angle of the nutrient canal from micro-CT scans

Fig. 6.81 shows the result of the calculation of the nutrient canal angle, on the XZ plane (side view). The blue lines represent the selected region of interest of the bone, after the surface determination and surface extraction processes. The nutrient canal was clearly visible in the 3D reconstruction of the selected regions, after surface determination and extraction were applied (Fig. 6.82).
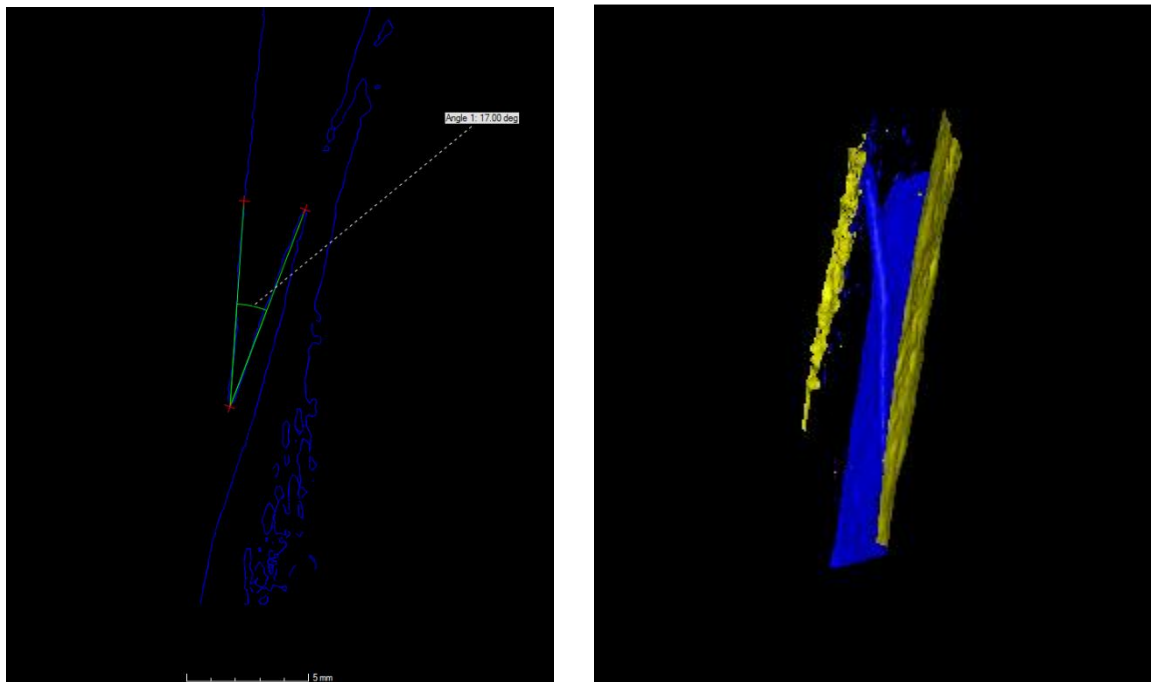
Fig. 6.81. Nutrient canal angle of a deer tibia, XZ view.

Fig. 6.82. 3D reconstruction of the main nutrient canal of a human left femur (canal entrance and cortical bone are on the right side of the image)

The table below (Table 6.16) shows the minimum and maximum angle values obtained for each bone.

	Human	Sheep	Deer	Pig	Chicken	Duck
Humerus	2.88°-2.9°	2.28°-3.08°	1.91°-2.51°	2.56°-2.88°	2.05°-2.21°	2.43°-2.76°
Radius	2.2°-2.36°	2.13°-2.36°	2.03°-3.23°	2.18°	2.28°-2.51°	1.96°-2.18°
Ulna	1.9°-2.43°	1.9°-2.28°	1.9°-2.25°	2°	2.16°-2.96°	2.61°-18.86°
Femur	1.9°-3°	2.21°-2.95°	2.2°-2.46°	1.95°-1.98°	2.46°-2.58°	2.36°-2.5°
Tibia	0.26°-0.3°	1.88°-1.91°	1.95°-2.08°	2.5°-2.63°	1.9°-1.91°	0.28°-1.86°

Table 6.16. Nutrient foramina angle degrees (minimum and maximum). As for pig radius and ulna, only one sample per bone was scanned, therefore only one value is available

The only two human bones whose nutrient canals seem to enter at a very specific angle are the humerus and the tibia.

In both human humeri the nutrient canal enters the bone at the same angle. However, the angle seen in human humerus, albeit very specific, cannot exclusively be linked to a human bone, as in sheep humerus and femur, deer radius, pig humerus, chicken and duck ulna the ranges of angles include 2.88° and 2.9°. This means that in these non-human bones the nutrient canal may enter at the same angle as observed in the human humerus.

In the human radius, the range of the angle degrees is slightly large. In sheep humerus, radius, ulna and femur; deer humerus, radius, ulna, and femur (which shows a range very similar to the one seen in human radius); chicken humerus, radius and ulna and duck femur, the range of the angle values includes 2.2°-2.36°; therefore, they can likely have the nutrient canal at the same angle as in human radius.

In the human ulna and femur, the range of angles becomes even larger, especially for the femur; in this case, the canal angle calculation might not be a useful tool for the identification of the human or non-human origin of a fragmented bone.

Among the human bones, the tibia seems to have a unique angle range; only in duck tibia the canal is seen to enter at a similar angle, although in this case the measurement range is larger than the one seen in the human tibia.

6.5 Cross-sectional shape

The following tables (Tables 6.17-6.22) show the mid-shaft cross-sectional shapes as seen from the micro-CT scans. Each table shows left and right limb bones of human (Table 6.17), sheep (Table 6.18), deer (Table 6.19), pig (Table 6.20), chicken (Table 6.21) and duck (Table 6.22). The images are not in scale.
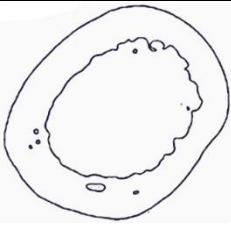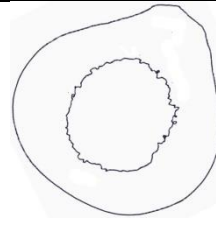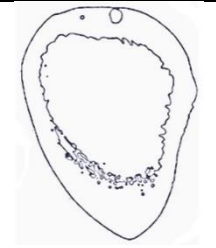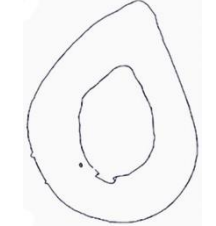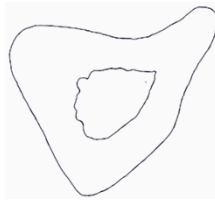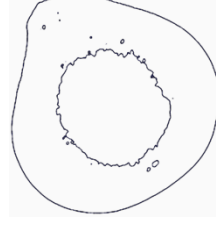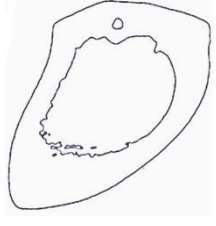
Human				
Humerus	**Radius**	**Ulna**	**Femur**	**Tibia**
Rounded rectangle	Drop-shaped	Scalene triangle with concave-convex sides	Pear-shaped	Comma-shaped

Table 6.17. Human limb bones cross-sectional shapes. In each column, the left bone is on the top
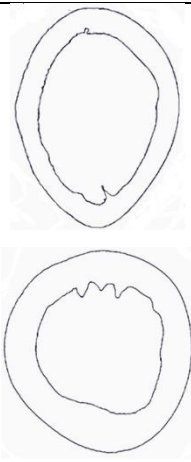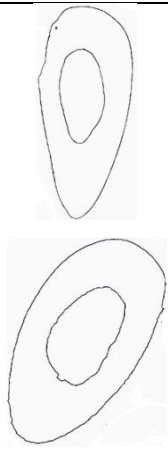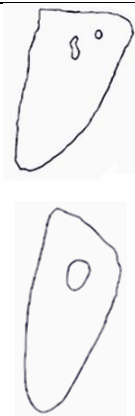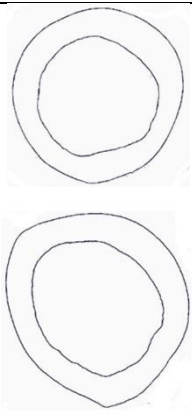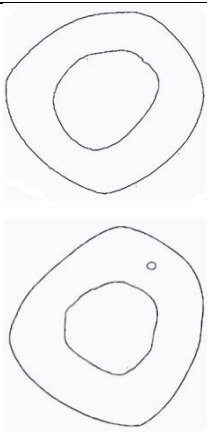
Sheep				
Humerus	**Radius**	**Ulna**	**Femur**	**Tibia**
Oval/rounded oval	Long oval	Isosceles triangle	Rounded (pointed tip is linea aspera)	Rounded trapezoid

Table 6.18. Sheep limb bones cross-sectional shapes. In each column, the left bone is on the top
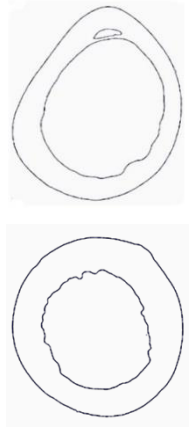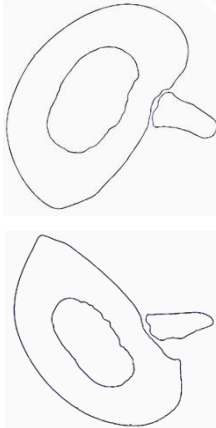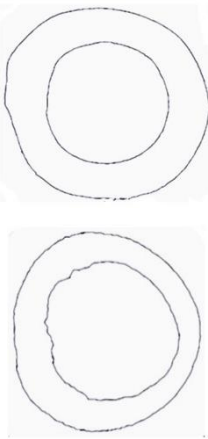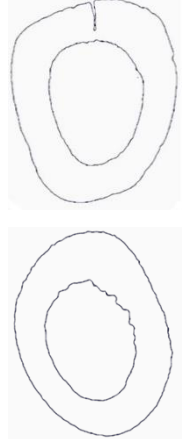
Deer			
Humerus	**Radius-ulna**	**Femur**	**Tibia**
Irregular rounded drop (roe)/rounded (fallow)	Radius: oval flattened posteriorly Ulna: rounded isosceles triangle (fallow)	Rounded, slightly flat on the linea aspera(roe, fallow)	Oval flared posteriorly (fallow, roe)

Table 6.19. Deer limb bones cross-sectional shapes. In each column, the left bone is on the top. Radius and ulna were scanned together as they are fused
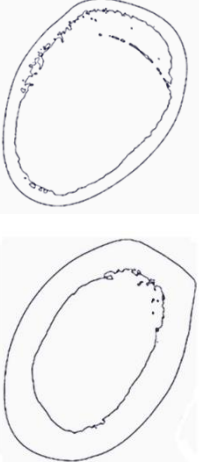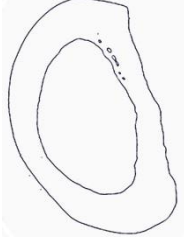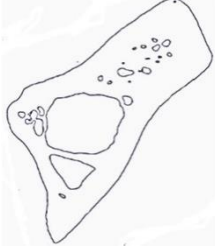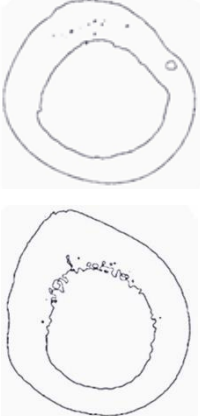
Pig				
Humerus	**Radius**	**Ulna**	**Femur**	**Tibia**
Oval, pointed at the deltoid tuberosity	Oval, flat posteriorly	Isosceles triangle with quadrangular tip	Irregular circle, pointed at the linea aspera	D-shaped (flat side is posterior)

Table 6.20. Pig limb bones cross-sectional shapes. In each column, the left bone is on the top. Only one left radius and ulna were available for scanning
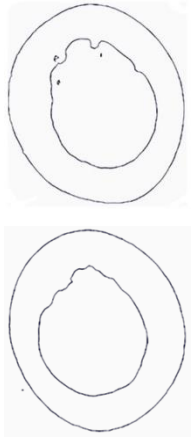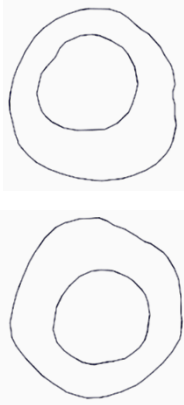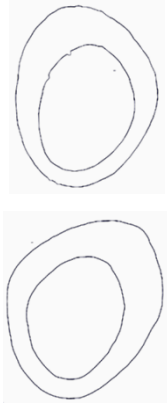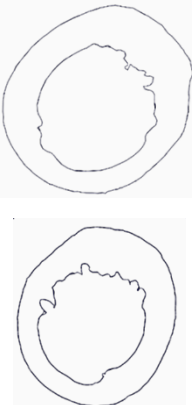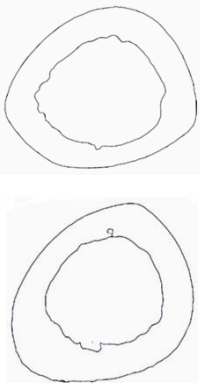
Chicken				
Humerus	**Radius**	**Ulna**	**Femur**	**Tibia**
Oval	Irregular circle	Irregular oval	Rounded, flat on the linea aspera	Rounded triangle

Table 6.21. Chicken limb bones cross-sectional shapes. In each column, the left bone is on the top
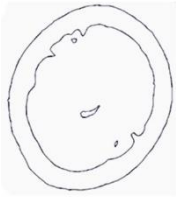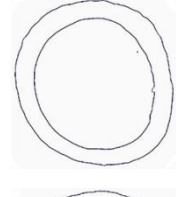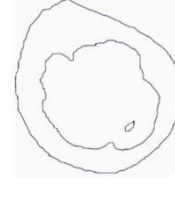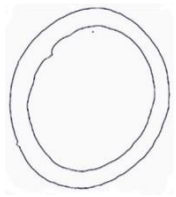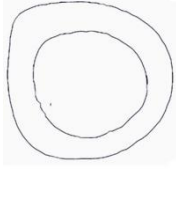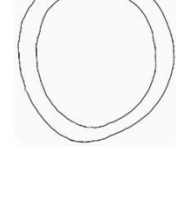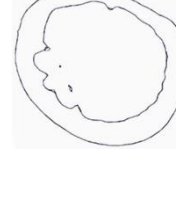
Duck				
Humerus	**Radius**	**Ulna**	**Femur**	**Tibia**
Oval	Rounded drop	Rounded	Irregular rounded drop (tip is linea aspera)	Irregular circle, flat posteriorly (up right)

Table 6.22. Duck limb bones cross-sectional shapes. In each column, the left bone is on the top

The cross-sectional shapes seen in human limb bones (rounded rectangle, drop, scalene triangle, pear, comma) were not seen in any other non-human species considered.

All human limb bones have a specific shape not seen on other mammals. Only ulna follows the more generic triangle shape pattern seen in other mammals. As for femur, its pear shape is given from the linea aspera, which is particularly pronounced in humans because of bipedalism; with a less marked linea aspera, the human femur would have a more rounded shape like the one seen in other mammals (Chevalier, 2008).

There is a specific scheme among sheep, deer and pig and between the two birds considered. Every bone is the variation of the same shape, as it can be seen in the following table (Table 6.23):
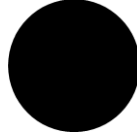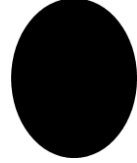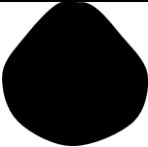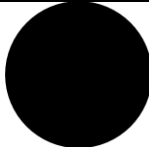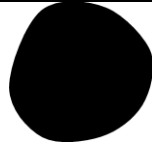
	Human	Non-human Mammals	Birds
Humerus	Rounded rectangle	Egg-shaped	Oval
Radius	Drop	Long oval	Circle
Ulna	Scalene triangle	Isosc. Triangle	Rounded oval
Femur	Pear	Rounded	Irregular circle
Tibia	Comma	Trapezoid	Rounded scalene triangle

Table 6.23. Limb bones cross-sectional shapes in human, non-human mammals and birds

There are some shapes that are not seen in human limb bones: oval, seen only in mammal humerus and radius and in bird humerus and ulna; trapezoid, seen only in mammal tibia; rounded scalene triangle, seen only in birds tibiae. Therefore, if one of these cross-sectional shapes is encountered, the bone might be non-human.

When bones of individuals of different ages could be observed, no age-related differences were noticed; the bones of both adult and juveniles individuals were scanned, and the resulting cross-sectional shapes have not shown any difference between young and adult individuals (an example in Fig. 6.83).
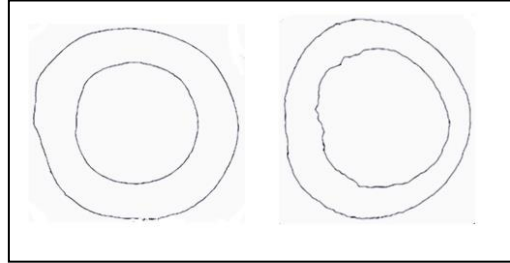
Fig. 6.83. Comparison of two deer femur cross-sectional shapes. The femur on the left is from an adult individual (5 years old), while the femur on the right is from a young individual (less than 1 year old)

The human cross-sectional shapes and most of the non-human ones are still identifiable if hypothetically cut in two or four halves, to simulate a potential fragmentation scenario. In the following images (Fig. 6.84-6.86) the human ulna is shown in an example of potential fragmentation:
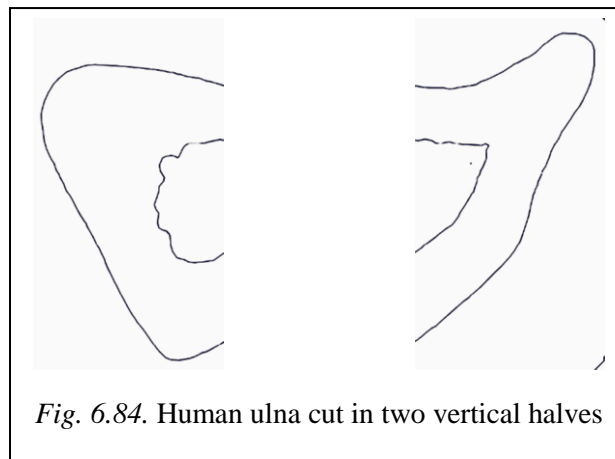
Fig. 6.84. Human ulna cut in two vertical halves

Fig. 6.85. Human ulna cut in two horizontal halves

Fig. 6.86. Human ulna cut in four halves
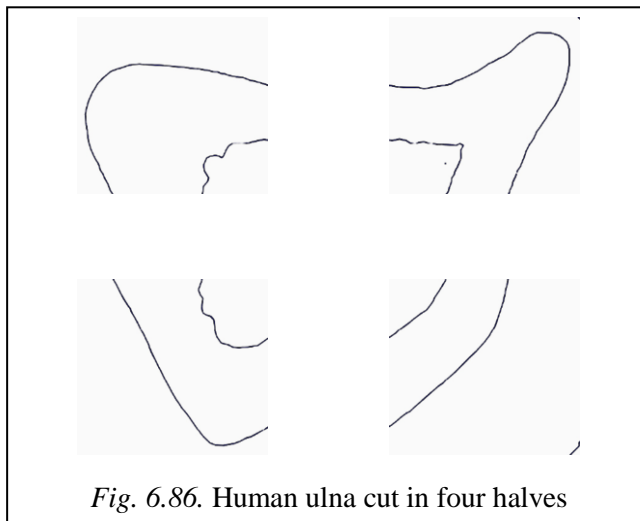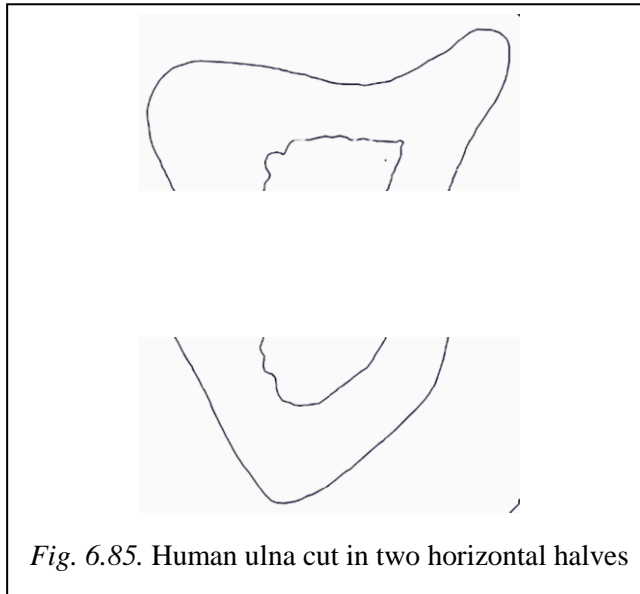
Human humerus, ulna and tibia are recognizable in any case. The shape of humerus is clearly quadrangular/rectangular; since this shape is not found on any other nonhuman species considered, a bone showing a quadrangular/rectangular shape can be considered human, and even be identified as humerus, since only human humerus has this shape. At a first glance, a similarity between human and mammal ulna might be seen, since the human ulna is a scalene triangle while the mammal one is an isosceles triangle; theoretically, if the complete triangle were not visible, it would not be possible to identify the specific triangle. However, deer and sheep ulnae are much smaller than the human one, and their medullary canal is narrower and sometimes is not even visible. As for pig ulna, it has usually a distinctive and more irregular shape, and is much more massive in comparison to the human one; even its cortical bone would appear much thicker (Fig. 6.87).

Fig. 6.87. Human, sheep and pig ulna. Images are not in scale
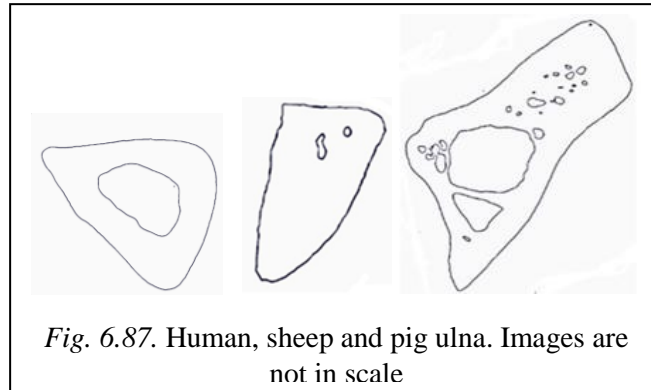
The only two human bones that might be partially problematic are radius and femur, both of them for the same reason. As for radius, in a hypothetical division in four equal parts, most of its sides even if fragmented would suggest a drop shape. However, if only part of the anterior portion were available, only the rounded shape would be visible, and the fragment could be misidentified as a mammal juvenile femur or as an adult bird radius or femur (Fig. 6.88). As for femur, if linea aspera is visible or partially visible the identification is still possible. However, if only the anterior portion of the femur were visible, this would appear rounded in shape and then mistakable as a mammal femur or a chicken femur in case of human juvenile bones (the latter only if the fragment does not show the linea aspera, which is a flat area in chicken). The human femur cannot be misidentified as a bird radius, despite a human radius does, because even a newborn human child would not have a femur thin and small like the radius of an adult chicken or duck (Fig. 6.89).

Fig. 6.88. Human radius cut in four halves. Part of the anterior portion (arrow) might resemble a rounded bone

Fig. 6.89. Human femur cut in four halves (left) and deer femur (right). The anterior portion of a human femur (arrows), if isolated, would suggest a rounded shape
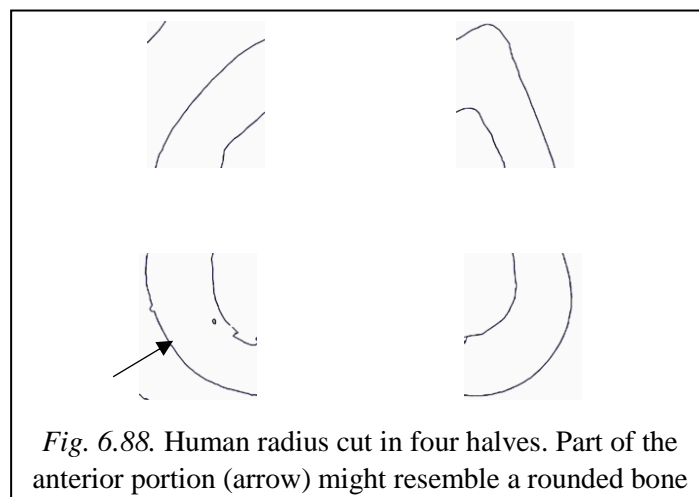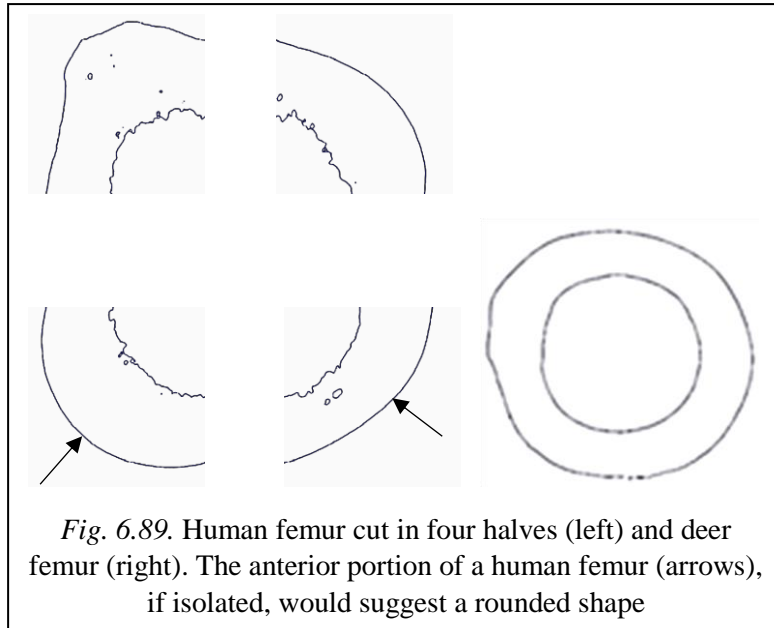
It is not advisable to try dividing the shapes in more than four parts, as in this case the fragments would be too small and the cross-sectional shape might not be helpful anymore. In case of extreme fragmentation, the cross-sectional shape can be used as an additional parameter but not as the only one.

6.6 Blind test on fragmented bones

31 bone fragments, whose human or non-human origin was not known, were observed. The aim was to test the applicability of the methods and features used in this study for the differentiation between human and non-human fragmented bones. For each fragment, the features and methods useful for origin identification were listed, starting from the most efficient. Methods involving the use of a GIS software or micro-CT were only suggested or advised, but not used for this test. 17 of the 31 bone fragments tested are shown in this Section.

Fig. 6.90. The 3 cm fragment in the photo above is an occipital bone fragment, showing a right occipital condyle and the hypoglossal canal. The condyle is 60% complete, as its superior portion is missing and weathering is visible throughout. The examination of the condyle can help in the origin identification. The condyle appears as bean-shaped, has bulbous borders and is not attached to the condyle on the opposite side; the portion of the foramen magnum visible suggests a rounded rhomboidal shape. Despite the texture of the condyles might have been changed by the weathering, the main characteristics of the condyle are still visible and suggest a human origin.

Fig. 6.91-6.92. The 8 cm fragment on the left is a radius proximal shaft, juvenile as the epiphysis is not attached; the 8 cm fragment on the right is a radius proximal shaft as well, with no epiphysis. The general shape of both shafts, their internal structure showing reduced or no trabecular bone, the sharp transition between cortical and spongy bone, and the cross-sectional shape (rounded anteriorly and flattened posteriorly) suggest a non-human mammal origin. The features listed are sufficient for the origin identification of the fragments; for further confirmation, the nutrient foramen can be observed.

Fig. 6.93 a-b. This fragment, long 7 cm, is a cremated, posterior, femoral shaft portion. The clear presence of the linea aspera identifies this fragment as a femur. The nutrient foramen is located on the linea aspera, has a distal-proximal direction, and appears as drop-shaped; the foramen alone could confirm that this fragment is human. The internal structure of the bone offers a further confirmation of the human origin of this fragment.
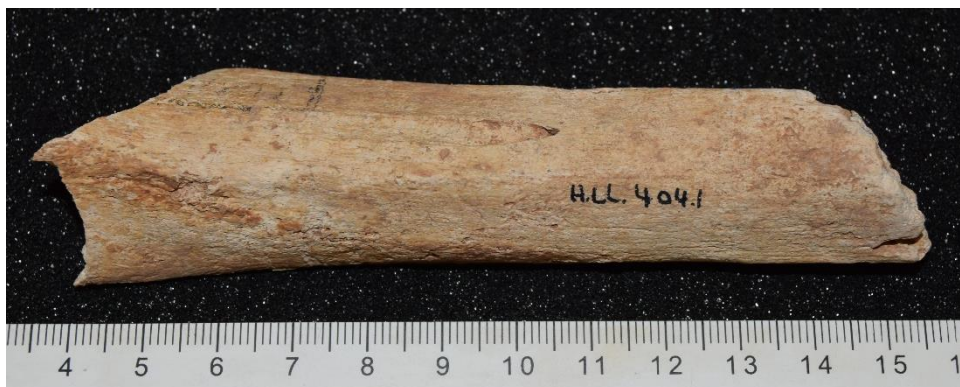
Fig. 6.94. This 11.5 cm long bone fragment is a tibia shaft. The morphology and the comma-like cross sectional shape allow to identify the fragment as a tibia; the nutrient foramen, with its posterior, proximal location, its proximal-distal direction, and its rounded V shape, with a long, widening, deep groove, allows to identify this tibia as human.

157

Fig. 6.95 a-b. This shaft fragment, 9.5 cm long, is clearly from a long bone, but its origin might be less clear, as no particular diagnostic landmarks are visible. However, its mid-shaft cross-sectional shape, which is visible in this case with no need for micro-CT use, is clearly drop-shaped (right image), and allows to identify this fragment as a human radius.

Fig. 6.96. This 11.5 cm long bone shaft is not severely fragmented, but can still be challenging to identify to an untrained eye. Its appearance identifies this shaft as a tibia. The smooth internal structure showing no trabecular bone, and the nutrient foramen, which does not resemble the human tibial foramen, allow to identify this shaft as non-human. Micro-CT can be applied, to detect cross-sectional shape and foramen shape, but it is not needed as the bone is not severely fragmented and the criteria stated above were enough to identify it as non-human.

Fig. 6.97-6.98. These fragments, measuring 8 cm and 8.5 cm respectively, are both long bone fragments. Their internal structure shows a relatively smooth medullary canal, with reduced trabecular bone. The fragment on the right shows a very smooth cortical bone, too. The mid-shaft cross-sectional shape, which is visible in both fragments, is rounded for the left fragment and oval for the one on the right. All these elements suggest a non-human origin, probably avian. The fragment in the right image is very light and has a visible nutrient foramen, but in this case further investigation of the nutrient foramen is not needed.

a)   b)

Fig. 6.99 a-b. This fragment, 7 cm long, appears as a long bone fragment, and is severely weathered. Despite the weathering, the visible linea aspera allows to identify this fragment as a femur. However, in this case the linea aspera cannot be used for origin identification, as its appearance is compromised. The nutrient foramen is visible; its location is typically human (on, medial or lateral to linea aspera), but its appearance might have

changed because of the weathering. Micro-CT scans of the foramen might allow to identify its origin. For this fragment, the cross-sectional shape is the diagnostic feature: the image on the right shows a clear pear-shaped cross-sectional shape, which identifies this femoral fragment as human.

Fig. 6.100. The fragment in the image above is clearly from an occipital bone. Both occipital condyles and ¾ of the foramen magnum are visible. The rounded-rhomboidal foramen magnum, and the bean shaped occipital condyles (with transverse grooves as non-metric trait), with their bulbous borders, allow to identify this occipital bone fragment as human.

Fig. 6.101 a-d. The images above show three bone fragments (*b* is related to the first fragment), which can be safely identified as cranial, as they are curved and show sutures. The sandwich-like structure of the diploe between two cortical layers (*b*) is visible in all three fragments, but using it as diagnostic feature for a human origin identification is not recommended, as this type of structure can also be seen in non-human cranial bones. The curvature calculation with a GIS software can be made. A suture is visible in all three fragments, however only for *c)* the use of a GIS software would be beneficial, as both sides of the suture are visible.

Fig. 6.102 a-b. The fragments shown in the images above are clearly two rib shaft fragments. The costal groove, visible in both fragments, might suggest a human origin. For safer results, the shaft curvature can be calculated using a GIS software.

Fig. 6.103 a-c. The long bone shown in the images above is not severely fragmented, but its grade of fragmentation might still make its human or non-human origin not clear, as only a portion of the shaft with a partial epiphysis is visible. The bone appears as an ulna, showing the attachment site for radius. The cross-sectional shape at the mid-shaft is not visible and its detection may require the use of micro-CT scanning; the visible cross-sectional shape is that of the distal shaft, but still corresponds to the human ulna shape identified in this research, namely a scalene triangle with convex sides. A further confirmation of the origin of this ulna comes from its nutrient foramen, whose medial-proximal location, distal-proximal direction, and rounded V shape allow to identify this bone as human.

Chapter 7: DISCUSSION

This chapter will discuss the findings presented in Chapter 6. In section 7.1, the results of the analysis of cranial curvature, cranial sutures and rib curvature carried out using ArcGIS are discussed. The findings of the morphological examination of human and non-human occipital condyles and linea aspera are discussed in sections 7.2 and 7.3, respectively. Section 7.4, which discusses the results of the nutrient foramina analysis, is divided in five subsections, focused on location, appearance, direction, shape from micro-CT scans and angle of the nutrient canal from micro-CT scans. Section 7.5 explains the results of the cross-sectional shape analysis carried out using micro-CT scanning. Section 7.6 briefly explains the concept of admissibility of evidence in forensics. A table with a summary of the research results is provided at the end of this chapter, in section 7.7.

7.1 Cranial curvature, sutures and rib curvature

7.1.1 Cranial curvature

The human cranial vault tends to be curved (due to a relatively large brain), with a clear sandwich-like cross-sectional structure, consisting of a layer of spongy bone between two outer tables of compact bone (Bruner, De La Cuetara and Halloway, 2011). Non-human crania are usually flatter, elongated and more irregular, and the sandwich-like appearance may be more or less clear (Christensen, Passalacqua and Bartelink, 2014). However, when morphologically observed, sheep, calf and fox crania seemed to have a curvature that looked very similar to the human one.

The aim of the curvature calculation in ArcScene and the statistical comparison of the values was to highlight differences between the species that were not visible at the naked eye. A t-test was performed, in order to determine whether there were a statistically significant difference between the means of sheep, calf and fox cranial curvature and the means related to human curvature. The parietal curvature of the three non-human species was not significantly different from the human one; the curvature in fox appeared to be equal to the human curvature. The curvature calculation and the t-test confirmed the similarities among the species observed before the analysis, but failed to highlight any differences; this means that the parietals of human and sheep, fox and calf cannot be distinguished on

the basis of their curvature as calculated by a GIS software. The same, unpromising results were obtained when the calculation was repeated using four human parietal bone fragments, as the difference between human and non-human curvature values was not statistically significant, with a high probability of type I error.

The calculations made by the GIS software did not show any significant difference between parietal curvature of human, sheep and calf, while confirmed fox as the most misleading species when it comes to curvature. Given the results, GIS has not proved to be a valuable method to securely assess the human or non-human origin of cranial fragments. An important limitation faced by the use of cranial curvature calculation with a GIS software was the high intra-species variability seen in curvature values; further research employing a larger sample size might be needed, in order to explore the variability of cranial curvature within the species and to reassess the validity of the method by using more samples.

Human and non-human skull fragments may also be confused when a pathological condition is present. For example, an anencephalic human cranium, although very rare, may be mistaken for non-human (because it is much flatter than a normal human skull), or a hydrocephalic cow skull neurocranium may resemble a human one, because it would be more bulbous and then human-like (France, 2009). Therefore, it is advisable to have a basic knowledge of the pathological conditions and malformations that may affect the cranial vault, because even if rare they may be present and lead to a misidentification of the bone fragments.

7.1.2 Sutures

The GIS software application in Forensic or Biological Anthropology is relatively new and still unexplored: one of the few examples of its use can be seen in Bolton (2013), where GIS has been used to "map" the pubic symphysis in order to find differences in slope, aspect and volume in relation to age. Since before this study a GIS software had not yet been used for cranial bone sutures and curvature analysis, all the applicable software features had to be explored, in order to find those suitable for the calculation of curvature and suture pattern analysis.

The images produced by ArcGIS showed significant differences between suture patterns. To the naked eye, calf, sheep and fox sagittal sutures looked very similar to the human ones, but when the same skulls were analysed with GIS the sutures could be easily distinguished. The contour lines

highlighted differences in the sutures pattern that could not be seen when the skulls were visualized. Despite the variability between individuals of the same species is high (sutures could be used for human identification, because each individual has unique cranial sutures, as seen in Sekharan, 1985 and Mann *et al.,* 2015), the main pattern within a species remains the same (as seen in Table 6.2).

Therefore, the differences between cranial suture patterns can be highlighted using a GIS software. The software helped to clearly distinguish between sutures that looked very similar at the naked eye, and it could also demonstrate that each species has a specific sagittal suture pattern (undulated in foxes, linear in calves, closely denticulated in sheep, largely denticulated in humans). The method has proven to be useful and it can be used when cranial bone fragments with visible sutures (even if just small portions) are found. Since similarities between species were noticed in lambdoid and coronal suture as well, the contour lines creation with GIS can be tested on other cranial sutures.

The main limitation of this method is that the data produced are qualitative and not quantitative. Furthermore, since the partial or total closure of a cranial suture prevents the creation of contour lines, this method may not fully work with older individuals, both human and non-human.

In a rare non-metric trait called "simple suture", a portion of a human suture, usually the sagittal, may appear linear (Mann, Hunt and Lozanoff, 2016). For this reason, when a cranial fragment showing a suture is found, it is advisable to use more methods of origin identification (e.g. sutures, morphology, texture) to prevent a single non-metric trait from leading to a misidentification of a human fragment for non-human, or vice versa.

7.1.3 Rib curvature

The ribs of quadruped mammals are usually straighter than the human ones, as their thorax is deep and narrow, while in humans this is shallow and broad (France, 2009). However, while the differences in curvature can be clearly observed on complete ribs, these become much less obvious when the ribs are fragmented and only a portion of their shaft is visible. Pig ribs are used for human consumption, therefore their fragments could be present in a forensic or archaeological scenario and be misidentified as human. For this reason, a quantitative method that can help distinguishing a human rib shaft fragment from a pig one is needed.

The same procedure seen in the comparison of parietal curvatures was followed. After calculating the curvature of the shafts with a GIS software, a t-test was performed, in order to determine whether

there was a statistically significant difference between the means of human and pig rib shaft curvature, in superior, inferior, and combined views.

In superior view, no significant difference in curvature was found between human and pig ribs. In inferior and combined superior-inferior views, the curvatures were significantly different. Therefore, when the rib shaft curvature was calculated from the inferior point of view, or when both superior and inferior views were considered, human ribs appeared as different from the pig ones. The curvature calculation with ArcGIS and the statistical comparison of the means could be useful methods to distinguish between human and pig fragmented rib shafts. Furthermore, the variability within the same species was low. The number of ribs used for each species was low (N = 4); a repetition of the same calculations with a larger sample size is advisable, in order to prove (or disprove) the validity of the method.

Pathologies and trauma must be taken into account when the identification of a rib shaft fragment is based on its curvature, as this latter can undergo alterations. Activities like coughing, childbirth, or heavy lifting can produce rib fractures, particularly in ribs 3 to 10 (Hanak, Hartman and Ryu, 2005). Furthermore, rib trauma can be a consequence of falls, motor vehicle accidents and interpersonal violence (de la Cova, 2017). An improperly healed rib fracture can produce changes in the curvature and main shape of the shaft; a change in the original curvature of the shaft might also be seen in properly healed ribs, because of the temporary bone callus formation that is part of the healing process (Talbot *et al.*, 2017). Infectious diseases like tuberculosis, or conditions like polyostotic fibrous dysplasia, scoliosis and ankylosing spondylitis can change the shape of the ribs (Steele and Bramblett, 2012). The ribs used for this study, both human and non-human, were from healthy individuals; in case of shape alterations caused by trauma or disease, the curvature of the shaft might not be a reliable feature to consider to identify the human or non-human origin of a rib fragment.

7.2 Occipital condyles

The specific location of the occipital condyles differs between human and non-human species. This is due to main differences in locomotion and spinal structure. In non-human species, the spine is more or less horizontally oriented, and the head protrudes anteriorly; therefore, the foramen magnum (thus the occipital condyles) is located on the posterior part of the cranium. In humans, the spine is vertically oriented, therefore the foramen magnum is located on the inferior part of the skull. In non-human primates and bipedal species, the foramen magnum is situated more anteriorly than in

167

quadrupeds; however, the human one is the most anteriorly positioned foramen magnum (Russo and Kirk, 2013).

In non-human species, flexion of the neck is a passive movement, since it is assisted by gravity, while extension is the main movement permitted at the atlanto-occipital joint. Therefore, animals tend to have strong posterior cervical muscles, thus pronounced muscular attachments and a thick occipital crest (Graf, Waele and Vidal, 1995). In human skeletons, the spine is weight-bearing, being it mainly vertical with the skull on its uppermost part. Accordingly, both flexion and extension of the neck are assisted by gravity, therefore the cervical muscles are weaker and the occipital nuchal crest much smaller in humans compared to animals. In contrast, human skulls show a large mastoid process, because they have large sternocleidomastoid muscles, whose function is to pull the head forward from a dorsal position and to turn the head (France, 2009).

Generally, the occipital condyles and the superior facets of the atlas (anterior in quadrupeds) are thicker and stronger in non-human species (Goel *et al.*, 2011). The facets of the first vertebra are usually cup-shaped, and the atlanto-occipital joint tends to be similar to a hinge-joint; these characteristics provide a higher stability and mobility than in humans. The total range of motion at the atlanto-occipital articulation is 90°-105° in quadrupedal mammals and only 11°-13° in humans (Graf, Vidal and Evinger, 1986).

Despite the differences dictated by locomotion, the occipital condyles of some non-human species can appear very similar to the human ones; therefore, these species may be considered a potential challenge whenever fragmented condyles are found. The main aim of this study was to identify the similarities and the differences between the most challenging non-human species and humans in the appearance of the foramen magnum and the occipital condyles, in order to be able to assess the origin of occipital fragments even in those cases where the fragments seem to be particularly challenging.

The method used was a thorough morphological examination of non-human skulls belonging to the most common bird and mammal species found in the United Kingdom, followed by a comparison of each skull with human skulls. The features considered for the comparison were: foramen magnum shape; occipital condyles shape; condyles texture and borders; whether condyles meet or do not meet inferiorly.

Birds were excluded from further analyses, as their occipital condyles appearance is very different from the one seen in humans; the differences between birds and humans are so clear that they could be noticed even if a small occipital fragment were found. Among mammals, each of the species considered showed at least one similarity with humans; however, most of the similarities noticed were

too weak to be considered challenging in a scenario where fragmented samples are found. The only two species whose occipital condyles seemed to be more human-like, and then more difficult to identify if fragmented, were fox and seal (grey and common seal). Despite the many apparent similarities with humans, even these two species were proved to be different and distinguishable from a human sample. As for the fox, it was concluded that it may be challenging only in a very rare if not impossible scenario; as for the seal, despite it is the most human-like species when it comes to occipital condyles, it can still be distinguished from the human species when a number of details are considered. Human occipital condyles have specific characteristics that would allow to safely identify the origin of a fragment as human or non-human (Table 6.7).

Some non-metric variations of the condyles, such as condyle dysplasia, the presence of median basioccipital canals (enlarged foramina on the upper part of the foramen magnum) or tertiary condyles, and asymmetry, should be taken into account. Occipital dysplasia is a congenital abnormality of the occipital bone formation, which in most cases leads to underdevelopment of the occipital and enlargement of the foramen magnum; more rarely, it can result in underdevelopment of the occipital condyles. Condyle dysplasia is a rare abnormality that is mostly observed in some dog breeds (Prescher, Brors and Adam, 1996). A third occipital condyle, oval in shape, can appear on the anterior margin of the foramen magnum, articulating with the tip of the dens of the axis, with the anterior atlantic arch, or with both. In humans, the presence of a third occipital condyle has been registered in only 0.25% to 1% of the considered cases (Kumar *et al.*, 2013). Asymmetry of the condyles, where one condyle is usually higher and steeper than the other one, is an uncommon abnormality that may result in torticollis (or wry neck; Eriksen and Rochester, 2007). Despite its serious clinical consequences, the asymmetry of the condyles does not result in a complete change in the appeareance of the condyles (Mann, Hunt and Lozanoff, 2016).

7.3 Linea aspera

The human or non-human origin of a whole femur or one where at least one of the epiphyses is visible would not be challenging. The identification of a femoral shaft with missing epiphyses might be a less straightforward process, as there are some non-human species whose femoral shaft is similar to the human one. In this case, linea aspera, nutrient foramina or cross-sectional shape (discussed in sections 7.4 and 7.5 respectively) can help understanding if the shaft is human or non-human. However, a fragmented femoral shaft showing only a portion of the linea aspera might be much more

challenging to identify as human or non-human, because the main shape of the linea aspera would not be visible. Given the lack of literature on the topic, the aim of this study was to carry out a detailed analysis of human and non-human linea aspera, in order to better understand whether there are differences and similarities that should be taken into account when a fragment showing a portion of linea aspera needs to be determined as human or non-human.

The linea aspera of most of the species considered for this study was proven to be different in any aspect from the human one, therefore not challenging in those cases where a fragmented femoral shaft is found. The species that can be excluded from a list of potentially challenging ones when it comes to linea aspera are pig, sheep/goat, horse, cow, fox, badger, rabbit/hare, cat, and goose.

As for pheasant, pigeon, chicken, turkey and duck, the main scheme of the distal portion of the linea aspera is similar to the human one; however, specific characteristics such as sharpness and outline of the lines, cross-sectional shape and texture make their femoral shafts different and under no circumstances identifiable as human. The only exception is the central portion of duck linea aspera, as its lateral nutrient foramen may lie in the same location as in human femur; further observations on nutrient foramina were made in sections 6.4 and 7.4.

The linea aspera in dog femur follows the same scheme of the human one in its proximal portion. Here the lateral line seemed to be particularly challenging as it shares position and outline with the human linea aspera. However, when better observed, the proximal lateral line in dog is hollow, while the human one is not; this detail could allow excluding dogs from the list of challenging non-human species in the origin assessment of femoral shaft fragments showing the linea aspera. Further research employing a larger quantity of dog femora can be carried out, in order to assess the consistency of the dog linea aspera characteristics observed in this study.

The only species that should be taken into account when identifying a femoral fragment through the linea aspera is deer. The main scheme of its linea aspera is extremely similar to the human one; roughness and sharpness of the lines were considered for the differentiation between deer and human, however it was noticed that these features may vary greatly, depending on the deer species and sex. The central portion of the linea aspera seems to be the most challenging part, as it shares location and outline with the human one. The only difference found was that in deer femur one of the two lines that make the central portion seems to be always wider than the other, with the other line being thin and sharp. However, further studies focused only on the comparison between human and deer femora are advised, as the sex-related differences can make the roughness and sharpness not very reliable criteria for the differentiation from the human linea aspera. Furthermore, there are six deer species living in the United Kingdom, whose femoral shafts can look different, as already seen in this study,

where a female roe deer and a male fallow deer were shown; an accurate study should consider all the six deer species and both sexes for each of them.

The roughness of the linea aspera (and of any other muscular marking) should not be used as the only parameter for the differentiation between human and non-human bone, as its degree is influenced by factors like sex and activity (Polguj *et al.*, 2013; Byers, 2017).

Despite the similarities observed between the linea aspera of human and some non-human species (e.g. deer and dog), specific characteristics that, if present, could help identifying the human/non-human origin of a femoral fragment, were detected (Table 6.9).

7.4 Nutrient foramina

The studies that have focused on nutrient foramina (site, size and direction) are mainly of clinical and surgical interest, as a thorough knowledge of the characteristics of the nutrient canal and the blood flow that passes through it is vital, for example, in orthopedic surgery, fracture diagnosis and union, tumor resection, and reconstructive surgery of skeletal abnormalities (Gainor and Metzler, 1986).

Trauma and surgical dissection can cause damage to the nutrient foramina and subsequent devascularization. The capability of bones to grow and repair depends on their blood supply, therefore poor therapy or surgery could impair the foramina and the blood supply that passes through them, and interfere with bone healing (Malukar and Joshi, 2011; Xue *et al.,* 2016). It is extremely important to know the precise location and direction of the nutrient foramina in delicate orthopedic or surgical procedures like bone grafting or microsurgical vascularized bone transplantation. In bone transplants, the knowledge of the nutrient foramina anatomy allows to place the graft without damaging the nutrient arteries and to preserve both the vascularization and the transplant consolidation (Pereira, Lopes, Santos and Silveira, 2011).

Very few studies have been carried out on non-human nutrient foramina (Dongchoon, 2013; Hughes, 1952; Sim and Dongchoon, 2014; Witkowska *et al.*, 2014). Those undertaken to date investigate the number, site, position and direction of the nutrient foramina of some common non-human species, such as dogs (Dongchoon, 2013; Sim and Dongchoon, 2014) and guinea pigs (Witkowska *et al.*, 2014), and fall within the field of veterinary medicine.

Even fewer studies have focused on the comparison between human and non-human nutrient foramina, in the field of comparative anatomy or forensic anthropology. Johnson, Beckett and Marquez-Grant (2017) measured location (based on the calculation of the foraminal index, not used in this study, see Subsection 5.3.2), direction, length, angle, circumference and area of the main nutrient canal in human, pig and sheep humeri and femora, in order to identify new parameters that could be used in the differentiation between human and non-human bones in forensic contexts. Johnson *et al.* found that circumference and area of the nutrient canal are not useful for the human/non-human differentiation, as there are no significant differences among the species considered; the canal length was found to be a discriminating parameter. However, only 36 bones were used, and only two non-human species were considered; furthermore, since Johnson's research focused only on humeri and femora, its results might not be applicable in cases where other long bones such as radii, ulnae or tibiae are found.

In the study presented in this thesis (section 6.4) 384 long bones were employed; the analyses were focused on location, appearance, direction, shape and angle of the nutrient foramina of human and non-human humeri, radii, ulnae, femora and tibiae.

7.4.1 Location

The location of the nutrient foramina does not follow a specific pattern in any of the species considered in this study; furthermore, none of the foramina locations can be associated to a specific species.

The only exception is the human humerus, as it is the only human bone having a unique foramen location: when a fragment is big enough to understand it is a humerus, if the foramen location is anterior, distal and medially located, the bone should be securely identified as human. The unique location of the humeral nutrient foramen, between the coracobrachialis and brachialis muscles, is well known in clinical medicine, as the humerus is supplied by a single nutrient artery that is usually affected in case of fractures (Menck, Dobler and Dohler, 1997; Xue *et al.*, 2016).

In all long bones, the primary nutrient foramina are located near major muscle attachments, as they are essential for a continuous blood supply (Kizilkanat, Boyan and Ozsahin, 2007). More precisely, foramina lay on the flexor surface of the bones (Buckwalter *et al.*, 2001).

The human radius, like humerus, does not share the foramen location with any other non-human bone considered in this study. However, unless the fragment is big enough to see the actual shape of the bone, its side or any other feature such as muscular attachments, location alone might not be useful for origin identification, as in a highly fragmented bone is not possible to see where the foramen is located. In any case, location can be useful if other parameters such as appearance are considered.

7.4.2 Appearance

The human species seems to be the one with the most varied pattern in terms of nutrient foramina appearance in the skeleton. None of the non-human species follows a specific pattern. Only chicken and deer have the drop-shape recurring in all bones, but this is not always the case; in any case, this detail would be beneficial only to a specific non-human species identification, which is not the aim of the present study.

Although variations in foramina appearance were seen on human radius and femur, and some similarities between human and non-human foramina (e.g. human radius and sheep femur) were noticed, the appearance resulted to be the most effective for the differentiation of human/nonhuman bone, among the parameters considered in the research focused on nutrient foramina.

There are some shapes that do not appear on human bones: V-shape, which was seen only in pig and duck; oval and linear, seen only in birds. If a nutrient foramen shows one of these shapes, the bone might be non-human. The appearance table shown in section 6.4 (Table 6.11) might be used as a reference in case of a nutrient foramina-based bone origin identification.

In case of very fragmented bones, the specific orientation of the foramen might not be noticeable, but it is useful to know it, because the foramina that have a specific orientation would appear oblique in any case, when compared to the direction of the bone growth lines (Iannotti, 1990). The orientation alone might even help understanding the origin, since among the human bones only humerus has a foramen with an orientation (medial-lateral).

7.4.3 Direction

In human limb bones, the nutrient canal opens towards the elbow in the upper limb and away from the knee in the lower limb (Longia, Ajmani, Saxena and Thomas, 1980; Williams *et al.*, 1995). The direction pattern of the nutrient foramina in non-human species does not always follow the same rule seen in human limb bones (Rao and Kothapalli, 2014). The present study shows that the porcine bones share the whole nutrient canal direction pattern with the human bones.

As there are only two possible directions, there is limited variability between species. Identifying the origin of fragmented bones only by direction of foramina is not possible, but in any case knowing the direction of every human long bone primary foramen might help in the process, when other features such as appearance and location are considered.

7.4.4 Shape from micro-CT scans

As for the nutrient foramina shape from the XY plane, human bones were the only ones that showed specific and consistent shapes that appeared very similar to each other, with the right bone equal to the left one. The foramina shapes of the non-human species showed less consistency and more variation.

The shape as seen in the XY plane was a very helpful parameter for the origin identification, as in most cases the human bones did not share the foramen shape with any other non-human bone.

Conversely, the shape as seen in the YZ plane was not useful. Indeed, in none of the bones, either human or non-human, the foramina shapes followed a fixed pattern that could be related to a specific species; in human bones there was no correspondence even between left and right of the same long bone (except for humerus).

It should be noted that the results of this part of the study might have some limitations, as only two of each long bone were scanned. With more bones, more (or less) inter- and intra-species variation might be expected.

7.4.5 Angle of the nutrient canal from micro-CT scans

In human bones, the angle at which the nutrient canal enters the bone went from 0.26° to 3°, which is a very large range that does not allow a secure origin identification. Furthermore, for most human bones the angle degree was shared with non-human species, meaning that in a non-human bone the nutrient canal may enter the cortex at the same angle as in a human bone.

This parameter alone is not reliable; it might be helpful only if used along other parameters. For example, if a bone fragment is thought to be a human tibia (on the basis of different parameters), the angle of the nutrient canal can be used to check whether it is consistent or not with a human tibia, in order to strengthen the diagnosis.

7.5 Cross-sectional shape

Most of the studies that have looked at the differences between human and non-human long bone cross sectional shapes have focused on the relation between morphology, body mass, biomechanical properties and mobility, and compared human limb bones to those of primates (Ruff, 1990; Carlson *et al.*, 2006; Ruff and Larsen, 2014). Fewer studies have focused on mammalian limb bones and their cross-sectional properties in relation to locomotion, body mass and mechanical loading (Polk *et al.*, 2000; Cosman, Sparrow and Rolian, 2016).

Cross-sectional shape, area, and second moments of area (geometrical property that calculates how the points of an area are distributed with regard to an arbitrary axis) of long bone diaphyses have been used in multiple studies as parameters to better understand human skeletal adaptation. Research has mainly focused on locomotion, manipulative behaviour, bone growth and the consequences of subsistence strategies on the skeleton (e.g., Stock and Pfeiffer, 2001; Holt, 2003; Ruff, 2003).

The long bones' cross-sectional shape has been used in studies focused on population comparison in terms of activity and nutrition (e.g. pre-agricultural vs agricultural), mobility patterns, or sexual dimorphism (Ogilvie and Hilton, 2011; Stock *et al.*, 2011). Some modern studies have considered the cross-sectional geometry of limb bones to compare individuals who practice different sports; an example is the study of Shaw and Stock (2009), where the tibial mid-shafts of young adult male cross-country runners, field hockey players, and controls were compared.

Despite the many studies focusing on the cross-sectional properties of long bones, very little research has been done regarding the differentiation between human and non-human long bones cross sectional shape applied to fragmented bones in archaeological or forensic contexts. There are few publications within the field of comparative anatomy focused on the cross-sectional shape of complete bones, such as Hillson (2003), which compares mammalian long bones, including human, using drawings. The cross-sectional shapes observed as a result of this study were compared to those shown in Hillson's book; the findings of the two studies are similar, both for human and non-human mammal bones.

In this study, the cross-sectional shapes of human limb bones were different from those seen in the non-human species considered. The uniqueness of the human shapes are due to bipedal locomotion and to a different range of movements (e.g. hand grasping) not seen in most non-human species (France, 2009).

The human humerus has a very distinctive rectangular/quadrangular cross-sectional shape that does not resemble the egg-shape or oval shape seen in non-human mammals and birds (see also Hillson, 2003). In humans, the humerus "twists" from the mid-shaft to the distal epiphysis and shows many ridges in the same area (where the non-human species observed are particularly smooth). The twisting and the ridges allow a greater movement of the forearm, and is therefore found only in humans and in those non-human species that have a more varied movement of the forearm, like primates (Beisaw, 2013; Currey, 2002).

For the same reasons the human radius appears as drop-shaped, while the non-human mammal ones, particularly in ungulates like the mammals observed in this study, are more massive and with no twisting, to be able to support the heavy limbs in standing position (see also Hillson, 2003).

In non-human mammals like sheep and deer, the ulna tends to be much smaller and more dense because of a very small or not present medullary cavity and the lack of interior spongy bone. In pigs, the ulna is asymmetrical and massive. In birds, on the lateral side of ulna there are attachments for the feathers, while the rest of its surface is very smooth (Beisaw, 2013). It should be taken into account that in deer and sheep the ulna is separate from the radius only in immature individuals, while in adult ones it is fused to the radius, therefore unlikely to be found alone.

The human femur has its unique pear shape because of the linea aspera (not visible before three years of age, more prominent with advancing age; Moore, 2014), which tends to be more marked in humans, who are bipedal and can do much more complex and diverse movements than any other non-human species. The shape of bird femora is similar to that seen in non-human mammals, although most bird bones are lighter and thinner than mammalian ones, which is why they should be considered only if

compared to human juveniles (Scheuer and Black, 2004; Christensen, Passalacqua and Bartelink, 2014).

The peculiar comma shape in human tibia is given by the presence of the anterior crest (Baker, Dupras and Tocheri, 2005), which arises from the tibial tuberosity and divides the anterior portion of the shaft into medial and lateral surfaces (Tersigni-Tarrant and Langley, 2017).

In a hypothetical scenario where the mid-shafts were cut in two or four halves, the cross-sectional shape of human long bones was still recognizable. The only exceptions were a portion of the anterior part of radius and the anterior part of femur, which if found isolated would suggest a rounded shape and could then be misidentified as a mammal femur, an adult bird radius or a bird femur.

When the bone fragmentation level makes the identification of a long bone by its cross-sectional shape difficult if not impossible, the internal morphology of the bone can help understanding whether the bone is human or non-human. In non-human mammals, the transition between the cortical and the spongy bone is sharp and clear, while in humans the transition is much less defined; birds bone tend to have a pneumatic internal structure (Komar and Buikstra, 2008; see Chapter 2 of this thesis).

The identification of the human or non-human origin of limb bones by their cross-sectional shape might get difficult with cremated bones, as the burning process can cause significant alteration of the shape of shafts (Imaizumi, 2015). Shrinkage, warping, spalling and fracturing may occur (Haglund and Sorg, 1997; Brickley, 2007). Significant deformation and fragmentation may be due to shrinkage, which can cause alteration of important morphological indicators of species, sex, age and stature (Imaizumi, 2015). Warping is also responsible for heat-induced shape changes in bones; its effects are limited in areas of dense bone, but it can cause great dimensional changes along the principal axis of loading and transverse diameters of long bones (Thompson, 2005). Warping is more prominent when the bone burns when still fleshed, because of the muscle fibres contraction induced by heat (Thompson, 2005).

7.6 The admissibility of evidence in forensic cases

In forensic cases, all evidence presented in court must conform to a series or rules and restrictions in order to be admissible and considered as relevant. In the United Kingdom, evidence is considered admissible if the following conditions are satisfied:

- The expert witness is impartial and sufficiently qualified in his/her field of expertise, which itself is considered to be reliable;
- The expert witness should only testify in relation to matters within his/her knowledge, as evidence of opinion or belief is inadmissible;
- The expert witness has acquired by study or experience sufficient knowledge of the relevant field to render his/her opinion of value;
- The expert evidence has a sufficiently reliable scientific basis, or is part of a body of knowledge/experience which is sufficiently organised to be accepted as reliable knowledge or experience;
- The evidence is based on validated methods, such as laboratory techniques and technologies; the methods are recognised as providing a sufficient scientific basis upon which the expert's conclusions can be reached;
- The expert's opinion relies on an inference from any findings, and the opinion properly explains how safe or unsafe the inference is, by reference to statistical significance or in other appropriate terms;
- If the expert's opinion relies on results obtained by using a qualitative method, the opinion takes proper account of matters affecting the accuracy or reliability of those results (The Crown Prosecution Service, 2014).

In the United States, similar regulations apply. Federal courts and most state courts use the Daubert standard, a rule of evidence regarding the admissibility of expert evidence in court. The Daubert standard takes its name from the Daubert v. Merrell Dow Pharmaceuticals case (1993), where the pharmaceutical company was accused of selling drugs that caused serious birth defects. The expert evidence submitted to prove that the drug caused birth defects was based on methodologies (in vitro and in vivo animal studies, and reanalysis of other published studies) that had not yet been accepted by the scientific community (Bernstein, 1994). The trial court dismissed the case for lack of admissible evidence, and the US Supreme Court defined the criteria by which scientific knowledge

could be used as evidence in court. The factors that a judge should consider when following the Daubert standard are:

- Whether the theory has been tested;

- The standards controlling the technique used;

- Whether the theory/technique has been subjected to peer review and publication;

- The known or potential error rate;

- The general acceptance of the theory and the method;

- Whether the expert has adequately accounted for alternative explanations (Saferstein, 2007).

Before the Daubert standard, the Frye standard was followed. It was established in 1923 by the US District of Columbia Circuit Court, after it rejected the scientific validity of the polygraph. The Frye standard was applied to decide if the procedure used by the expert was generally accepted by the relevant scientific community (Fisher, 2016). In 1975 the federal courts introduced the Federal Rules of Evidence, which were more flexible than the Frye standard, as they considered a suitable witness any individual qualified as an expert by knowledge, skill, experience, training, or education. The testimony had to be based on sufficient data, as a result of reliable methods, reliably applied to the facts of the case (Federal Rules of Evidence, 2014).

After the Kumho Tire Co. v. Carmichael case in 1999, the Supreme Court expanded the Daubert rule to include scientific and technical expert testimony. Kumho Tire Co., a tire manufacturer, was sued because its defective tires were considered the cause of a deadly vehicle accident. The expert witness was a tire failure expert, whose methodology was considered not scientifically valid (Schwartz, 2000).

7.7 Concluding remarks

Table 7.1 Summarizes the research presented in this study, showing the parts of the human and non-human skeleton considered, the specific features analysed and the method used, the effectiveness of each feature/method in the human-nonhuman bone differentiation, and the potential limitations.

Bone(s)	Feature	Method	Human/Nonhuman Differentiation	Limitations
Parietals	Curvature	GIS	Not Possible	High error rate; Intra-species variability
Parietals	Sagittal suture pattern	GIS	Possible	Qualitative method; Less effective on partially obliterated sutures; Not effective with one-sided sutures
Ribs (3rd to 10th)	Shaft curvature	GIS	Possible	Only one non-human species used; small sample size
Occipital	Occipital condyles/foramen magnum morphology	Morphological examination	Possible	Qualitative method
Femur	Linea aspera morphology	Morphological examination	Possible	Qualitative method
Limb bones, except fibula	Nutrient foramen (location, direction, appearance, shape, angle)	Morphological examination, micro-CT	Possible	Number of bones scanned; Possible intra-species variation
Limb bones, except fibula	Mid-shaft cross-sectional shape	Micro-CT	Possible	Less effective in case of high fragmentation

Table 7.1. Summary of the research and its results.

Chapter 8:

CONCLUSIONS, LIMITATIONS, AND FURTHER RESEARCH

The results presented within this thesis have provided a new insight into the human-nonhuman fragmented bone differentiation. Bone features about which little research has been done or that have never been used for the human-nonhuman distinction were investigated: cranial bone curvature, cranial sutures, rib shaft curvature, occipital condyles, linea aspera, nutrient foramina and cross-sectional shape of limb bones. 34 non-human species were considered and more than 700 human and non-human bones were analysed in this study; more than 1000 bones were initially observed and then excluded from further analyses. Non-destructive methods that have the potential of speeding up the origin identification process were employed. A GIS software was used to calculate cranial and rib curvature, and to identify cranial suture patterns; morphological examination was used to analyse occipital condyles and linea aspera, while micro-CT was employed to investigate nutrient foramina and cross-sectional shape. In this chapter, the conclusions of the research are stated, along with its limitations and the recommendations for further research.

8.1 Research conclusions

The use of a GIS software to calculate rib curvature and to identify suture patterns proved to be an effective method of differentiation between human and non-human cranial bones and ribs. However, the calculation of parietals curvature did not allow to differentiate non-human cranial vaults from the human ones; there were no significant differences between the species, and the probability of error was high. The calculation of rib curvature produced more reliable results. The curvature of a rib shaft fragment without any visible indicative feature, whose human or non-human origin needs to be identified, can be quickly calculated using ArcScene. The numerical values obtained can be statistically compared to the ones shown in this study, or new calculations with human (and non-human if needed) reference samples can be done and used for comparison. The human and non-human sagittal suture patterns were identified and distinguished; the method was successfully tested on human cranial vault fragments.

The human origin of complete or fragmented occipital condyles can be identified, despite the fact that human condyles share their features with some non-human species. It was demonstrated that a thorough morphological examination of specific characteristics of the occipital condyles allows to distinguish between human and non-human bone fragments showing complete or partial condyles, and to identify the specific non-human species, if needed. Even those species whose condyles seemed to be particularly similar to the human ones, such as fox and seal, could be distinguished and identified. Given the visible differences between the human and non-human species, the occipital condyles, if found in a fragmentation context, can be used to assess the origin of occipital bone fragments.

As regards linea aspera, it was shown that the differences between human and non-human may not be clear in case of fragmentation of the posterior femoral shaft, as in some non-human species the linea aspera has human-like features that can lead to origin misidentification. A thorough examination of the linea aspera of each non-human species considered was performed, and specific portions of each non-human linea aspera were compared with the corresponding portions of the human linea aspera. Very specific differences were found, even in those species that seemed to have a linea aspera, or parts of it, very similar to the human one. Therefore, the human or non-human origin of femoral shaft fragments showing the linea aspera can be assessed using the linea aspera as diagnostic feature.

There are noticeable differences among nutrient foramina of human and non-human long bones. Nutrient foramina can be used to identify the human or non-human origin of fragmentary or incomplete long bones shafts. The location of the foramen can be a very useful parameter, especially if the anatomy of human long bones (and possibly of some common non-human species) is known; when the samples are too fragmented, location becomes less useful alone, but can still be helpful if considered alongside other data. Direction as a parameter is impossible to use alone, as it can be only proximal-distal or distal-proximal, but it can be useful as complimentary data that can be cross-checked with others. Among the parameters morphologically examined, the appearance of the nutrient foramina was proven to be the most effective one; in any case, it is advisable to use the other parameters for safer results. As regards the features requiring the use of a micro-CT scanner, the canal entrance shape proved to be very useful, as most of the shapes seen in the human bones were not seen on any other non-human bone; however, only the XY plane should be considered. Since the shapes as seen on the micro-CT scans and those visible by the naked eye are not the same (because the latter include the vascular groove), the CT-scanning method does not represent just an additional verification, but a very useful tool for bone identification. The angle of the canal at the cortical bone was the least informative parameter; it cannot be used alone, but just for a data cross-check. If micro-

CT scanning is employed anyway, it is recommended to calculate the angle, since its calculation takes seconds; conversely, a CT-scan made with the sole purpose of angle calculation is not recommended.

The cross-sectional shape of the limb bones can help identifying their human or non-human origin. The method is accurate when the shaft shows its complete cross-sectional shape, because of the uniqueness of the human bones due to adaptation and evolution. The cross-sectional shape of human limb bones proved to be diagnostic even in a fragmentation scenario, where shapes were hypothetically cut in four halves. In cases of extreme fragmentation, the method can be less useful alone but can be still used to cross-check data obtained using other parameters (e.g. cortical-spongy bone transition). The comparison between human and non-human long bones cross-sectional shape allowed to group mammals and birds in different specific categories, in relation to their morphology, size, and the way they move or fly. When fragmented bones are found and their human or non-human origin has to be assessed, the anatomy and the locomotion of the main non-human species that might be present on the scene should be taken into account, in order to ease the identification of the remains. The micro-CT scanning method is accurate, quick and non-invasive, as it allows to look at the cross-section of bones without sectioning already fragmented bones.

8.2 Limitations

The calculation of parietals curvature did not help distinguishing between human and non-human cranial bones; the accuracy of the results might have been affected by the high intra-species variability, as shown by the high values of standard deviation in the means comparison.

The creation of contour lines in ArcScene for the suture pattern comparison in mainly a visual and qualitative method that does not run on a statistical basis. Furthermore, the method cannot be applied when only one side of a suture is available. The method is also less effective on partially obliterated sutures, but this might not be considered a limitation as a closed suture would not be visible in any case, regardless of the method used.

The rib curvature calculation method itself did not show any limitation. The small sample size and the comparison with only one non-human species are limitations related to the unavailability of non-human ribs for the study. The fact that only 13th and 14th pig ribs were used might be considered a limitation, although their use was justified by the lack of availability of other pig ribs.

The morphological examination of occipital condyles and linea aspera was a qualitative research, based on the detailed observation and on the comparison of features present in human bones with those present in a number of non-human species. The qualitative nature of the studies might not be considered as a limitation, as the data obtained did not require quantification.

In the study focused on nutrient foramina, while the visual examination of location, appearance and direction was performed on a relatively high number of bones, both human and non-human, the micro-CT scanning was used on a lower quantity of bones, more precisely on an average of ten bones per species. With a higher number of scanned bones, intra-species variation in foramina shape and canal angle might be noticed.

There are some limitations in the use of the cross-sectional shape as a parameter to distinguish human from non-human bones. Very small fragments might not suggest the cross-sectional shape of the bone, and cremated bones can undergo a shape alteration. Furthermore, all the individuals considered for this study were healthy, with the exception of some osteoarthritis cases; stress, rickets, spina bifida, cancer and trauma might change the shape of the bones affected (Ralis *et al*., 1976; Lin *et al*., 2015).

8.3 Recommendations for further research

The differentiation between human and non-human bone fragments represents a very important and challenging aspect of both forensic and biological anthropology. Furthermore, most of the methodologies currently used to identify the human or non-human origin of bone fragments are destructive and time-consuming; further research on potential non-destructive methods of origin identification is needed. Some of the bone features and methods used for the research presented in this thesis, such as cranial sutures and GIS, were never used before for human and non-human bone differentiation; therefore, further research using the same bone features and methods is recommended.

As for cranial curvature, a higher number of samples from the same species used in this study could improve the accuracy of the results, given the high intra-species variability in cranial curvature values.

The suture considered in this study was the sagittal; further research on the comparison between human and non-human cranial sutures can be extended to the coronal and the lambdoid suture, as similarities in these sutures were noticed between human and non-human crania.

The linea aspera of deer and dog and its strong similarities with the human one should be better investigated, given the variety of types and breeds that characterize these two non-human species.

Further research can be done on the differentiation between human and non-human nutrient foramina, possibly involving different non-human species and a larger sample number to use for micro-CT scanning, in order to evaluate the presence (or absence) or intra-species variability.

The use of cross-sectional shape as means for the differentiation between human and non-human limb bones can be further investigated, taking into consideration different locations in the proximal and distal shaft. Furthermore, the impact of cremation and pathological conditions on the cross-sectional shape of human and non-human limb bones and the possible effect on their differentiation can be an interesting subject for future research.

Further studies can consider any of the features and methods used in this thesis and apply them on other non-human species, whose skeletal remains may be potentially found in a forensic or bioarchaeological context in countries with a different fauna from that found in the United Kingdom.

REFERENCES

Adams, B.J. (2007), *Forensic Anthropology*, New York (NY): Chelsea House Publishers.

Adams, B.J. and Byrd, J.E. (eds). (2008), *Recovery, Analysis and Identification of Commingled Human Remains,* Totowa (NJ): Humana Press.

Adams, B.J., Crabtree, P.J. and Santucci, G. (2008), *Comparative Skeletal Anatomy. A Photographic Atlas for Medical Examiners, Coroners, Forensic Anthropologists, and Archaeologists,* Totowa (NJ): Humana Press.

Albert, M.J. (2012), "La forense policial del 'caso Ruth y José' echa en falta un hueso de las pruebas", El País, 16 October 2012, https://elpais.com/ccaa/2012/10/16/andalucia/1350391997_752786.html (accessed January 2018).

Albert, M.J. (2013), "José Bretón sentenced to 40 years for murder of his two young children", El País, 22 July 2013, https://elpais.com/elpais/2013/07/22/inenglish/1374497071_160243.html (accessed January 2018).

Andronowski, J.M., Pratt, I.V. and Cooper, D.M.L. (2017), "Occurrence of osteon banding in adult human cortical bone", *American Journal of Physical Anthropology*, vol. 164, no. 3, pp. 635-642.

Anstett, E. and Dreyfus, J.M. (2015), *Human Remains and Identification: Mass Violence, Genocide and "the Forensic turn",* Manchester: Manchester University Press.

Apps, J., Vesely, L., Alys, L.L. and Blythe, T. (2014), Two sides of the same coin, missing and unidentified people. In Mallett, X., Blythe, T. and Berry, R. (eds), *Advances in forensic human identification,* Boca Raton (FL): CRC Press, pp. 3-19.

Arbabi, A. (2009), "A quantitative analysis of the structure of human sternum", *Journal of Medical Physics*, vol. 34, no. 2, pp. 80-86.

Arcoverde, N., Euclides, N., Duarte, R.M., Barreto, R.M., Magalhaes, J.P., Bastos, C.M., Ren, T.I. and Cavalcanti, G.C. (2014), "Enhanced real-time head pose estimation system for mobile device", *Integrated Computer-Aided Engineering,* vol. 21, no. 3, pp. 281-293.

Aspinall, V. and Cappello, M. (2015), *Introduction to Veterinary Anatomy and Physiology Textbook,* Toronto (ON): Elsevier.

Baker, B.J., Dupras, T.L. and Tocheri, M.W. (2005), *The Osteology of Infants and Children,* Texas A&M University Anthropology Series, no.12, Texas A&M University Press.

Barrios Mello, R., Regis Silva, M.R., Seixas Alves, M.T., Evison, M.P., Guimarães, M.A., Francisco, R.A., Dias Astolphi, R. and Miazato Iwamura, E.S. (2017), "Tissue Microarray Analysis Applied to Bone Diagenesis", *Scientific Reports*, vol. 7, Article number: 39987.

Bartosiewicz, L. (2013), *Shuffling Nags, Lame Ducks. The Archaeology of Animal Disease,* Oxford: Oxford Books.

BBC News (2013), "April Jones trial: Bone fragments from 'human skull'", 21 May 2013, http://www.bbc.co.uk/news/uk-wales-22596503 (accessed January 2018).

Becker, M.J. (1986), "Mandibular symphysis (medial suture) closure in modern Homo sapiens: Preliminary evidence from archaeological populations", *American Journal of Physical Anthropology,* vol. 69, no. 4, pp. 499-501.

Beisaw, A.M. (2013), *Identifying and Interpreting Animal Bones. A Manual,* Texas A&M University Anthropology Series, no. 18. China: Everbest Printing & Co.

Bellis, C., Ashton, K.J., Freney, L., Blair, B. and Griffiths, L.R. (2003), "A molecular genetic approach for forensic animal species identification", *Forensic Science International*, vol. 134, pp. 99-108.

Benedix D. (2004), *Differentiation of fragmented bone from Southeast Asia: the histological evidence*, Doctoral dissertation. Knoxville (TN): University of Tennessee-Knoxville.

Bernstein, D. E. (1994), "The Admissibility of Scientific Evidence after Daubert v. Merrell Dow Pharmaceuticals, Inc.", *Cardozo Law Review*, no. 15, pp. 2139–337.

Bolton, J.I. (2013), *The Pubic Symphysis Landscape - Investigating the Feasibility for a Quantitative Method of Age Determination, Using Geographical Information Systems.* A

thesis submitted in partial fulfilment of the requirements of Cranfield University for the degree of Master of Science. Shrivenham, United Kingdom: Cranfield University.

Boschin, F., Zanolli, C., Bernardini, F., Princivalle, F. and Tuniz, C. (2015), "A Look from the Inside: MicroCT Analysis of Burned Bones", *Ethnobiology Letters*, vol. 6, no. 2, pp. 258-266.

Boston, C. and Webb, H. (2012), Early Medical Training and Treatment in Oxford: A Consideration of the Archaeological and Historical Evidence. In Mitchell, P.D. (ed), *Anatomical Dissection in Enlightenment England and Beyond: Autopsy, Pathology and Display,* Farnham: Ashgate, pp. 43-68.

Bostrom, M., Yang, X. and Koutras, I. (2000), "Biologics in bone healing", *Current Opinion in Orthopaedics,* vol. 11, pp. 403-412.

Boulter, B.L. (2016), *Inventory and Demographic Analysis of Anatomical Teaching Specimens: The Teaching of Anatomy at the University of Oxford in the 19th Century.* A thesis submitted in partial fulfilment of the requirements of Cranfield University for the degree of Master of Science. Shrivenham, United Kingdom: Cranfield University.

Brickley, M.B. (2007), A Case of Disposal of Body Through Burning and Recent Advances in the Study of Burned Human Remains. In Brickley, M.B. and Ferllini, R. (eds), *Forensic Anthropology: Case Studies From Europe,* Springfield (IL): Charles Thomas Publisher, pp. 69-85.

Brickley, M.B. and Ferllini, R. (2007), *Forensic Anthropology: Case Studies from Europe,* Springfield (IL): Charles Thomas Publisher.

Brogdon, B.G. (1998), *Forensic Radiology,* Boca Raton (FL): CRC Press.

Brook, A.H., Griffin, R.C., Townsend, G., Levisianos, Y., Russell, J. and Smith, R.N. (2009), "Variability and patterning in permanent tooth size of four human ethnic groups", *Archives of Oral Biology,* vol. 54, no. 1, pp. 79-85.

Bruner, E., De La Cuetara, J.M. and Halloway, R. (2011), "A Bivariate Approach to the Variation of the Parietal Curvature in the Genus *Homo*", *The Anatomical Record,* vol. 294, no. 9, pp. 1548-1556.

Buckley, M., Collins, M., Thomas-Oates, J. and Wilson, J.C. (2009), "Species identification by analysis of bone collagen using matrix-assisted laser desorption/ionisation time-of-flight mass spectrometry", *Rapid Communications in Mass Spectrometry,* vol. 23, no. 23, pp. 3843-3854.

Buckley, M., Whitcher Kansa, S., Howard, S., Campbell, S., Thomas-Oates, J. and Collinse, M. (2010), "Distinguishing between archaeological sheep and goat bones using a single collagen peptide", *Journal of Archaeological Science,* vol. 37, no.1, pp. 13-20.

Buckley, M., Fraser, S., Herman, J., Melton, N.D., Mulville, J. and Pálsdóttir, A.H. (2014), "Species identification of archaeological marine mammals using collagen fingerprinting", *Journal of Archaeological Science,* vol. 41, pp. 631-641.

Buckley, M. (2017), Zooarchaeology by Mass Spectrometry (ZooMS) Collagen Fingerprinting for the Species Identification of Archaeological Bone Fragments. In Giovas, C.M. and LeFebvre, M.J. (eds), *Zooarchaeology in Practice. Case Studies in Methodology and Interpretation in Archaeofaunal Analysis,* Cham (Switzerland): Springer, pp. 227-247.

Buckwalter, J.A., Stanish, W.D., Rosier, R.N., Schenck, R.C. Jr, Dennis, D.A. and Coutts, R.D. (2001), "The increasing need for non-operative treatment of patients with osteoarthritis", *Clinical Orthopaedics and Related Research*, vol. 385, pp. 36-45.

Budimlija, Z.M., Prinz, M.K., Zelson-Mundorff, A., Wiersema, J., Bartelink, E., MacKinnon, G., Nazzaruolo, B.L., Estacio, S.M., Hennessey, M.J., Shaler, R.C. (2003), "World Trade Center Human Identification Project: Experiences with Individual Body Identification Cases", *Croatian medical journal*, vol. 44, no. 3, pp. 259-263.

Buikstra, J.E. and Ubelaker, D.H. (1994), *Standards for Data Collection from Human Skeletal Remains,* Fayetteville: Arkansas Archaeological Survey Research Studies No. 44.

Byers, S.N. (2017), *Introduction to Forensic Anthropology,* fifth edition, Abingdon: Routledge.

Campbell Hibbs, A.R. and Finnegan, M. (2010), Age estimation by root dentin transparency of single rooted teeth. In Latham, K.E. and Finnegan, M. (eds), *Age Estimation of the Human Skeleton*, Springfield (IL): Charles Thomas Publisher, pp. 36-47.

Campos, F.F., Pellico, L.G., Alias, M.G. and Fernández-Valencia, R. (1987), "A study of nutrient foramina in human long bones", *Surgical and Radiologic Anatomy*, vol. 9, no. 3, pp. 251-255.

Carlson, K.J., Doran-Sheehy, D.M., Hunt, K.D., Nishida, T., Yamanaka, A. and Boesch, C. (2006), "Locomotor behavior and long bone morphology in individual free-ranging chimpanzees", *Journal of Human Evolution,* vol. 50, pp. 394-404.

Cartmill, M. and Smith, F.H. (2009), *The Human Lineage,* Hoboken (NJ): John Wiley & Sons.

Casanova, P.M. (2012), "Basicranial analysis in young bovines reveals a relation to breed and sex", *Anatomia, Histologia, Embryologia*, vol. 42, pp. 398-401.

Cattaneo, C., Gelsthorpe, K. and Sokol, R.J. (1994), "Immunological detection of albumin in ancient human cremation using ELISA and monoclonal antibodies", *Journal of Archaeological Science,* vol. 21, pp. 565-571.

Cattaneo, C., DiMartino, S., Scali, S., Craig, O. E., Grandi, M. and Sokol, R.J. (1999), "Determining the human origin of fragments of burnt bone: a comparative study of histological, immunological and DNA techniques", *Forensic Science International*, vol. 102, pp. 181-191.

Chandra Sekharan, P. (1985), "Identification of skull from its suture pattern", *Forensic Science International*, vol. 27, pp. 205-214.

Chang, K. (2010), *Introduction to Geographic Information Systems,* fifth edition, New York (NY): McGraw-Hill Higher Education.

Chevalier, T. (2008), "Linea aspera: criterion of bipedalism?", *Biometrie Humaine et Anthropologie*, vol. 26, no. 3-4, pp. 225-237.

Chilvarquer, I., Katz, J.O., Glassman, D.M., Phrihoda, T.J. and Cottone, J.A. (1987), "Comparative radiographic study of human and animal long bone patterns", *Journal of Forensic Sciences*, vol. 32, no. 6, pp. 1645-1654.

Christensen, A.M., Smith, M.A. and Thomas, R.M. (2012), "Validation of X-ray fluorescence spectrometry for determining osseous or dental origin of unknown material", *Journal of Forensic Sciences,* vol. 57, no. 1, pp. 47-51.

Christensen, A.M., Passalacqua, N.V. and Bartelink, E.J. (2014), *Forensic Anthropology. Current Methods and Practice,* San Diego (CA): Elsevier.

Christensen, A.M., Passalacqua, N.V., Schmunk, G.A., Fudenberg, J., Hartnett, K., Mitchell, R.A., Love, J.C., DeJong, J. and Petaros, A. (2015), "The value and availability of forensic anthropological consultation in medicolegal death investigations", *Forensic Science, Medicine and Pathology,* vol. 11, no. 3, pp. 438-441.

Conolly, J. and Lake, M. (2006), *Geographical Information Systems in Archaeology. Cambridge Manuals in Archaeology,* Cambridge: Cambridge University Press.

Copes, L.E., Lucas, L.M., Thostenson, J.O., Hoekstra, H.E. and Boyer, D.M. (2016), "A collection of non-human primate computed tomography scans housed in MorphoSource, a repository for 3D data", *Scientific Data,* vol. 3, Article number: 160001, doi:10.1038/sdata.2016.1.

Cosman, M.N., Sparrow, L.M. and Rolian,C. (2016), "Changes in shape and cross-sectional geometry in the tibia of mice selectively bred for increases in relative bone length", *Journal of Anatomy,* vol. 228, no. 6, pp. 940-951.

Covington, A.D, Song, L., Suparno, O., Koon, H. and Collins, M.J. (2008), "Link-lock: an explanation of the chemical stabilisation of collagen", *Journal of the Society of Leather Technologists and Chemists,* vol. 92, no. 1, p. 1.

Crescimanno, A. and Stout, S.D. (2012), "Differentiating fragmented human and nonhuman long bone using osteon circularity", *Journal of Forensic Sciences*, vol. 57, no. 2, pp. 287-294.

Croker, S.L., Clement, J.G. and Donlon, D. (2009), A comparison of cortical bone thickness in the femoral midshaft of humans and two non-human mammals, *HOMO – Journal of Comparative Human Biology,* vol. 60, no. 6, pp. 551-565.

Cuijpers, S. A. (2009), "Distinguishing between the bone fragments of medium-sized mammals and children. A histological identification method for archaeology". *Anthropologischer Anzeiger,* vol. 67, pp. 181–203.

Currey, J.D. (2002), *Bones. Structure and Mechanics,* Oxford: Princeton University Press.

Dawnay, N., Oqden, R., McEwing, R., Carvalho, G.R. and Thorpe, R.S. (2007), "Validation of the barcoding gene COI for use in forensic genetic species identification", *Forensic Science International*, vol. 173, no. 1, pp. 1-6.

Deisboeck, T. and Kresh, J.Y. (2006), *Complex Systems Science in Biomedicine,* New York (NY): Springer.

De la Cova, C. (2017), Fractured lives: structural violence, trauma, and recidivism in urban and industrialized 19th-century-born African American and Euro-Americans. In Tegtmeyer, C.E. and Martin, D.L. (eds), *Broken Bones, Broken Bodies. Bioarchaeological and Forensic Approaches for Accumulative Trauma and Violence,* Lanham (MD): Lexington Books, pp. 153-180.

De Lahunta, E. (2015), *Miller's Anatomy of the Dog,* fourth edition, St Louis (MO): Elsevier.

Dennis, M.Y, Paracchini, S., Scerri, T.S., Prokunina-Olsson, L., Knight, J.C., Wade-Martins, R., Coggill, P., Beck, S., Green, E.D. and Monaco, A.P. (2009), "A Common Variant Associated with Dyslexia Reduces Expression of the *KIAA0319* Gene", *PLOS Genetics,* Published: March 27, 2009, *https://doi.org/10.1371/journal.pgen.1000436.*

De Oliviera, O.F., Tinoco, R.L.R, Daruge, J.E., Araujo, L.G., Silva, R.H.A. and Paranhos, L.R. (2013), "Sex Determination from Occipital Condylar Measurements by Baudoin Index in Forensic Purposes", *Internal Journal of Morphology,* pp. 1297-1300.

Dettmeyer, R.B. (2011), *Forensic Histopathology. Fundamentals and Perspectives,* Berlin: Springer.

Dettmeyer, R.B. (2018), *Forensic Histopathology. Fundamentals and Perspectives,* Second Edition, Berlin: Springer.

De Witte, S.N. (2015). "Bioarchaeology and the Ethics of Research Using Human Skeletal Remains", *History compass*, vol. 13, no. 1, pp. 10-19.

Dirkmaat, D. (ed). (2014), *A Companion to Forensic Anthropology,* Chichester: Wiley-Blackwell.

Dix, J.D., Stout, S.D. and Mosley, J. (1991), "Bones, blood, pellets, glass, and no body", *Journal of Forensic Sciences,* vol. 36, no. 3, pp. 949-952.

Dogăroiu, C., Dermengiu, D. and Viorel, V. (2012), "Forensic comparison between bear hind paw and human feet. Case report and illustrated anatomical and radiological guide", *Romanian Society of Legal Medicine*, vol. 20, pp. 131-134.

Domínguez-Rodrigo, M. and Barba, R. (2007), *Deconstructing Olduvai: A Taphonomic Study of the Bed I Sites,* Dordrecht (The Netherlands): Springer.

Domínguez, V.M. and Crowder, C.M. (2012), "The utility of osteon shape and circularity for differentiating human and non-human Haversian bone", *American Journal of Physical Anthropology,* vol. 149, no. 1, pp. 84-91.

Dongchoon, A. (2013), "Anatomical study on the diaphyseal nutrient foramen of the femur and tibia of the German shepherd dog", *Journal of Veterinary Medical Science,* vol. 75, pp. 803 – 808.

Du Plessis, A., Broeckhoven, C., Guelpa, A. and le Roux, S.G. (2017), "Laboratory x-ray micro-computed tomography: a user guideline for biological samples", *GigaScience*, vol. 6, no. 6, pp. 1-11.

Duhig, C. and Martinsen, N. (2007), Many Layers of Taphonomy: Dismemberment and Other Body Processing. In Brickley, M.B. and Ferllini, R. (eds), *Forensic Anthropology: Case Studies From Europe,* Springfield (IL): Charles Thomas Publisher, pp. 86-98.

Dumont, E.R. (2010), "Bone density and the lightweight skeletons of birds", *Proceedings of the Royal Society B: Biological Sciences*, vol. 277, no. 1691, pp. 2193-2198.

Dwyer, J. (2006), "Pieces of Bone Are Found on Building at 9/11 Site", New York Times, April 6, http://www.nytimes.com/2006/04/06/nyregion/pieces-of-bone-are-found-on-building-at-911-site.html (accessed December 2017).

Elbroch, M. (2006), *Animal Skulls: A Guide to North-American Species,* Mechanicsburg (PA): Stackpole Books.

Eriksen, K. and Rochester, R.P. (2007), *Orthospinology procedures. An Evidence Based Approach to Spinal Care,* Philadelphia (PA): Lippincott Williams & Wilkins.

Esri, "What is GIS?", https://www.esri.com/en-us/what-is-gis/overview (accessed June 2018).

Evans, E. (2016), Avian Anatomy. In Lovette, I.J. and Fitzpatrick, J.W. (eds), *The Cornell Lab of Ornithology Handbook of Bird Biology,* third edition, Chichester: Wiley, pp. 169-214.

Evidence Technology Magazine (2016), "Expert Q & A: Diane L. France", vol. 14, no. 2, pp. 26-27.

Ewer, R.F. (1998), *The Carnivores*, New York: Cornell University Press.

Fairgrieve, S.I. (2008), *Forensic cremation. Recovery and Analysis*, Boca Raton (FL): Taylor & Francis Group.

Fantner, G.E., Birkedalb, H., Kindta, J.H, Hassenkama, T., Weaverd, J.C., Cutronia, J.A., Bosmad, B.L., Bawazerb, L., Fincha, M.M., Cidadea, G.A.G., Morsed, D.E., Stuckyc, G.D., and Hansmaa, P.K. (2004), "Influence of the degradation of the organic matrix on the microscopic fracture behaviour of trabecular bone", *Bone*, vol. 35, pp. 1013-1022.

Federal Rules of Evidence (2014), Printed for the use of The Committee on the Judiciary House of Representatives, U.S. Government Printing Office, Washington http://www.uscourts.gov/sites/default/files/Rules%20of%20Evidence.

Ferllini, R. (2003), *Raising the Dead. How the Forensics of the Future are Solving the murders of the Past,* London: John Blake Publishing.

Fisher, B.A.J. (2016), "Moving Toward New Requirements for the Admissibility of Evidence", *Forensic Science Policy & Management: An International Journal,* vol. 7, no. 3-4, pp. 51-53.

Fox, A.J., Wanivenhaus, F. and Rodeo, S.A. (2012), "The basic science of the patella: structure, composition, and function", *The Journal of Knee Surgery,* vol. 25, no. 2, pp. 127-141.

France, D.L. (2009), *Human and Nonhuman Bone Identification: A Colour Atlas,* Boca Raton (FL): CRC Press.

France, D.L. (2011), *Human and Non-Human Bone Identification. A Concise Field Guide,* Boca Raton (FL): CRC Press.

Franklin, D., Swift, L. and Flavel, A. (2016), "'Virtual anthropology' and radiographic imaging in the Forensic Medical Sciences", *Egyptian Journal of Forensic Sciences,* vol. 6, no. 2, pp. 31-43.

Franklin, D. and Marks, M.K. (2013), Species: Human versus Nonhuman. In Siegel, J.A., Saukko, P.J. and Houck, M.M. (eds). *Encyclopaedia of Forensic Sciences,* second edition, San Diego (CA): Academic Press.

Franklin, D. and Marks, M.K. (2017), Species: Human versus Nonhuman. In Houck, M.M. (ed). *Forensic Anthropology,* London: Academic Press, pp. 129-136.

Gainor, B.J. and Metzler, M. (1986), "Humeral shaft fracture with brachial artery injury", *Clinical Orthopaedics and Related Research*, vol. 204, pp. 154–61.

Gantt, D.G., Grine, F.E. and Martin, L.B. (2007), HRXCT analysis of hominoid molars: A quantitative volumetric analysis and 3D reconstruction of coronal enamel and dentin. In Bailey, S.E. and Hublin, J.J. (eds.). *Dental Perspectives on Human Evolution. State-of-the-Art Research in Dental Palaeoanthropology,* Dordrecht (The Netherlands): Springer, pp. 117-138.

Gapert, R., Black, S. and Last. J. (2009), "Sex determination from the occipital condyle: discriminant function analysis in an eighteenth and nineteenth century British sample", *American Journal of Physical Anthropology,* vol. 138, no. 4, pp. 384-394.

Gates, H.R. (2003), *Infectious Diseases Secrets,* Second Edition, Philadelphia (PA): Hanley & Belfus, Elsevier.

Daniel García-Martínez, D., Recheis, W., and Bastir, M. (2015), "Ontogeny of 3D rib curvature and its importance for the understanding of human thorax development", *American Journal of Physical Anthropology,* vol. 159, no.3, pp. 424-431.

Garrod, B. (2016), "No more monkey business: why primates should never be pets", The Guardian, February 28, 2016, https://www.theguardian.com/lifeandstyle/2016/feb/28/why-primates-should-never-be-pets (accessed January 2018).

Gilbert. M.T.P., Willerslev, E., Hansen, A.J., Barnes, I., Rudbeck, L., Lynnerup, N. and Cooper, A. (2003), "Distribution Patterns of Postmortem Damage in Human Mitochondrial DNA", *The American Journal of Human Genetics*, vol. 72, no. 1, pp. 32-47.

Gilchrist, R., Vooght, S. and Soames, R. (2011), Comparative Osteology. In Black, S. and Ferguson, E. (eds). *Forensic Anthropology. 2000 to 2010,* Boca Raton (FL): CRC Press, pp. 319-328.

Glenny, M. (1997), *The Fall of Yugoslavia. The Third Balkan War,* London: Penguin Books.

Goel, A., Shah, A., Kothari, M., Gaikwad, S. and Dhande, P.L. (2011), "Comparative quantitative analysis of osseous anatomy of the craniovertebral junction of tiger, horse, deer and humans", *Journal of Craniovertebral Junction and Spine*, vol. 2, no. 1, pp. 32-37.

Gosman, J.H. (2012), Growth and Development: Morphology, Mechanisms and Abnormalities. In Crowder, C. and Stout, S. (eds). *Bone Histology: An Anthropological Perspective*, Boca Raton: CRC Press, pp. 23-44.

Graf. W., Vidal, P.P. and Evinger, L.C. (1986), "How animals move their heads", *Proceedings of the International Union of Physiological Sciences*, vol. 16, pp. 394-411.

Graf, W., de Waele, C. and Vidal, P.P. (1995), "Functional anatomy of the head-neck movement system of quadrupedal and bipedal mammals", *Journal of Anatomy*, vol. 186, pp. 55-74.

Gross, J.H. (2017), *Mass Spectrometry. A Textbook,* Third Edition, Cham (Switzerland): Springer, pp. 1-2.

Guharaj, P.V. (2003), *Forensic Medicine,* second edition, Telangana (India): Orient Blackswan Pvt. Limited.

Haglund, W.D. and Sorg, M.H. (1997), Method and theory of forensic taphonomic research. In Haglund, W.D. and Sorg, M.H., *Forensic Taphonomy. The Post-mortem Fate of Human Remains,* Boca Raton: CRC Press.

Hanak, V., Hartman, T.E. and Ryu, J.H. (2005), "Cough-induced rib fractures", *Mayo Clinic Proceedings,* vol. 80, no. 7, pp. 879-882.

Harms-Paschal, J.L. and Schmidt, C.W. (2010), The Estimation of Age at Death through the Examination of Root Transparency. In Latham, K.E. and Finnegan, M. (eds), *Age Estimation of the Human Skeleton*, Springfield (IL): Charles Thomas Publisher, pp. 19-35.

Hefner, J.T. (2009), "Cranial Nonmetric Variation and Estimating Ancestry", *Journal of Forensic Sciences,* vol. 54, no. 5, pp. 985-995.

Hershkovitz, N.Y. (2004), "Interrelationship between various aging methods, and their relevance to palaeodemography", *Human Evolution*, vol. 19, no. 2, pp. 145-155.

Hillier, M.L. and Bell, L.S. (2007), "Differentiating Human Bone from Animal bone: A Review of Histological Methods", *Journal of Forensic Sciences*, vol. 52, no. 2, pp. 249-263.

Hillson, S. (1996), *Dental Anthropology,* Cambridge University Press.

Hillson, S. (2003), *Mammal Bones and Teeth. An Introductory Guide to Methods of Identification,* Institute of Archaeology, University College London.

Hindelang, F., Zurbach, R. and Roggo, Y. (2015), "Micro Computed Tomography for medical device and pharmaceutical packaging analysis", *Journal of Pharmaceutical and Biomedical Analysis,* vol. 108, pp. 38-48.

Hiroshige, K., Soejima, M., Nishioka, T., Kamimura, S. and Koda, Y. (2009), "Simple and sensitive method for identification of human DNA by allele-specific polymerase chain reaction of FOXP2", *Journal of Forensic Sciences,* vol. 54, pp. 857-861.

Holt, B.M. (2003), "Mobility in Upper Palaeolithic and Mesolithic Europe: evidence from the lower limb", *American Journal of Physical Anthropology*, vol. 122, pp. 200-215.

Hughes, H. (1952), "The factors determining the direction of the canal for the nutrient artery in the long bones of mammals and birds", *Acta Anatomica* (Basel), vol. 15, pp. 261–80.

Human Tissue Act 2004. http://www.legislation.gov.uk/ukpga/2004/30/contents

Iannotti, J.P. (1990), "Growth plate physiology and pathology", *The Orthopedic Clinics of North America*, vol. 21, no. 1, pp. 1-17.

Imaizumi, K., Saitoh, K., Sekiguchi, K. and Yoshino, M. (2002), "Identification of fragmented bones based on anthropological and DNA analyses: case report", *Legal Medicine*, vol. 4, pp. 251-256.

Imaizumi, K. (2015), "Forensic Investigation of Burnt Human Remains", *Research and Reports in Forensic Medical Science*, vol. 5, pp. 67-74.

Javed, N. (2016), "Bones found on Vaughan construction site "non-human", TheStar.com, August 8, 2016 https://www.thestar.com/news/gta/2016/08/08/bones-found-on-vaughan-construction-site-non-human.html (accessed September, 2017).

Jayaprakash, P.T and Srinivasan, G.J. (2013), "Skull sutures: Changing morphology during preadolescent growth and its implications in forensic identification", *Forensic Science International*, vol. 229, 166.e1-166.e13.

Johnson, V.O., Beckett, S. and Marquez-Grant, N. (2017), "Differentiating human versus non-human bone by exploring the nutrient foramen: implications for forensic anthropology", *International Journal of Legal Medicine*, vol. 131, no. 6, pp. 1757-1763.

Johnston, S.A. and Tobias, K.M. (2018), *Veterinary Surgery. Small Animal,* second edition, St. Louis (MO): Elsevier.

Jurmain, R., Kilgore, L., Trevathan, B. and Ciochon, R.L. (2014), *Introduction to Physical Anthropology*, 2013-2014 Edition, Belmont (CA): Cencage Learning.

Kaiser, G.W. (2007), *The Inner Bird. Anatomy and Evolution,* Vancouver (BC): UBC Press.

Kalthur, S.G., Padmashali, S., Gupta, C. and Dsouza, A.S. (2014), "Anatomic study of the occipital condyle and its surgical implications in transcondylar approach", *Journal of Craniovertebral Junction and Spine*, vol. 5, no. 2, pp. 71-77.

Kardong, K.V. (1995), *Vertebrates. Anatomy, Function, Evolution*, Dubuque (IA): Wm. C. Brown Communications, Inc.

Kavitha, S., Chandrasekaran, S., Anand, A. and Shanthi, K.C. (2013), "Morphometric study of occipital condyles in adult human skulls", *International Journal of Current Research and Review*, vol. 5, no. 15, pp. 31-34.

Kizilkanat, E., Boyan, N. and Ozsahin, E.T. (2007), "Location, number and clinical significance of nutrient foramina in human long bones", *Annals of Anatomy*, vol. 189, pp. 87-95.

Klein-Nulend, J. and Bacabac, R.G. (2012), "Bone Adaptation and Regeneration – New Developments", *International Journal of Modern Physics: Conference Series,* vol. 17, pp. 34-43.

Klein, R.G. and Cruz-Uribe, K. (1984), *The Analysis of Animal Bones from Archaeological Sites,* Chicago: University of Chicago Press.

Klepinger, L.L. (2006), *Fundamentals of Forensic Anthropology*, Hoboken (NJ): John Wiley & Sons.

Klonowski, E.E. (2007), Exhumations in Bosnia and Herzegovina: Caves as Mass Graves, From Recovery to Identification. In Brickley, M.B. and Ferllini, R. (eds). *Forensic Anthropology: Case Studies From Europe,* Springfield (IL): Charles Thomas Publisher, pp. 183-202.

Knüsel, C.J. and Outram, A.K. (2004), "Fragmentation: the Zonation Method Applied to Fragmented Human Remains from Archaeological and Forensic Contexts", *Environmental Archaeology,* vol. 9, pp. 85-97.

Komar, D.A. and Buikstra, J.E. (2008), *Forensic Anthropology. Contemporary Theory and Practice,* Oxford University Press.

Konecny, G. (2014), *Geoinformation. Remote Sensing, Photogrammetry, and Geographic Information Systems,* second edition, Boca Raton (FL): CRC Press.

König, H.E., Korbel, R., Liebich, H.G. and Klupiec, C. (2016), *Avian Anatomy: Textbook and Colour Atlas,* second edition, Stuttgard (Germany): Schattauer.

Kontanis, E. and Sledzik, P. (2008), Resolving commingling issues during the medicolegal investigations of mass fatality incidents. In Bird, J. and Adams, B.J (eds.). *Recovery, Analysis and Identification of Commingled Human Remains,* Totowa, NJ: Humana Press, pp. 317-336.

Kulkarni, N.V. (2012), *Clinical Anatomy. A Problem Solving Approach,* second edition, New Delhi: Jaypee Brothers Medical Publishers.

Kumar, V., Rao, A.S., Rao KG, M., Jyothsna, P., Ashwini, L.S. and Sapna, M. (2013), "Presence of an articulating condylus tertius on the basilar part of the occipital bone - A rare anatomical abnormality", *Gülhane Tıp Dergisi*, vol. 55, pp. 217-219.

Kumar, A. and Nagar, M. (2015), "Human Adult Occipital Condyles: A Morphometric Analysis", *Research & Reviews: Journal of Medical and Health Sciences,* vol. 3, no. 4, pp. 112-116.

Lai, C.S., Fisher, S.E., Hurst, J.A., Vargha-Khadem, F. and Monaco, A.P. (2001), "A forkhead-domain gene is mutated in a severe speech and language disorder", *Nature*, vol. 413, pp. 519–23.

Latham, K.E. and Finnegan, M. (2010), *Age Estimation of the Human Skeleton*, Springfield (IL): Charles Thomas Publisher.

Lebrasseur, O., Ryan, H. and Abbona, C. (2018). Bridging Archaeology and Genetics. In Piskin, E., Marciniak. A. and Bartkowiak, M. (eds), *Environmental Archaeology. Current Theoretical and Methodological Approaches,* Cham (Switzerland): Springer, pp. 111-132.

Lee, H.C. (2007), Collection and Preservation of Biological Evidence from the Crime Scene. In Coyle, H.M. (ed), *Non-Human DNA Typing. Theory and Casework Applications,* Boca Raton (FL): CRC Press, pp. 11-22.

Leung, B. (2008), *Traditional Chinese Medicine. The Human Dimension,* Abingdon: Taylor & Francis.

Lieberman, D.E. and Crompton, A.W. (2000), "Why fuse the mandibular symphysis? A comparative analysis", *American Journal of Physical Anthropology,* vol. 112, no. 4, pp. 517-540.

Lieberman, D.E., Polk, J.D. and Demes, B. (2004), "Predicting long bone loading from cross-sectional geometry", *American Journal of Physical Anthropology,* vol. 123, pp. 156-171.

Liebich, H.E. and König, H.G. (2007), Hyoid bone, hyoid apparatus (os hyoideum, apparatus hyoideus). In Liebich, H.E. and König, H.G., *Veterinary Anatomy of Domestic Animals. Textbook and Colour Atlas,* third edition, Stuttgart (Germany): Schattauer, pp. 71-72.

Lin, C. and Miller, J (2002), "Cone beam X-ray microtomography—a new facility for three-dimensional analysis of multiphase materials", *Minerals Metallurgical Processing*, vol. 19, no. 2, pp. 65-71.

Lin, T., Wong, W., Chandra, A., Hsu, S.Y., Jia, H., Zhu, J., Tseng, W.J., Levine, M.A., Zhang, Y., Yan, S.G., Liu, X.S., Sun, D., Young, W. and Qin, L. (2015), "A comprehensive study of long-term skeletal changes after spinal cord injury in adult rats", *Bone Research*, 3: 15028, published online on 27/10/15. doi: 10.1038/boneres.2015.28.

Lloyd, C.D. (2010), *Spatial Data Analysis – An Introduction for GIS Users,* Oxford University Press.

Longia, G.S., Ajmani, M.L., Saxena, S.K. and Thomas, R.J. (1980), "Study of diaphyseal nutrient foramina in human long bones", *Acta Anatomica* (Basel), vol. 107, pp. 399-406.

Lovejoy, C.O., Meindl, R.S., Pryzbeck, T.R. and Mensforth, R.P. (1985), "Chronological metamorphosis of the auricular surface of the ilium: A new method for determination of adult skeletal age at death", *American Journal of Physical Anthropology,* vol. 68, no. 1, pp. 15-28.

Lydekker, R. and Sclater, P.L. (2011), *The Royal Natural History,* Charleston (SC): Nabu Press.

Lyman, R.L. (1994), *Vertebrate Taphonomy*, Cambridge University Press.

Lyman, R.L. (2013), Bone density and bone attrition. In Pokines, J.T. and Symes, S.A. (eds), *Manual of Forensic Taphonomy,* Boca Raton (FL): CRC Press, pp. 51-72.

Maass, P. (1997), *Love thy Neighbour: A Story of War,* New York: Vintage Books.

Maddux, S.D., Sporleder, A.N. and Burns, C.E. (2015), "Geographic Variation in Zygomaxillary Suture Morphology and its Use in Ancestry Estimation", *Journal of Forensic Sciences*, vol. 60, no. 4, pp. 966-973.

Maggiano, C.M. (2012), Making the Mold: A Microstructural Perspective on Bone Modelling During Growth and Mechanical Adaptation. In pp. Crowder, S. and Stout, S. (eds), *Bone Histology. An Anthropological Perspective,* Boca Raton (FL): CRC Press, pp. 45-90.

Malcolm, N. (2002), *Bosnia: a Short History,* London: Pan Books.

Mallett, X., Blythe, T. and Berry, R. (2014), *Advances in Forensic Human Identification*, Boca Raton (FL): CRC Press, Taylor & Francis Group.

Malmström, H., Storå, J., Dalén, L., Holmlund, G. and Götherström, A. (2005), "Extensive Human DNA Contamination in Extracts from Ancient Dog Bones and Teeth", *Molecular Biology and Evolution*, vol. 22, no. 10, pp. 2040–2047.

Malukar, O. and Joshi, H. (2011), "Diaphysial Nutrient Foramina In Long Bones And Miniature Long Bones", *National Journal of Integrated Research in Medicine*, vol. 2, no. 2, pp. 23-26.

Manhein, M.H., Listi, G.A. and Leitner, M. (2006), "The application of geographic information systems and spatial analysis to assess dumped and subsequently scattered human remains", *Journal of Forensic Sciences*, vol. 51, no. 3, pp. 469-474.

Mann, R.W., Manabe, J., Byrd, G.E., Sam, S.A., Holland, T.D., Tuamsuk, P. (2015). The sagittal suture as an indicator of age and sex. In Berg, G.E. and Ta'ala, S.C. (eds), *Biological Affinity in Forensic Identification of Human Skeletal Remains. Beyond Black and White,* Boca Raton (FL): CRC Press, pp. 95-132.

Mann, R.W., Hunt, D.R. and Lozanoff, S. (2016), *Photographic Regional Atlas of Non-Metric Traits and Anatomical Variants in the Human Skeleton,* Springfield (IL): Charles Thomas Publisher.

Marelli, C.A. and Simons, L.R. (2014), "Microstructure and Cross-Sectional Shape of Limb Bones in Great Horned Owls and Red-Tailed Hawks: How Do These Features Relate to Differences in Flight and Hunting Behavior?", *PLOS one*, published August 27, 2014, https://doi.org/10.1371/journal.pone.0106094.

Marenzana, M. and Arnett, T.R. (2013), "The key role of the blood supply to bone", *Bone Research*, vol. 1, no. 3, pp. 203-215.

Martini, F.H., Timmons, M.J. and Tallitsch, R.B. (2012), *Human Anatomy,* seventh edition, Oxford: Pearson Education.

Mayne Correia, P.M. (1997), Fire Modification of Bone: A Review of the Literature. In Haglund, W.D. and Sorg, M.H. (eds). *Forensic Taphonomy. The Postmortem Fate of Human Remains,* Boca Raton: CRC Press, pp. 275-293.

Mays, S., Elders, J., Humphrey, L., White, W. and Marshall, P. (2013). "Science and the Dead. A guideline for the destructive sampling of archaeological human remains for scientific analysis", Advisory Panel on the Archaeology of Burials in England, English Heritage Publishing.

McLaughlin, G. and Lednev, I.K. (2012), "Spectroscopic discrimination of bone samples from various species", *American Journal of Analytical Chemistry*, vol. 3, pp. 161-167.

Meindl, R.S. and Lovejoy, C.O. (1985), "Ectocranial suture closure: A revised method for the determination of skeletal age at death based on the lateral-anterior sutures", *American Journal of Physical Anthropology,* vol. 68, no. 1, pp. 57-66.

Menck, J., Dobler, A. and Dohler, J.R. (1997), "Vascularization of the humerus", *Langenbecks Archives of Surgery*, vol. 382, pp. 123–27.

Mimura, N., Yasuhara, K., Kawagoe, S., Yokoki, H. and Kazama, S. (2011), "Damage from the Great East Japan Earthquake and Tsunami - A quick report", *Mitigation and Adaptation Strategies for Global Change,* vol. 16, no. 7, pp. 803-818.

Mnich, B., Skrzat, J. and Szostek, K. (2017), "Estimating age at death from an archaeological bone sample – a preliminary study based on comparison of histomorphometric methods", *Anthropological Review,* vol. 80, no. 1, pp. 37-55.

Moore, S.R., Milz, S. and Knothe Tate, M.L. (2014), "The Linea Aspera: A Virtual Case Study Testing Emergence of Form and Function", *The Anatomical Record*, vol. 297, no. 2, pp. 273-280.

Moreno, F. (2013), Sexual Dimorphism in Human Teeth from Dental Morphology and Dimensions: A Dental Anthropology Viewpoint. In Moriyama, H. (ed), *Sexual Dimorphism*, InTech, pp. 81-96.

Moss, M.L. and Young, R.W. (1960), "A functional approach to craniology", *American Journal of Physical Anthropology,* vol. 18, pp. 281-292.

Mulhern. D.M. and Ubelaker, D.H. (2001), "Differences in osteon banding between human and nonhuman bone", *Journal of Forensic Sciences*, vol. 46, no. 2, pp. 220-2.

Mulhern, D.M. and Ubelaker, D.H. (2009), "Bone microstructure in juvenile chimpanzees", *American Journal of Physical Anthropology,* vol. 140, no. 2, pp. 368-375.

Mulhern, D. M. and Ubelaker, D. H. (2012), Differentiating Human from Nonhuman Bone Microstructure. In Crowder, C. and Stout, S. (eds), *Bone Histology: An Anthropological Perspective,* Boca Raton: CRC Press, pp. 109-134.

Mulhern, D.M. (2016), Differentiating Human from Nonhuman Skeletal Remains. In Blau, S. and Ubelaker, D.H (eds), *Handbook of Forensic Anthropology and Archaeology,* New York: Taylor & Francis.

National Geographic (2017), "GIS (geographic information system)", https://www.nationalgeographic.org/encyclopedia/geographic-information-system-gis/ (accessed June 2018).

Newton, C.D. and Nunamaker, D.M. (1985), *Textbook of Small Animal Orthopaedics,* Philadelphia (PA): Lippincott Williams & Wilkins.

Nicklas, J.A. and Buel, E. (2006), "Simultaneous determination of total human and male DNA using a Duplex Real-Time PCR Assay", *Journal of Forensic Sciences*, vol. 51, no. 5, pp. 1005-1015.

Nielsen-Marsh, C.M., Ostrom, P.H., Gandhi, H., Shapiro, B., Cooper, A., Hauschka, P.V. and Collins, M.J. (2002), "Sequence preservation of osteocalcin protein and mitochondrial DNA in bison bones older than 55 ka", *Geology,* vol. 30, no. 12, pp. 1099, 1102.

Noakes, D.E., Parkinson, J.T. and England, G.C.W. (2001), *Arthur's Veterinary Reproduction and Obstetrics*, Philadelphia (PA): Saunders.

Obenson, K. (2014), "In consideration of subspecialty training in forensic anthropology for pathologists", *Forensic Science, Medicine and Pathology*, vol. 10, pp. 114-115.

Ogilvie, M.D. and Hilton, C.E. (2011), *"*Cross-sectional geometry in the humeri of foragers and farmers from the prehispanic American Southwest: exploring patterns in the sexual division of labor", *American Journal of Physical Anthropology*, vol. 144, no. 1, pp. 11-2.

O'Rahilly, R., Muller, F., Carpenter, S. and Swenson, R. (2008), *Basic Human Anatomy. A Regional Study of Human Structure*, Philadelphia (PA): W. B. Saunders Co.

Payne-James, J. and Byard R. (2015), *Encyclopaedia of Forensic and Legal Medicine,* second edition, Amsterdam: Elsevier.

Pearson, M. (2015), "Jeffrey Dahmer's killer explains why he did it", Cnn.com, April 30, 2015 https://edition.cnn.com/2015/04/30/us/feat-jeffrey-dahmer-killer-explanation/index.html (accessed July 2015).

Pereira, F., Carneiro, J. and van Asch, B. (2010), A Guide for Mitochondrial DNA Analysis in Non-Human Forensic Investigations, *The Open Forensic Science Journal,* vol. 3, pp. 33-44.

Pereira, G.A.M., Lopes, P.T.C., Santos, A.M.P.V. and Silveira, F.H.S. (2011), "Nutrient Foramina in the Upper and Lower Limb Long Bones: Morphometric Study in Bones of Southern Brazilian Adults", *International Journal of Morphology*, vol. 29, no. 2, pp. 514-520.

Pickering, R.B., and Bachman, D. (2009), *The use of Forensic Anthropology*, second edition, Boca Raton (FL): CRC Press.

Polguj, M., Blizniewska, K., Jedrzejewski, K., Majos, A. and Topol, M. (2013), "Morphological study of linea aspera variations – a proposal of classification and sexual dimorphism", *Folia Morphologica*, vol. 72, no. 1, pp. 72-77.

Polk, J.D., Demes, B., Jungers, W.L., Biknevicius, A.R., Heinrich, R.E. and Runestad, J.A. (2000), "A comparison of primate, carnivoran and rodent limb bone cross-sectional properties: are primates really unique?", *Journal of Human Evolution*, vol. 39, no. 3, pp. 297-325.

Porwit, A., Mc Cullough, J. and Erber, W.N. (2011), *Blood and Bone Marrow Pathology,* London: Churchill Livingstone Elsevier.

Potter, A., Reuther, J.D., Lowenstein, J.M. and Scheuenstuhl, G. (2010), "Assessing the reliability of pRIA for identifying ancient proteins from archaeological contexts", *Journal of Archaeological Science*, vol. 37, pp. 910-918.

Prescher, A., Brors, D. and Adam, G. (1996), "Anatomic and Radiologic Appearance of Several Variants of the Craniovertebral Junction", *Skull Base Surgery*, vol. 6, pp. 83-94.

Pritchard, J.J., Scott, J.H. and Girgis, F.G. (1956), "The structure and development of cranial and facial structures", *Journal of Anatomy*, vol. 90, pp. 73-86.

Queen, L. (2016), *"*Bones found at Thornhill golf club turn out to be 'non-human'", YorkRegion.com, August 9, 2016 https://www.yorkregion.com/news-story/6801080-bones-found-at-thornhill-golf-club-turn-out-to-be-non-human-/ (visited December 2017).

Ralis, Z.A., Ralis, H.M., Randall, M., Watkins, G. and Blake, P.D. (1976), "Changes in shape, ossification and quality of bones in children with spina bifida", *Developmental Medicine and Child Neurology,* Supplement, vol. 37, pp. 29-41.

Rao, S., Kothapalli, J. (2014), "The Diaphyseal nutrient foramina architecture - a study on the human upper and lower limb long bones", *Journal of Pharmacy and Biological Sciences*, vol. 9, no. 1, pp. 36-41.

Reichs, K.J. (ed) (1998), *Forensic Osteology. Advances in the Identification of Human Remains,* Springfield (IL): Charles C. Thomas Publisher.

Reitz, E.J. and Wing, E.S. (2008), *Zooarchaeology,* second edition, Cambridge University Press.

Rerolle, C., Saint-Martin, P., Dedouit, F., Rousseau, H. and Telmon, N. (2013), "Is the corticomedullary index valid to distinguish human from nonhuman bones: a multislice computed tomography study", *Forensic Science International,* vol. 231, no. 1-3, 406.e 1-5.

Rimm, S.A. (2007), "Sexual Selection and Genital Evolution in Mammals: A Phylogenetic Analysis of Baculum Length", *The American Naturalist,* vol. 169, no. 3, pp. 360-369.

Robinson, M.E. (2007), *Crime Scene Photography,* London: Academic Press.

Rogers, T.L. and Allard, T.T. (2004), "Expert testimony and positive identification of human remains through cranial suture patterns", *Journal of Forensic Sciences*, vol. 49, no. 2, pp. 203-207.

Rohde, D. (2012), *Endgame: The Betrayal and Fall of Srebenica, Europe's Worst Massacre Since World War II,* New York: Penguin Books.

Rouge-Maillart, C., Telmon, N., Rissech, C., Malgosa, A. and Rouge, D. (2004), "The determination of male adult age at death by central and posterior coxal analysis. A preliminary study", *Journal of Forensic Sciences,* vol. 49, no. 2, pp. 208-214.

Ruengdit, S., Prasitwattanaseree, S., Mekjaidee, K., Sinthubua, A. and Mahakkanukrauh, P. (2018), "Age estimation approaches using cranial suture closure: A validation study on a Thai population", *Journal of Forensic and Legal Medicine*, vol. 53, pp. 79-86.

Ruff, C. (1990), Body mass and hindlimb bone cross-sectional and articular dimensions in anthropoid primates. In Damuth, J. and MacFadden, B.J. (eds). *Body size in mammalian paleobiology: estimation and biological implications,* Cambridge University Press, pp. 119-149.

Ruff, C. (2003), "Ontogenetic adaptation to bipedalism: age changes in femoral to humeral length and strength proportions in humans, with a comparison to baboons", *Journal of Human Evolution*, vol. 45, pp. 327-349.

Ruff, C.B. and Larsen, C.S. (2014), Long Bone Structural Analyses and the Reconstruction of Past Mobility: A Historical Review. In Carlson, K.J. and Marchi, D. (eds). *Reconstructing Mobility – Environmental, Behavioural, and Morphological Determinants,* New York: Springer, pp. 13-29.

Russo, G.A. and Kirk, E.C. (2013), Foramen Magnum Position in Bipedal Mammals, *Journal of Human Evolution,* vol. 65, no. 5, pp. 656-670.

Saferstein, R. (2007), *Criminalistics: An Introduction to Forensic Science*, Upper Saddle River (NJ): Pearson Education.

Samuels, M.E., Regnault, S. and Hutchinson, J.R. (2017), "Evolution of the patellar sesamoid bone in mammals", *PeerJ,* March 21, 5: e3103, doi: 10.7717/peerj.3103.

Savolainen, P. and Lundeberg, J. (1999), "Forensic evidence based on mtDNA from dog and wolf hairs", *Journal of Forensic Sciences,* vol. 44, no. 1, pp. 77-81.

Schaefer, M., Black, S. and Schaefer, L. (2009), *Juvenile Osteology: A Laboratory and Field Manual,* Oxford: Elsevier.

Scheuer, L. and Black, S. (2004), *The Juvenile Skeleton,* Oxford: Elsevier.

Schmitt, A., Cunha, E. and Pinheiro, J. (2006), *Forensic Anthropology and Medicine. Complementary Sciences from Recovery to Cause of Death,* Totowa (NJ): Humana Press.

Schwark, T., Heinrich, A., Preusse-Prange, A., von Wurmb-Schwark, N. (2011), "Reliable genetic identification of burnt human remains", *Forensic Science International. Genetics*, vol. 5, no. 5, pp. 393-399.

Schwartz, J.H. (2007), *Skeleton Keys. An Introduction to Human Skeletal Morphology, Development, and Analysis,* Oxford University Press.

Schwartz, M.A. (2000), "Kumho Tire Co. v. Carmichael: The Supreme Court Follows Up on the Daubert Test", 16 *Touro Law Review* 297, Touro Law Center Legal Studies Research Paper.

Sekharan, C.P. (1985), "Identification of skull from its suture pattern", *Forensic Science International*, vol. 27, no. 3, pp. 205-214.

Seymour, R.S., Smith, S.L., White, C.R., Henderson, D.M. and Schwarz-Wings, D. (2012), "Blood flow to long bones indicates activity metabolism in mammals, reptiles and dinosaurs", *Proceedings of the Royal Society B: Biological Sciences,* vol. 279, pp. 451-456.

Shaw, C.N. and Stock, J.T. (2009), "Intensity, repetitiveness, and directionality of habitual adolescent mobility patterns influence the tibial diaphysis morphology of athletes", *American Journal of Physical Anthropology,* vol. 140, no. 1, pp. 149-159.

Shewale, J.G., Schneida, E., Wilson, J., Walker, J.A., Batzer, M.A., Sinha, S.K. (2007), "Human genomic DNA quantitation system, H-Quant: development and validation for use in forensic casework", *J Forensic Sciences,* vol. 52, no. 2, pp. 364–70.

Silber, L., and Little, A. (1997), *Yugoslavia: Death of a Nation,* London: Penguin Books.

Sim, J.H. and Dongchoon, A. (2014), "Anatomy of the diaphyseal nutrient foramen in the long bones of the pectoral limb of German Shepherds", *Korean Journal of Veterinary Research*, vol. 54, no. 3, pp. 179-184.

Singhal, A., Grande, J.C. and Zhou, Z. (2013), "Micro/nano CT for visualization of internal structures", *Microscopy Today*, vol. 21, no. 2, pp. 16-22.

Sisniega, A., Vaquero, J.J. and Desco, M. (2014), Design and Assessment Principles of Semiconductor Flat-Panel Detector-Based X-Ray Micro-CT Systems for Small Animal Imaging. In Farncombe, T. and Iniewski, K. (eds). *Medical Imaging: Technology and Applications,* Boca Raton (FL): CRC Press, pp. 109-146.

Sledzik, P.S, Dirkmaat, D., Mann, R.W., Holland, T.D., Mundorff, A.Z., Adams, B.J., Crowder, C.M. and DePaolo, F. (2009), Disaster Victim Recovery and Identification. Forensic Anthropology in the Aftermath of September 11. In Steadman, D.W. (ed). *Hard Evidence. Case Studies in Forensic Anthropology,* Upper Saddle River (NJ): Pearson Education, pp. 289-302.

Steadman, D.W. (2009), *Hard Evidence. Case Studies in Forensic Anthropology,* Upper Saddle River (NJ): Pearson Education.

Steele, D.G. and Bramblett, C.A. (2012), *The Anatomy and Biology of the Human Skeleton*, College Station: Texas A&M University Press.

Stock., J. and Pfeiffer, S. (2001), "Linking structural variability in long bone diaphyses to habitual behaviours: foragers from the southern African Later Stone Age and the Andaman Islands", *American Journal of Physical Anthropology*, vol. 115, pp. 337-348.

Stock, J.T., O'Neill, M.C., Ruff, C.B., Zabecki, M., Shackelford, L. and Rose, J. (2011), Body size, skeletal biomechanics, mobility and habitual activity from the Late Palaeolithic to the mid-Dynastic Nile Valley. In: Pinhasi, R. and Stock, J.T. (eds), *Human bioarchaeology of the transition to agriculture*, New York: Wiley-Blackwell, pp. 347–367.

Stock, S.R. (2011), *Micro-Computed Tomography. Methodology and Applications,* Boca Raton (FL): CRC Press.

Stout, S.D. and Ross, L.M. (1991), "Bone fragments a body can make", *Journal of Forensic Sciences*, vol. 36, no. 3, pp. 953-957.

Stout, S.D. (1998), Estimating time since death: the use of histological methods in forensic anthropology. In: Reichs, K.J. (ed). Forensic *osteology: advances in the identification of human remains.* Springfield (IL): Charles C. Thomas, pp. 237–252.

Stout, S.D. (2009), Small Bones of Contention. In Steadman, D.W. (ed). *Hard Evidence. Case Studies in Forensic Anthropology,* Upper Saddle River (NJ): Pearson Education, pp. 239-247.

Streeter, M. (2012), Histological Age at Death Estimation. In pp. Crowder, S. and Stout, S. (eds), *Bone Histology. An Anthropological Perspective,* Boca Raton (FL): CRC Press, pp. 135-152.

Stubbs, G. (1976), *The Anatomy of the Horse,* Mineola (NY): Dover Publications.

Takezawa, S. (2016), *The Aftermath of the 2011 East Japan Earthquake and Tsunami. Living Among the Rubble,* London: Lexington Books.

Talbot, B.S., Gange, C.P., Chaturvedi, A., Klionsky, N., Hobbs, S.K. and Chaturvedi, A. (2017), "Traumatic Rib Injury: Patterns, Imaging Pitfalls, Complications, and Treatment", *RadioGraphics*, vol. 37, no. 2, https://doi.org/10.1148/rg.2017160100.

Tersigni-Tarrant, M.A. and Langley, N.R. (2017), Human Osteology. In Langley, N.R. and Tersigni-Tarrant, M.A. (eds.). *Forensic Anthropology. A Comprehensive Introduction*, Boca Raton (FL): Taylor & Francis Group, p. 105.

The British Deer Society (2015), "Deer Species", http://www.bds.org.uk/index.php/advice-education/species (accessed January 2016).

The Crown Prosecution Services (2014), "Expert Evidence", https://www.cps.gov.uk/sites/default/files/documents/legal_guidance/expert_evidence_first_edition_2014.pdf (accessed September 2018).

The Japan Times (2016), "Hunt for missing disaster victims still confounds rescuers", March 11, 2016 https://www.japantimes.co.jp/news/2016/03/11/national/hunt-missing-disaster-victims-still-confounds-rescuers/ (accessed September 2016).

The Telegraph (2017), "What happened to murdered April Jones and who is Mark Bridger?", 20 June 2017, http://www.telegraph.co.uk/news/0/happened-murdered-april-jones-mark-bridger/ (accessed January 2018).

Thompson, T.J. (2005), "Heat-induced dimensional changes in bone and their consequences in forensic anthropology", *Journal of Forensic Sciences,* vol. 50, no. 5, pp. 1008-1015.

Tobe, S.S. and Linacre, A.M. (2008), "A multiplex assay to identify 18 European mammal species from mixtures using the mitochondrial cytochrome b gene", *Electrophoresis*, vol. 29, no. 2, pp. 340–347.

Ubelaker, D.H. (1989), *Human Skeletal Remains: Excavation, Analysis, Interpretation,* Washington, D.C.: Taraxacum.

Ubelaker, D.H., Ward, D.C., Braz, V.S. and Stewart, J. (2002), "The use of SEM/EDS analysis to distinguish dental and osseous tissue from other materials", *Journal of Forensic Sciences*, vol. 47, no. 5, pp. 940-943.

Ubelaker, D.H., Lowenstein, J.M. and Hood, D.G. (2004), "Use of solid-phase double-antibody radioimmunoassay to identify species from small skeletal fragments", *Journal of Forensic Sciences,* vol. 49, no. 5, pp. 924-929.

Ubelaker, D. H. and Scammell, H. (2006), *Bones. A Forensic Detective's Casebook,* Lanham (MD): M. Evans.

Ubelaker, D.H. (2010), Recent Advances in the Estimation of Age at Death from the Assessment of Immature Bone. In Latham, K.E. and Finnegan, M. (eds). *Age Estimation of the Human Skeleton*, Springfield (IL): Charles Thomas Publisher, pp. 177-189.

Ubelaker, D.H. (2016), "The Dynamic Interface of Bioarchaeology and Forensic Anthropology", *Intersecciones en Antropologia*, vol. 17, no. 2, pp. 137-156.

Uhl, N.M. (2013), Age at death estimation. In DiGangi, E.A. and Moore, M.K. (eds). *Research Methods in Human Skeletal Biology,* Oxford: Academic Press, pp. 63-90.

Urbanova, T. and Novotny, V. (2005), "Distinguishing between human and non-human bones: histometric method for forensic anthropology", *Anthropologie*, vol. 43, no. 1, pp. 77-85.

Vass, A.A., Madhavi, M., Synstelien, J. and Collins, K. (2005), "Elemental characterization of skeletal remains using laser-induced breakdown spectroscopy (LIBS)", *Proceedings of the American Academy of Forensic Sciences,* vol. 11, pp. 307-308.

Vigorita, V.J. (2008), *Orthopaedic Pathology,* second edition, Philadelphia (PA): Lippincott Williams & Wilkins.

Von Wurmb-Schwark, N., Simeoni, E., Ringleb, A., Oehmichem, M. (2004), "Genetic investigation of modern burned corpses", *International Congress Series* 1261, pp. 50-52.

Walker, P.L. (2008), Bioarchaeological Ethics: A Historical Perspective on the Value of Human Remains. In Katzenberg, M.A. and Saunders, S.R. (eds), *Biological Anthropology of the Human Skeleton*, second edition, Hoboken (NJ): John Wiley & Sons, pp. 3-40.

Walter, B.S. and Schultz, J.J. (2013), "Mapping simulated scenes with skeletal remains using differential GPS in open environments: an assessment of accuracy and practicality", *Forensic Science International*, vol. 228, no. 1-3, pp. 33-46.

Ward, M. R., Pasterkamp, G., Yeung, A. C. and Borst, C. (2000), "Arterial remodeling. Mechanisms and clinical implications", *Circulation,* vol. 102, pp. 1186 – 1191.

Warden, S.J., Mantila, R.S.M., Kersh, M.E., Hurd, A.L., Fleisig, G.S., Pandy, M.G. and Fuchs, R.K. (2014), "Physical activity when young provides lifelong benefits to cortical bone size and strength in men", *Proceedings of the National Academy of Sciences of the United States of America,* vol. 111, no. 14, pp. 5337-5342.

Watson, J. and McClelland, J., *n.d.*, "Distinguishing Human from Animal Bone". The University of Arizona, Arizona State Museum. http://www.statemuseum.arizona.edu/crservices/human_animal_bone.shtml (accessed 23 November 2014).

White, T.D. and Folkens, P.A. (2005), *The human Bone Manual*, Elsevier Academic Press.

White, T., Black, M. and Folkens, P. (2011), *Human Osteology,* third edition, San Diego (CA): Academic Press.

Wilbert, D.M. and Finnegan, M. (2010), Age Estimation by Root Dentin Transparency of Double Rooted Mandibular Molars. In Latham, K.E. and Finnegan, M. (eds). *Age Estimation of the Human Skeleton*, Springfield (IL): Charles Thomas Publisher, pp. 48-56.

Wild, D. (2013), *The Immunoassay Handbook,* Fourth Edition, Oxford: Elsevier.

Williams, P.L., Bannister, L.H., Berry, M.M., Collins, P., Dyson, M., Dussek, J.E. and Ferguson, M.W.J. (1995), Pelvic girdle and lower limb. In H. Gray (*ed*), *Gray's Anatomy*, 38th edition, Philadelphia (PA): Churchill Livingstone, pp. 1434-1567.

Williams, S.A. and Russo, G.A. (2015), "Evolution of the hominoid vertebral column: The long and the short of it", *Evolutionary Anthropology,* vol. 24, no. 1, pp. 15-32.

Witkowska, A., Alibhai, A., Hughes, C., Price, J., Klisch, K., Sturrock, C.J. and Rultand, C.S. (2014), "Computed tomography analysis of guinea pig bone: architecture, bone thickness and dimensions throughout development", *PeerJ* 2: e615.

Wu, X. and Schepartz, L.A. (2009), "Application of computed tomography in paleoanthropological research", *Progress in Natural Science,* vol. 19, no. 8, pp. 913-921.

Xue, Z., Ding, H., Hu, C., Xu, H. and An, Z. (2016), "An anatomical study of the nutrient foramina of the human humeral diaphysis", *Medical Science Monitor*, vol. 22, pp. 1637-1645.

Young, W.C. (1989), *Roark's Formulas for Stress and Strain,* New York: HcGraw-Hill.

Young, B., Lowe, J.S., Stevens, A. and Heath, J.W. (2006), *Wheater's Functional Histology. A Text and Color Atlas,* fifth edition, Philadelphia (PA): Churchill Livingstone Elsevier.

Zachary, J.F. (2017), *Pathologic Basis of Veterinary Disease*, Expert Consult, 6th Edition, Maryland Heights (MO): Mosby Elsevier.

Zimmermann, H.A., Schultz, J.J. and Sigman, M.E. (2014), "Preliminary validation of handheld X-ray fluorescence (HHXRF) spectrometry: distinguishing osseous and dental tissue from non-bone material of similar chemical composition", *Journal of Forensic Sciences,* vol. 60, no. 2, pp. 382-390.

Zimmermann, H.A., Meizel-Lambert, C.J., Schultz, J.J. and Sigman, M.E. (2015), "Chemical Differentiation of Osseous, Dental, and Non-skeletal Materials in Forensic Anthropology using Elemental Analysis", *Science and Justice,* vol. 55, pp. 131-138.

Appendix A

CLASSIFICATION STATISTICS: CRANIAL CURVATURE

This appendix contains the classification statistics produced in ArcScene as a result of the cranial bones curvature calculation process.

Count:	515816
Minimum:	-63.300
Maximum:	78.500
Sum:	35.035.633,73
Mean:	67,92273548
Standard Deviation:	2.129,744116

Count:	515816
Minimum:	-77.200
Maximum:	84.100
Sum:	-7.888.024,314
Mean:	-15,2923219
Standard Deviation:	2.436,372141

Count:	515816
Minimum:	-69.900
Maximum:	86.200
Sum:	-51.732.080,78
Mean:	-100,2917335
Standard Deviation:	2.481,536768

Count:	515816
Minimum:	-72.400
Maximum:	63.200
Sum:	-21.704.315,29
Mean:	-42,07763097
Standard Deviation:	2.210,335043

Fig. A.1. Classification statistics produced in sheep cranial curvature calculation

Count:	515816	Count:	515816
Minimum:	-62.400	Minimum:	-71.200
Maximum:	57.600	Maximum:	66.000
Sum:	71.454.776,47	Sum:	-61.862.881,57
Mean:	138,5276464	Mean:	-119,9320718
Standard Deviation:	1.956,515735	Standard Deviation:	2.228,238395

Count:	515816	Count:	515816
Minimum:	-65.500	Minimum:	-65.700
Maximum:	65.200	Maximum:	69.500
Sum:	40.497.985,49	Sum:	15.191.093,33
Mean:	78,5124647	Mean:	29,45060513
Standard Deviation:	1.947,771662	Standard Deviation:	2.610,082104

Fig. A.2. Classification statistics produced in calf cranial curvature calculation

Count:	515816	Count:	515816
Minimum:	-61.100	Minimum:	-60.100
Maximum:	60.500	Maximum:	58.400
Sum:	-17.037.330,2	Sum:	-48.705.929,41
Mean:	-33,02985986	Mean:	-94,425007
Standard Deviation:	2.289,436581	Standard Deviation:	2.101,874154

Count:	515816	Count:	515816
Minimum:	-82.800	Minimum:	-68.000
Maximum:	60.800	Maximum:	58.100
Sum:	-4.081.483,922	Sum:	91.948.577,25
Mean:	-7,912674135	Mean:	178,2584822
Standard Deviation:	2.302,432509	Standard Deviation:	2.161,699132

Fig. A.3. Classification statistics produced in fox cranial curvature calculation

Count:	515816	Count:	515816
Minimum:	-62.400	Minimum:	-67.000
Maximum:	58.800	Maximum:	64.400
Sum:	-43.379.896,47	Sum:	-3.629.021,177
Mean:	-84,09955579	Mean:	-7,035495558
Standard Deviation:	1.991,124488	Standard Deviation:	2.034,887545

Count:	515816	Count:	515816
Minimum:	-61.500	Minimum:	-68.400
Maximum:	59.900	Maximum:	76.300
Sum:	-24.875.967,84	Sum:	94.926.203,14
Mean:	-48,22643703	Mean:	184,0311335
Standard Deviation:	2.334,205415	Standard Deviation:	2.120,801803

Fig. A.4. Classification statistics produced in human cranial curvature calculation

Count:	4288068	Count:	24000000
Minimum:	-6.200	Minimum:	-5.000
Maximum:	6.000	Maximum:	6.500
Sum:	29.650.923,92	Sum:	-72.934.949,02
Mean:	6,914751334	Mean:	-3,038956209
Standard Deviation:	420,2758379	Standard Deviation:	301,986965

Count:	24000000	Count:	24000000
Minimum:	-5.400	Minimum:	-6.000
Maximum:	8.300	Maximum:	7.700
Sum:	-158.536.170,2	Sum:	-111.886.062,7
Mean:	-6,605673758	Mean:	-4,661919281
Standard Deviation:	255,465389	Standard Deviation:	303,3067177

Fig. A.5. Classification statistics produced in curvature calculation of human fragments

Appendix B

CLASSIFICATION STATISTICS: RIB SHAFT CURVATURE

This appendix contains the classification statistics produced in ArcScene as a result of the rib shaft curvature calculation process.

Count:	10130184
Minimum:	-4.100
Maximum:	9.400
Sum:	-168.659.947,1
Mean:	-16,64924813
Standard Deviation:	263,0570777

Count:	11173248
Minimum:	-3.000
Maximum:	5.700
Sum:	12.171.703,53
Mean:	1,089361261
Standard Deviation:	256,7760049

Count:	12004020
Minimum:	-4.100
Maximum:	10.300
Sum:	-136.659.543,5
Mean:	-11,38448149
Standard Deviation:	242,5307801

Count:	10689305
Minimum:	-2.900
Maximum:	5.900
Sum:	-22.690.787,06
Mean:	-2,122756069
Standard Deviation:	261,7731894

Fig. B.1. Classification statistics produced in human rib shaft curvature calculation (rib superior view)

Count: 7995968	Count: 9441036
Minimum: -5.800	Minimum: -5.400
Maximum: 9.300	Maximum: 8.300
Sum: -39.684.905,49	Sum: -56.451.951,76
Mean: -4,963114596	Mean: -5,97942342
Standard Deviation: 262,5396181	Standard Deviation: 249,5624444

Count: 10007040	Count: 10006164
Minimum: -3.100	Minimum: -2.700
Maximum: 6.100	Maximum: 6.100
Sum: -42.497.606,27	Sum: -74.041.632,94
Mean: -4,246770901	Mean: -7,399602179
Standard Deviation: 249,7178155	Standard Deviation: 251,4730559

Fig. B.2. Classification statistics produced in human rib shaft curvature calculation (rib inferior view)

Count: 5267535	Count: 8160000
Minimum: -5.800	Minimum: -4.100
Maximum: 4.200	Maximum: 4.500
Sum: 20.798.843,14	Sum: 83.550.506,67
Mean: 3,948496429	Mean: 10,23903268
Standard Deviation: 286,8066561	Standard Deviation: 241,261584

Count: 7219900	Count: 6586712
Minimum: -3.700	Minimum: -3.000
Maximum: 7.700	Maximum: 2.500
Sum: -43.506.185,88	Sum: -7.489.943,137
Mean: -6,025870979	Mean: -1,13712929
Standard Deviation: 253,1988726	Standard Deviation: 253,0315003

Fig. B.3. Classification statistics produced in pig rib shaft curvature calculation (rib superior view)

Count:	6469245	Count:	6964524
Minimum:	-2.600	Minimum:	-5.100
Maximum:	2.900	Maximum:	2.700
Sum:	7.580.960,784	Sum:	28.490.468,24
Mean:	1,171846295	Mean:	4,09079906
Standard Deviation:	236,5492231	Standard Deviation:	240,1159012

Count:	7902183	Count:	7344904
Minimum:	-3.000	Minimum:	-2.600
Maximum:	2.900	Maximum:	2.700
Sum:	1.003.210,588	Sum:	-4.565.118,039
Mean:	0,126953601	Mean:	-0,621535426
Standard Deviation:	252,5030024	Standard Deviation:	258,3812898

Fig. B.4. Classification statistics produced in pig rib shaft curvature calculation (rib inferior view)